Investigating the Rapid Clearance of Oscillating Transcripts during Vertebrate Segmentation

Dissertation

Presented in Partial Fulfillment of the Requirements for the Degree Doctor of Philosophy in the Graduate School of The Ohio State University

By

Kiel Tietz, B.S.

Graduate Program in Molecular, Cellular, and Developmental Biology

The Ohio State University

2019

Dissertation Committee

Sharon L. Amacher, PhD., Advisor

Susan E. Cole, PhD.

Guramrit Singh, PhD.

James D. Jontes, PhD.

Abstract

Vertebrate segmentation is regulated by the segmentation clock, a biological oscillator that controls periodic formation of embryonic segments. This molecular oscillator generates cyclic gene expression in the tissue that generates somites and has the same periodicity as somite formation. Molecular components of the clock include the *Hes/her* family of transcriptional repressors, but additional transcripts also cycle. Maintenance of oscillatory gene expression requires that transcriptional activation and repression, RNA turnover, translation, and protein degradation are rapid (one cycle is 30 minutes in the zebrafish). Little is known about post-transcriptional control of cyclic transcripts during somitogenesis and my work employs genetic and biochemical approaches to better understand rapid cyclic transcript turnover.

The lab previously isolated a zebrafish segmentation clock mutant, *tortuga*, that has elevated levels of cyclic transcripts. Loss of proline-rich nuclear receptor coactivator protein Pnrc2 is responsible for cyclic transcript accumulation in *tortuga* deletion mutants and a new *pnrc2* loss-of-function mutant displays an identical phenotype (Chapter 2). The *her1* 3'UTR confers instability to otherwise stable transcripts in a Pnrc2-dependent manner indicating that the 3'UTR of cyclic transcripts is critical for Pnrc2-mediated decay.

Interestingly, cyclic protein levels do not accumulate in *pnrc2*-deficient embryos, suggesting that stabilized cyclic transcripts are not efficiently translated and that translation may be controlled by an additional post-transcriptional mechanism. Together, these findings demonstrate Pnrc2 regulates cyclic transcript turnover though 3'UTR interactions and suggests another level of post-transcriptional regulation maintains proper oscillations of cyclic genes in *pnrc2* mutants during somitogenesis.

To identify *her1* 3'UTR cis-regulatory elements critical for Pnrc2-mediated decay (Chapter 3), I show the last 179 nucleotides of the 725 nt *her1* 3'UTR is sufficient and necessary to confer Pnrc2-dependent rapid instability to reporter transcripts. Additionally, I show the 3'UTR of the *deltaC (dlc)* cyclic transcript also confers Pnrc2-mediated decay. I hypothesize that mechanisms regulating cyclic transcript turnover are shared among cyclic transcripts and have identified two putative decay-inducting motifs that are present in the destabilizing 179 nt region of the *her1* 3'UTR and are conserved in the *dlc* 3'UTR, a Pumilio response element (PRE) and a AU-rich element (ARE). I show here the PRE and ARE of the *her1* 3'UTR functions in the turnover of reporter transcripts. These results suggest Pnrc2 may function with Pumilio, a known decay factor, to regulate the rapid turnover of cyclic transcripts during somitogenesis. My work explores mechanisms regulating oscillation dynamics during vertebrate segmentation and will further our understanding of pathways that control post-transcriptional gene regulation.

Dedication

I dedicate this to my mother Susan, sister Lauren, and father Gregg. They have always provided great support and helped comfort me through the hardest times of graduate school. I also dedicate this to my cat Max who is the best companion a cat can be to a human.

Acknowledgments

Numerous people have contributed to my development throughout graduate school, but I must first thank my advisor Dr. Sharon Amacher for being the best mentor I could have possibly asked for. Sharon allowed me to develop as an independent scientist while also pushing me to do the best work I can. The wonderful culture Sharon creates in her lab is ideal for learning and working as a team to address difficult questions of biology. I attribute my successes in graduate school and my ability to obtain a great post-doctoral position to Sharon and I will forever be grateful for that.

I must also thank Dr. Thomas Gallagher for my development as an independent scientist. Tom was a large reason I joined the Amacher lab, and he showed me how a great scientist and mentor can also be a great friend. Tom is like a second advisor to me, and I also attribute my successes in graduate school to his mentorship. Tom taught me more than just technical skills, he taught me how to think as a scientist and I will continue to use that mindset throughout my scientific career. We have shared many great experiences in and outside of the lab together and will always think of Tom as a great mentor and a great friend.

I thank Dr. Susan Cole, Dr. Guramrit Singh, and Dr. James Jontes for being great committee members that truly care about my success and always

providing excellent feedback on my project. I thank Dr. Jared Talbot for providing training and support throughout graduate school. Jared helped me consider the next steps of my career and provided invaluable perspective on what is best for me and my overall career goals. I thank Dr. Michael Berberoglu for teaching me numerous technical skills and also being a great friend in and outside the lab. I thank Dr. Kim Hromowyk, we started graduate school together, and it was wonderful to be able to help each other throughout the demanding times of being a graduate student. I also thank Dr. Nicolas Derr, Zachary Morrow, and Dr. Adrienne Maxwell for always being positive influences in the lab and providing great energy to be around. I thank Danielle Pvirre and the army of undergraduates who have maintained and fed my fish throughout my graduate career. I thank The Center for RNA Biology at OSU for funding my research and for being such a great community that is purely focused on a better understanding of RNA biology. I also want to thank Dr. Joseph Greene and Janelle Gabriel for being amazing friends throughout graduate school and making Friday nights so enjoyable (left on Maynard).

Importantly, I want to thank my girlfriend Dr. Katie Doran for being a staple of support throughout my journey and always motivating me to keep doing my best. I also deeply thank my mother Susan Tietz, and sister Lauren Tietz. They were always just a phone call away and without their love I would not be where I am today.

Vita

2003-2007……Cooper High School

2007-2012……B.S. Applied Science, The University of Wisconsin-Stout

2012-2019……Graduate Research Associate, The Ohio State University

Publications

Gallagher TL[+], **Tietz KT**[+], Morrow ZT, McCammon JM, Goldrich ML, Derr NL, Witzki AM, Amacher SL (2017) Pnrc2 regulates 3'UTR-mediated decay of cyclic transcripts during zebrafish segmentation. *Dev Biol*. 429, 225-239, 2017. [+]Co-first authors.

Fields of Study

Major Field: Molecular, Cellular, and Developmental Biology

Research Area: Post-Transcriptional Gene Regulation

Table of Contents

List of Tables

List of Figures

Chapter 1: Introduction

1.1 Somitogenesis

Somitogenesis is a conserved process that governs the organization of the adult body of many species. The formation of somites (segments) is important for development of all vertebrate species as somites give rise to the vertebral column, ribs, skeletal muscle, cartilage, and tendons. This developmental process is critical for proper locomotion of the species and defects in somitogenesis can lead to severe immobility[1,2]. Somites are bilaterally paired blocks of mesoderm that form sequentially along the anterior-posterior axis of the developing embryo (Figure 1.1A). They mature from an area of mesenchymal cells termed the presomitic mesoderm (PSM). A region of multipotent cells called the tailbud, forms the posterior-most part of the vertebrate embryo, and is the source of PSM cells. As the embryo elongates, cells from the tailbud are continuously displaced into the posterior PSM; anteriorly, PSM cells become incorporated into forming somites (Figure 1.1B)[3,4]. Thus, cells transition through the PSM as immature mesoderm progenitors in the posterior and develop to more mature cells in the anterior. The progression of cell differentiation is regulated by cellular oscillations and a permissive gradient of gene expression across the PSM (Figure 1.1C). Cyclic expression of various key

segmentation genes is required for proper segmentation[3,5-7] and it is one of many examples of genetic oscillators regulating cell fate.

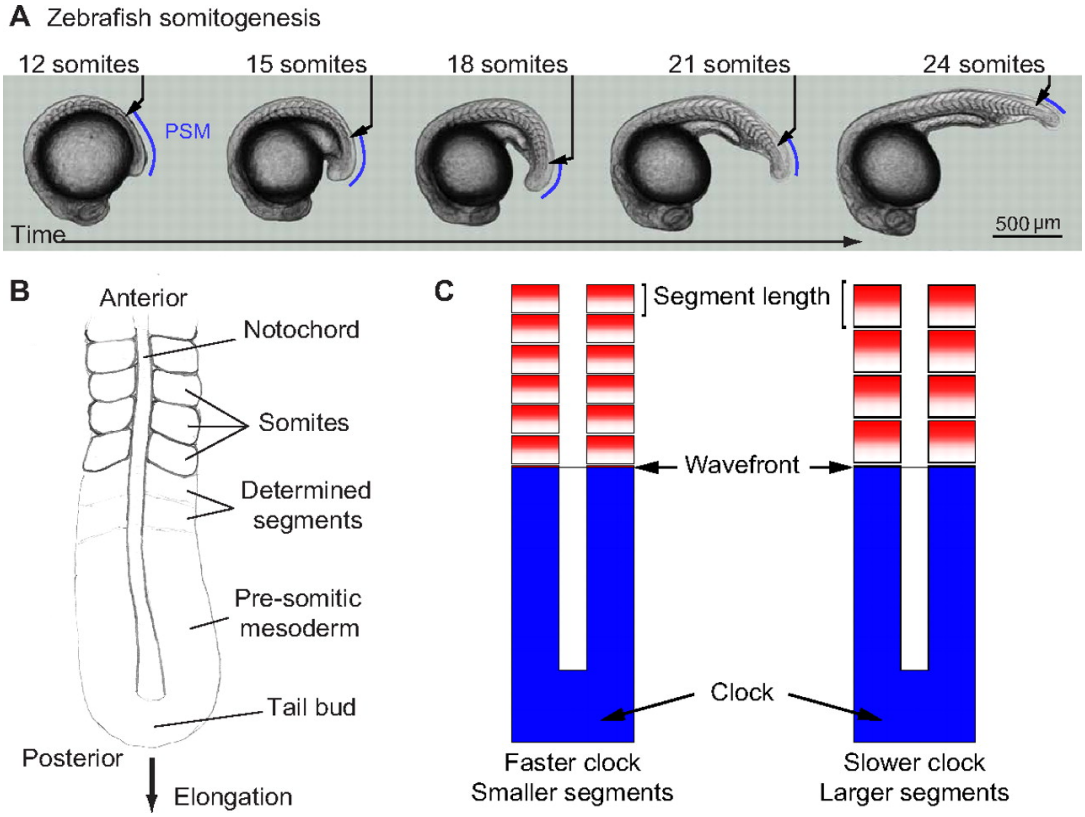

Figure 1.1. Anatomy of the rhythmic and sequential segmentation process. (**A**) Advancing stages of zebrafish embryo somitogenesis, lateral view. Somites bud sequentially from the posterior unsegmented tissue: the pre-somitic mesoderm (PSM, blue line). The position of the last formed somite is indicated with an arrow. Embryonic growth and the segmentation process are coordinated. (**B**) Dorsal view of the posterior of a segmenting vertebrate embryo. Somites form in pairs on each side of the notochord. (**C**) The Clock and Wavefront mechanism of vertebrate segmentation. The Clock consists of oscillating gene expression in the PSM (blue) and the Wavefront by a posteriorly-moving front that arrests the oscillations of the Clock. Resulting segments (red/white) have a length that is determined by the period of the Clock multiplied by the regression velocity of the Wavefront. (Figure from Oates et al, 2012. This figure was approved for use by Company of Biologists)

1.2 Human defects in somitogenesis

In humans, disruption of somitogenesis is linked to diseases such as Alagille syndrome (AGS) and spondylocostal dysostosis disorders (SCDO). AGS is a developmental disorder that occurs in at least 1:70,000 live births and has variable expressivity[1,2]. Individuals with AGS display skeletal deformities such as butterfly vertebrae. Mutation of the Notch ligand gene *Jagged1* is mapped to the AGS critical region and deletion of a single *JAG1* allele is sufficient for AGS to present, suggesting disruption of Notch signaling during somitogenesis may play a role in vertebral segmentation defects observed with AGS[8,9]. SCDO is a group of disorders characterized by short trunk dwarfism with vertebral segmentation defects along the entire spinal column. Individuals with SCDO can display butterfly vertebrae and may also have increased or decrease number of total vertebrae. Like AGS, many cases of SCDO are caused by mutation of genes involved in the Notch signaling pathway[10-12]. Both these diseases are linked to disruption of genetic oscillations in the Notch pathway and illustrate a need to better understand mechanisms by which genetic oscillators function.

1.3 Genetic oscillation in biological systems

Rhythms of gene expression are present in a large array of cellular events. The circadian clock, neuronal differentiation, and segmentation are some of the many examples. While gene expression is rhythmic in each of these processes, the periodicity of the gene expression can vary vastly. One of the

most well-studied examples of biological oscillation is the circadian clock. The circadian clock coordinates physiology and behavior of an organism on a 24-hour time scale. In mammals, molecular expression of transcriptional activators such as CLOCK (circadian locomotor output cycles kaput) and BMAL1 (brain and muscle ARNT-like 1) and repressors PER (period) and CRY (cryptochrome) function in two interlocking transcription/translation feedback loops to produce robust rhythms of gene expression[13,14]. The rhythmic expression of these circadian genes coordinates the organism's internal response to external stimuli such as light, and it has been found that between 2 and 10% of the total genome is transcribed in a circadian manner in various mouse tissues[15-17] emphasizing the importance oscillatory expression holds in biology.

Differentiation of neurons is another example of regulation by biological oscillation. In mice, high concentrations of Hes1 maintain a progenitor state in dividing neural progenitors by repressing proneural genes. Low amounts of Hes1 allow proliferation but permit differentiation away from the progenitor state. This balance of neuronal cells between a progenitor and non-progenitor state is accomplished through oscillation of Hes1 in neuronal cells every 2-3 hours[18]. This oscillatory expression of Hes1 allows cells to balance between the two states without commitment to a single fate and illustrates regulation of cellular differentiation by genetic oscillation.

Segmentation is another well-studied process by which genetic oscillators play a critical role. Expression of various cyclic genes in the PSM comprises the

segmentation clock and functions with a molecular Wavefront to coordinate the differentiation of cells in the PSM (Figure 1.1C). This mechanism was first termed the Clock and Wavefront model by Cooke and Zeeman in 1976 and is still the most widely accepted model for regulation of segmentation.

1.4 The Clock and Wavefront model

The Clock and Wavefront model is described as the mechanism by which vertebrate models regulate the formation of segments during somitogenesis. The 'Clock' consists of molecular oscillations that keep neighbor cells in a synchronized state while the 'Wavefront' moves across the PSM, arresting cells that are in the permissive oscillation phase and driving differentiation[19,20]. The first molecular evidence of the 'Clock' was discovered 1997 when the first oscillating ("cyclic") gene was identified in chick embryos[21]. In this study, the authors discovered that an avian homolog of the *Drosophila* segmentation gene *hairy* oscillated within the chick PSM and oscillation periodicity was the same as the periodicity of somite formation. The gene was named c-*hairy1* and was the first direct evidence for a developmental clock linked to segmentation. This developmental clock would later be termed the segmentation clock as homologs of the *hairy1* gene were found in mouse, fish, frog, and snake[22-26].

The Wavefront is defined as the intersection of two opposing gradients: Fgf8, Fgf4, and Wnt3a are expressed in the tailbud and decrease anteriorly and retinoic acid is expressed in formed somites and decreases posteriorly[27-30]. As somites form from anterior to posterior and the tailbud grows posteriorly, the

wavefront also shifts posteriorly. The continual movement of the tailbud posteriorly creates a gradient of expression such that cells positioned more posterior in the PSM have strong levels of Fgf8 and cells more anterior in the PSM have weaker presence of Fgf8. In mouse and chick, *Fgf8* is transcribed in the tail bud and progressive decay of *Fgf8a* mRNA and presumably *Fgf4* and *Wnt3a* mRNA in the PSM generates the posterior gradient[27,30]. When cells in the permissive phase of the segmentation clock contact the Wavefront, they undergo cellular differentiation and form mature somites.

The Clock and Wavefront function together to repeatedly coordinate the formation of segments along the anterior-posterior axis of the developing embryo. Disruption of the Wavefront through manipulation of WNT and FGF ligands in the PSM affects the position of somite boundaries[27-29,31]. Disruption of key segmentation clock genes such as *her1* and *her7* in zebrafish or *Hes7* in mice have also been shown to disrupt somite boundary formation[6,7,32-35]. These data emphasize the importance of both the segmentation clock and Wavefront in regulating the formation of segments in vertebrate species and motivates studies to better understand molecular mechanisms that govern these processes.

1.5 Components of the segmentation clock:

Since the discovery of c-*hairy1*, many genes with oscillatory expression have been identified and segmentation clock dynamics have been well-studied in the zebrafish and mouse systems[3,4]. The mouse c-*hairy1* homolog *Hes7* and zebrafish c-*hairy1* homologs *her1* and *her7* cycle dynamically in the PSM of each

species respectively[6,23,33,36,37]. These genes encode basic helix-loop-helix transcriptional repressors and oscillate through a negative feedback loop in which the Hes/Her protein inhibits its own transcription[36-39]. The period of the oscillation at the Wavefront defines somite size, and each species has a specific periodicity as zebrafish form a new somite pair every 30 minutes, chick every 90 minutes and mice every 2 hours[26]. Once an oscillation is completed, boundaries of elongating somites are formed and prolonged or shortened oscillation of the *Hes/her* genes can increase or decrease somite size respectively (Figure 1.1C)[7,34,35]. The expression cycle of these genes initiate in tailbud cells and then continues to oscillate as cells become progressively anteriorly displaced in the PSM[7,23]. Each new oscillation begins from a more posterior location as the tailbud extends posteriorly (Figure 1.1A). Of the *Hes* genes in mice, *Hes7* has been shown to be the most functionally important for the segmentation clock as knockdown or overexpression of *Hes7* causes failure of segmentation and fusion of somites[34,35,40]. In zebrafish, the *her* genes *her1* and *her7* are both necessary for proper segmentation[5-7,24]. *her1* is necessary for formation of anterior somite boundaries, while *her7* is necessary for formation of more posterior somite boundaries[33]; deletion or depletion of both *her1* and *her7* disrupts segmentation along the entire axis[5,33]. Expression of *Hes/her* genes must be tightly regulated as deletion of only two introns in the mouse *Hes7* gene has shown to accelerate the segmentation clock enough to abolish oscillations and cause somite fusion[34]. Various *Hes/her* genes have been identified to oscillate, but *Hes7* in mice and

her1 and *her7* in zebrafish have been defined to be the core components of the segmentation clock.

1.6 Post-transcriptional regulation segmentation clock genes:

In order to sustain oscillatory expression of segmentation clock genes, mathematical modeling suggests both protein and transcript must be cleared rapidly [39,41]. While many studies have explored the activation and negative feedback inhibition on oscillatory transcription[32,36,39,42-44], post-transcriptional mechanisms that govern cyclic transcripts are still not well-understood. Studies that have focused on post-transcriptional regulation of segmentation clock genes have shown splicing[34,35], mRNA export[45], and translational delays[38] all attribute to limited gene expression in the PSM. Studies examining turnover of oscillating mRNAs have revealed the 3'UTR of cyclic transcripts account for some of the differences in half-life[37,46-48]. In chick embryos, the miRNA miR-125a-5p was shown to induce the destabilization of *LFNG* mRNA and inhibiting miR-125a-5p-mediated repression of *LFNG* arrests the oscillations of *LFNG* and leads to segmentation defects[49]. In zebrafish it was shown that removal of the *her1* or *her7* 3'UTR more than doubled the half-life of the mRNA in vivo[32], and our own work demonstrates the *her1* 3'UTR is sufficient to rapidly destabilize a reporter transcript[48], suggesting features in the 3'UTR of cyclic transcripts are important for rapid instability. Studies have illustrated the importance of post-transcriptional regulation of key segmentation genes for sustaining somitogenesis, but mechanisms that function to sustain oscillatory expression

through mRNA turnover are still not well-understood.

1.7 mRNA decay pathways

Over the past 25 years, discoveries on mechanisms of mRNA decay have highlighted the importance of transcript half-life in regulating gene expression. mRNAs largely exist to produce protein product and the amount of protein produced can in part be attributed by stability of the transcript. Most mRNA decay occurs by exonuclease activities from either the 5' or 3' end of the transcript (Figure 1.2A), but some mRNAs undergo endonucleolytic activity within their body followed by decay of both upstream and downstream cleavage products (Figure 1.2B). All mRNAs contain a 7-methyl guanosine cap (m^7G-cap) at their 5' termini that protects the transcript from 5' to 3' exonucleases[50]. With exception to histone mRNAs, the 3' termini of mRNAs also contain a stretch of adenylate residues, termed the poly(A) tail, that functions with Poly(A)-binding protein (PABP) to protect the transcript from 3' to 5' exonucleases[51]. The process of mRNA decay begins with shortening of the poly(A) tail on the 3' end of the transcript by a multisubunit deadenylating CCR4-NOT complex followed by the hydrolysis of the 5' cap by the mRNA-decaping enzyme DCP2 and the body of the RNA is degraded with either 5' to 3' polarity by the exoribonuclease 1 (XRN1) and/or 3' to 5' polarity by exosome-assoicated exonucleases RRP44 or EXOSC10 (Figure 1.2A)[52,53]. How long the mRNA maintains the poly(A) tail and the m^7G-cap can vary dramatically and regulating the removal of these features can affect the amount of protein product generated. Sequence elements within

the transcript and trans-acting factors that trigger removal of the m^7G-cap and poly(A) tail and the downstream decay of the mRNA have remained a large interest of RNA biology and new factors and features involved in mRNA turnover are continuously being discovered.

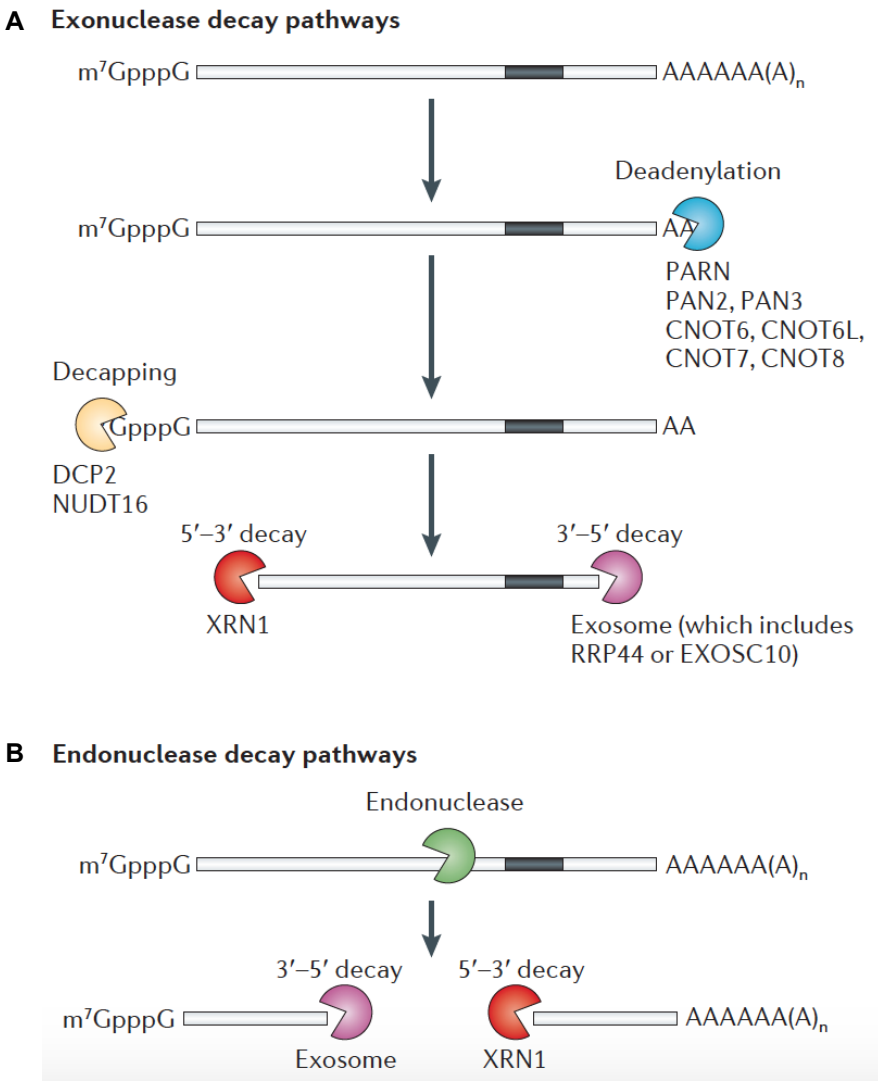

Figure 1.2. Major pathways of mRNA turnover.
(**A**) Exonuclease-mediated decay pathway. This process begins with deadenylation of the poly(A) tail through the complex of PAB-specific ribonucleases PAN2 and PAN3 and the CCR4-NOT transcription complex or by the deadenylase poly(A) ribonuclease PARN. Next the mRNA-decapping enzyme Dcp2 hydrolyses the m^7G-cap and 5' to 3' decay occurs through 5' to 3' exonuclease XRN1 and/or 3' to 5' decay occurs through the Exosome. (**B**) Endonuclease-mediated decay pathway. Some mRNAs undergo endonuclease cleavage within their body resulting in upstream and downstream cleavage products. Decay of these cleavage products is similar to the exonucleolytic decay process with 5' to 3' decay of downstream products occurring by XRN1 and 3' to 5' decay of upstream products by the Exosome. (Modified from Schoenberg and Maquat, 2012. This figure was approved for use by Springer Nature.)

1.8 Mechanisms that regulate mRNA turnover

The steady-state concentration of mRNA is determined by both the rates of synthesis and decay. Many mechanisms exist that regulate the turnover of nascent or aberrant mRNAs to avoid overexpression of potentially toxic proteins or to change abundance of functional proteins because of cellular conditions. Examples of these mechanisms are Nonsense-mediated mRNA decay (NMD), STAU1-mediated mRNA decay (SMD), ARE-mediated mRNA decay, PUM-mediated repression (PMR), and microRNA-mediated turnover.

Nonsense-mediated mRNA decay is one of the most well-studied quality control mechanisms in the cell and is coupled to the process of translation. This mechanism functions to prevent expression of defective transcripts that are routinely generated during gene expression and post-transcriptional events[54]. After the splicing of exons occurs, the exon-junction complex (EJC) is deposited ~20-24 nucleotides[55] upstream of the exon-exon junction. A termination codon sensed ~50-55 nts upstream of an EJC is defined as a premature termination codon and triggers NMD. The EJC serves many purposes but a major role is to function in determination of a premature termination codon[56]. In short, up-frameshift 1 (UPF1), a key nonsense-mediated mRNA decay factor, functions with suppressor of morphogenetic effect on genitalia 1 (SMG1), eukaryotic release factor 1 (eRF1), and eRF3 to form the SURF complex at the premature termination codon[57]. A SMG1-UPF1 complex then associates with a downstream EJC, resulting in phosphorylation of UPF1 and subsequent translational

repression and recruitment of mRNA decay factors[58]. Studies have shown knockdown of UPF1 causes upregulation of ~5% of properly functioning transcripts in HeLa cells suggesting NMD may also function in non-aberrant transcript decay in addition to quality control[59].

STAU1-mediated mRNA decay (SMD) is another mechanism regulating mRNA turnover that targets transcripts carrying a STAU1-binding site (SBS) in the 3'UTR. Unlike traditional NMD targets, these transcripts are functional and typically use the normal termination codon. However, factors involved in SMD overlap with NMD as SBS bound Staufen1 (STAU1) has been shown to recruit UPF1 to the 3'UTR and elicit presumably very similar downstream decay[60]. A large difference between SMD and NMD is that SMD targets are not only newly synthesized mRNAs but also older mRNAs[61], and that SMD is independent of EJC function. Targets of SMD vary but the mechanism has been implicated in myogenesis and adipogenesis through influencing stability of mRNAs involved in those pathways[62,63].

ARE-meditated mRNA decay is another mechanism of regulation that functions through elements in the 3'UTR of the mRNA. An AU-rich element (ARE) is defined as an AU-rich sequence within the 3'UTR and the canonical motif generally contains one or more copies of the 5' AUUUA pentamer and is surrounded in a U rich context. If classifying on sequence alone, ~9% of total mRNAs contain canonical AREs[64]. Decay of ARE-containing transcripts is similar to the downstream decay of other pathways beginning with shortening of the

poly(A) tail and subsequence steps to decay the mRNA 5' to 3' and 3' to 5' (Figure 1.2)[65]. ARE-binding proteins (ARE-BP) not only effect instability but can also function to stabilize the transcript and ARE-BPs are classified by this effect. Well-studied examples of destabilizing ARE-BPs are ARE/poly(U)-binding/degradation factor 1 (AUF1), tristetrapolin (TTP), butyrate response factor 1 (BRF1), BRF2, and KH-type splicing regulatory protein (KSRP)[66-68]. These factors function to recruit one or more of the degradative enzymes outlined in Figure 1.2[66]. The ARE-BP HuR is a well-characterized stabilizer of ARE-containing mRNAs and counteracts the destabilizing effect of AUF1, BRF1, BRF2, and KSRP[69]. AREs function in mRNAs that encode proto-oncogene proteins and inflammatory mediators and have important physiological and pathological functions that are not all linked to mRNA turnover[67,70-73].

PUM-mediated repression (PMR) is another form of mRNA regulation that functions through recognition of one or more Pumilio Response Elements (PREs) within the 3'UTR of the transcript. Pumilio proteins PUM1 and PUM2 have been shown to interact with PREs in 3'UTRs of mRNAs and reduce levels of mRNA and the encoded protein through translational repression[74-76]. The PRE consensus sequence is 5' UGUAHAUA, and the binding of Pumilio proteins to the PRE is well conserved from *Drosophila* to humans[77]. Transcriptome-wide analyses found that the PRE is among the features most strongly correlated with mRNA instability[78-80], and massive parallel reporter assays showed PREs destabilize mRNAs during vertebrate embryogenesis[81]. PMR causes

destabilization of the mRNA by recruitment the CCR4-NOT complex leading to deadenylation of the poly(A) tail and subsequent decay of the transcript[82,83]. In invertebrate systems, PMR has also been shown to cause decay of the transcript through promoting decapping[84]. Studies have revealed the importance of Pumilio proteins and PMR in the regulation of a wide array of biological events ranging from stem cell biology, growth, development, infertility, neurological disorders, and even cancer[77].

MicroRNA-mediated repression is yet another mechanism that functions to affect mRNA translation and stability through 3'UTR interactions. MicroRNAs (miRNAs) are endogenous ~22 nt long RNAs that bind to partially complementary sequences of the target mRNA and silence them by inducing mRNA degradation or inhibiting translation[85]. To date, over 2000 miRNAs have been identified in the human genome[86], and they control a broad array of biological processes from development, differentiation, proliferation and stress response[87-91]. The miRNA process of silencing begins with formation of the RNA-induced silencing complex (RISC) on the target mRNA consisting of at least a small RNA and Argonaute protein[92]. In mammals, the RISC complex will elicit mRNA decay through recruitment of deadenylases such as the CCR4-NOT complex causing deadenylation of target mRNA and decay through the downstream 5' to 3' exonucleolytic pathways (Figure 1.2)[93,94]. RISCs have also been shown to recruit decapping factors to the target mRNA to enhance degradation through removal of the m^7G-cap[95]. Although it is still unclear how

miRNAs repress translation, studies have shown that translational repression occurs at the initiation step prior and prior to mRNA decay in systems such as zebrafish[96]. New miRNAs are continually being discovered and their role in development and homeostasis through mRNA suppression is a large focus of the RNA community.

Research on mRNA turnover has shown that 3'UTRs are significant components for transcript stability and contain features such as miRNA-binding sites, AREs, and PREs that regulate decay of the transcript[81,97,98]. However, other "destabilizing" 3'UTRs contain no currently defined decay element[99], emphasizing our need to better understand cis features and trans-acting factors that regulate mRNA turnover.

1.9 Molecular identification of *tortuga*

To identify regulatory genes of the segmentation clock, our lab conducted an ENU mutagenesis screen examining expression of key segmentation genes during mid-segmentation. A segmentation clock mutant, *tortuga*, was identified where *her1* transcripts persist in regions of the PSM that are otherwise cleared during specific stages of the oscillation pattern[100]. In these mutants, expression of other cyclic genes such as *her7* and the Notch pathway gene *deltaC* (*dlc)*, and the segmentation clock-associated gene *deltaD* (dld) are also affected. Surprisingly, despite accumulation of cyclic transcripts, *her1* is still cyclically transcribed in *tortuga* mutants[100]. *tortuga* mutants form about three less somites than wildtype embryos (unpublished data) and somite boundaries appear

relatively normal (Figure 1.3)[100]. The *tortuga* mutation maps to a 1.47 Mb deletion on chromosome 16. A variety of experiments, including rescue experiments, identified Proline-rich nuclear receptor co-activator 2 protein (Pnrc2) as the gene responsible for cyclic transcript accumulation in *tortuga* mutants[48]. I conducted CRISPR/Cas9 mutagenesis frameshifting the *pnrc2* locus and in *pnrc2*^{oz22} mutants, *her1*, *her7*, *dlc*, and *dld* are misexpressed like in *tortuga* mutants[48]. *pnrc2*^{oz22} mutants do not display head necrosis or develop less total somites than WT siblings attributing those phenotypes to other genes in the *tortuga* deletion. Survivorship of *pnrc2*^{oz22} mutants to adulthood is rare, and the *pnrc2*^{oz22} mutants that reach adulthood appear lean much like mouse *pnrc2* mutants[101]. *pnrc2* mRNA is maternally provided and zygotically expressed throughout early development and we have shown that maternally provided Pnrc2 also functions in turnover of cyclic transcripts during somitogenesis (Chapter 3).

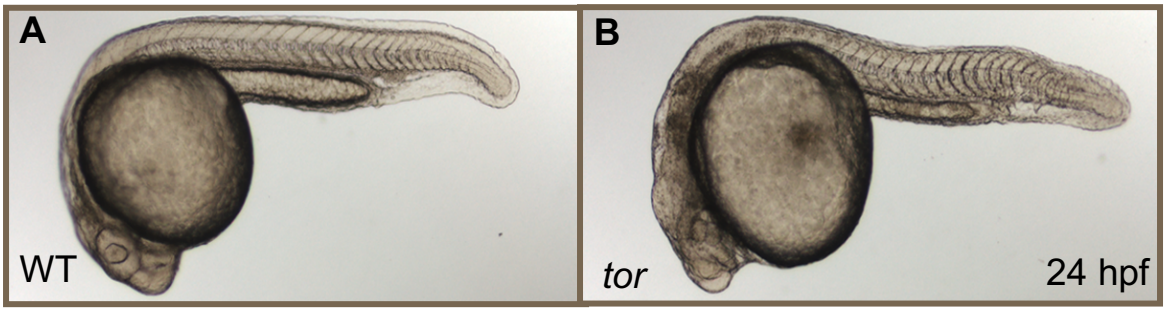

Figure 1.3. Visible phenotype of the *tortuga* mutant.
Brightfield images of **(A)** WT siblings and **(B)** *tortuga* mutants 24 hours post-fertilization (hpf). *tortuga* mutants display head necrosis and form roughly 3 less somites than WT siblings. Interestingly, somite boundaries are relatively normal in *tortuga* mutants. (Images from Thomas L. Gallagher)

1.10 Pnrc2 in development and mRNA turnover

The *pnrc2* gene encodes a 148 amino acid protein in zebrafish with two highly conserved domains across various vertebrate species, a SRC-Homology 3 (SH3) domain and a Nuclear Receptor (NR-box) domain[48]. Our lab was the first to characterize function of Pnrc2 in zebrafish, and research on mouse and human PNRC2 has implicated two roles for the protein; nuclear receptor co-activation and mRNA decay[102,103]. The earliest research on human and mouse PNRC2 determined an interaction with Estrogen Receptor α (ERα)[104], and knockout suggests a role in energy expenditure and adiposity[101]. More recent studies using human cell culture have shown PNRC2 interacts with UPF1 through the NR-box domain, mRNA-decapping enzyme 1A (DCP1A) through the SH3-domain, and copurifies with STAU1, suggesting a role in SMD and NMD[62,103,105]. Data from our lab supports a genetic interaction of Upf1 and Pnrc2 as sub-optimal depletion of both gene-products increases *her1* transcript accumulation[48]. Our lab performed RNA-seq analysis on Pnrc2 KD early-segmentation embryos and Upf1 KD early-segmentation embryos found more than 200-shared transcripts become up-regulated after knockdown of Upf1 and Pnrc2 (Figure 1.4), some of which are characterized as cyclic mRNAs[106]. This data highlights that Pnrc2 and Upf1 may function together to regulate non-aberrant cyclic transcripts during somitogenesis.

A recent study supports interaction of PNRC2 and UPF1 but questions whether PNRC2 functions in NMD as turnover of PTC containing reporter transcripts appear unaffected by Pnrc2 KD[107]. This inconsistency in the field illustrates a need to better understand how Pnrc2 functions to regulate turnover of natural, non-reporter targets. In collaboration with othrers, I have identified endogenous targets of Pnrc2 during early development (Chapter 2) and the mechanisms by which Pnrc2 regulates these targets (Chapter 3).

A

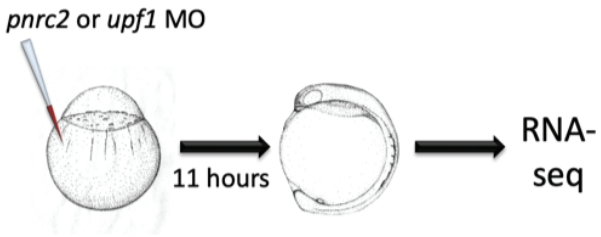

B RNA-seq results: > 800 transcripts upregulated including cyclic mRNAs

pnrc2 MO	821 up-regulated	Zebrafish cyclic genes: ***her1***, ***tbx16***, ***rhov***, *hs6st2, maf1*, *snrpd3l*, *sp4* Homologs of mouse and/or chick cyclic genes: ***shisa2***, ***dact1***
pnrc2 MO & *upf1* MO	220 up-regulated common to both	Homologs of mouse and/or chick cyclic genes: ***lfng***, ***mycb,*** *snai1a, sp5l*

Figure 1.4. RNA-seq results of Upf1 and Pnrc2 KD during early segmentation.
A) Diagram of the *pnrc2* or *upf1* KD experiment. 30 embryos were injected at the 1-cell stage with 6 ng *pnrc2* morpholino or 2 ng *upf1* morpholino and raised to 11hpf then processed in biological triplicates for RNA-seq analysis.
B) Results from RNA-seq analysis. KD of *pnrc2* caused up-regulation of over 800 transcripts including many cyclic transcripts such as *her1*, *tbx16*, *rhov*, *shisa2*, and *dact1* (bolded). Upregulation of over 200 transcripts are shared between *pnrc2* KD and *upf1* KD including cyclic genes such as *lfng* and *mycb*, suggesting Pnrc2 and Upf1 may function together in regulating these transcripts. Cyclic transcripts were previously defined[106].

Chapter 2: Pnrc2 regulates 3'UTR-mediated decay of segmentation clock-associated transcripts during zebrafish segmentation

This chapter contains published work. The publication reference is:

*Gallagher, T. L., *Tietz, K. T., Morrow, Z. T., McCammon, J. M., Goldrich, M. L., Derr, N. L., & Amacher, S. L. (2017). Pnrc2 regulates 3'UTR-mediated decay of segmentation clock-associated transcripts during zebrafish segmentation. *Developmental biology*, *429*(1), 225-239.

*Authors contributed equally to this work.

Contributions from authors other than myself will be denoted in the figure legends.

2.1 Abstract

Vertebrate segmentation is controlled by the segmentation clock, a molecular oscillator that regulates gene expression and cycles rapidly. Expression of many genes oscillate during segmentation, including *hairy/Enhancer of split-related* (*her* or *Hes*) genes, which encode transcriptional repressors that auto-inhibit their own expression, and *deltaC* (*dlc*), which encodes a Notch ligand. We previously identified the *tortuga (tor)* locus in a zebrafish forward genetic screen for genes involved in cyclic transcript regulation

and showed that cyclic transcripts accumulate post-splicing in *tor* mutants. Here we show that cyclic mRNA accumulation in *tor* mutants is due to loss of *pnrc2*, which encodes a proline-rich nuclear receptor co-activator implicated in mRNA decay. Using an inducible *in vivo* reporter system to analyze transcript stability, we find that the *her1* 3'UTR confers Pnrc2-dependent instability to a heterologous transcript. *her1* mRNA decay is Dicer-independent and likely employs a Pnrc2-Upf1-containing mRNA decay complex. Surprisingly, despite accumulation of cyclic transcripts in *pnrc2*-deficient embryos, we find that cyclic protein is expressed normally. Overall, we show that Pnrc2 promotes 3'UTR-mediated decay of developmentally-regulated segmentation clock transcripts and we uncover an additional post-transcriptional regulatory layer that ensures oscillatory protein expression in the absence of cyclic mRNA decay.

2.2 Introduction

Ultradian oscillatory circuits, with periods of minutes or hours, are pervasive in biological systems[108-110]. Oscillatory expression encodes an enormous amount of potential information; for example, there can be critical information in the number, amplitude, duration, or frequency of oscillations, as well as signal integration among multiple oscillators that collectively determine cellular response. A well-studied example of biological oscillation is the segmentation clock, a rapid molecular oscillator that generates periodic expression in developing embryos[3,22,111]. The segmentation clock controls vertebrate somitogenesis, the process by which the mesoderm is sequentially

divided into segmental units called somites that later give rise to vertebrae and ribs, body musculature, and dermis. Molecular oscillations during vertebrate segmentation were first described for *c-hairy1,* a chick homolog of the *Drosophila* pair rule gene *hairy.* In chick embryos, *c-hairy1* expression cycles in the presomitic mesoderm (PSM) and the period of each cycle corresponds with segment formation[21]. Since its discovery, *c-hairy1* orthologs have been identified in many vertebrate species. Mouse orthologs *Hes1* and *Hes7* and zebrafish orthologs *her1* and *her7* cycle dynamically in the PSM (2 hours in mouse and 30 minutes in zebrafish) and are required for proper segmentation[5,7,23,24,33,36,43,112,113]. In zebrafish, overexpression of *her* mRNA is associated with severe segmentation defects[32,113], and more recent work has confirmed that oscillatory expression is important for somite formation[114].

Several studies have explored activation and negative feedback inhibition of oscillatory transcription[32,36,39,42-44]. More recently, studies have also investigated post-transcriptional mechanisms regulating transcript processing and clearance[47,115-117]. Notable are studies that indicate splicing is a critical parameter[34,35], mRNA export is a rate-limiting step[45], translational delays contribute to traveling waves of expression[38], oscillatory protein turnover is required for transcriptional and post-transcriptional clock function[40], cyclic transcript 3'UTRs can promote decay[32,116,118], and miRNAs regulate decay of some cyclic transcripts[49,119-121]. Rapid clearance of cyclic transcripts likely occurs using mRNA decay machinery that promotes deadenylation, 5' cap removal,

and/or exonucleolytic cleavage of natural, non-aberrant transcripts[122-126], though how cyclic transcripts are efficiently targeted and cleared remains largely unknown.

In a forward genetic screen, we discovered a zebrafish mutant, *tortuga* (*tor*), with post-transcriptional accumulation of clock-associated transcripts, such as *her1*, *her7*, *deltaC* (*dlc*), and *deltaD* (*dld*)[100]. For simplicity, we refer collectively to clock-associated transcripts as cyclic through the body of this work, although *deltaD* (*dld*) expression does not oscillate[24]. Normally, cyclic expression appears as dynamic stripes of expression in the anterior PSM due to rapid oscillatory transcription followed by rapid mRNA decay; in *tortuga* mutants, the accumulation of cyclic transcripts obscures the striped expression pattern even though cyclic transcription appears normal[100]. Although many genes are deleted in the *tortuga* deficiency allele, we hypothesized that loss of *pnrc2* specifically leads to accumulation of segmentation clock transcripts in *tortuga* mutants. PNRC2 was first identified in a yeast two-hybrid screen of a human mammary gland cDNA library using mouse steroidogenic factor 1 (SF1) as bait[102] and subsequently shown to interact with several classes of steroid hormone receptors *in vitro*[55,102,104]. More recently, Pnrc2 has been described as an adapter protein of mRNA decay machinery that promotes decay of reporter mRNA containing a premature termination codon (PTC)[62,103,105,127-130]. We show here that Pnrc2 is required for rapid turnover of cyclic transcripts during vertebrate segmentation. We demonstrate that the *her1* 3'UTR confers Pnrc2-dependent instability,

extending previous work in cultured cells that shows that Pnrc2 affects mRNA stability of synthetic PTC-containing reporters via NMD[103,105]. We find that Pnrc2-mediated decay of *her1* transcripts does not require Dicer-dependent miRNAs and likely occurs via interaction with the mRNA decay factor Upf1. Our work identifies novel targets regulated by Pnrc2 in a developmental context and implicates the existence of an additional post-transcriptional regulatory mechanism that ensures proper oscillatory protein expression.

2.3 Materials and Methods

2.3.1 Animal stocks and husbandry

Adult zebrafish strains (*Danio rerio*) were kept at 28.5°C on a 14 hour (h) light/10h dark cycle and obtained by natural spawning or *in vitro* fertilization, and were staged according to Kimmel et al (1995). The *tortuga* (*tor*) mutant allele, *b644*, was isolated in a screen designed to identify mutations that disrupt segmental gene expression[100]. The segmentation clock reporter line, *Tg(her1:her1-Venus)*^{bk15}, was generated previously to visualize cyclic gene expression[118,131]. The stable *hsp70l:Venus-her1* 3'UTR reporter line and the *pnrc2*^{oz22} allele, described below, were generated in this study. Animal experiments were performed in accordance with institutional and national guidelines and regulations and were approved by the UC Berkeley and Ohio State University Animal Care and Use Committees.

2.3.2 Recombination mapping

Initial recombination mapping of the *tor*^{b644} deletion allele was performed using bulk segregant analysis[132] to identify polymorphic CA-repeat microsatellite markers showing biased representation in pooled genomic DNA from haploid progeny derived from an F1 AB/SJD hybrid female carrying the *tor*^{b644} allele. Recombination frequency for linked markers was calculated by analyzing marker segregation among many mutant and wildtype F1 hybrid individuals. The extent of the *tor*^{b644} deletion was defined as described in Results. Mapping marker locations and sequences are available at the Zebrafish Model Organism Database (ZFIN), University of Oregon, Eugene, OR 97403-5274; URL: http://zfin.org/.

2.3.3 BAC injection

A total of 4 BACs spanning the *tortuga*^{b644} deletion were injected at doses of 0.4–30 pg directly into 1-cell stage embryos from a cross between heterozygous *tor*^{b644} carriers. At 18 hpf, embryos in each BAC-injected clutch were sorted for neural degeneration (a visible *tor* phenotype), and then fixed in 4% PFA for 5 hours at room temperature, processed for *her1* in situ hybridization, scored for *her1* expression phenotype, and PCR genotyped. Only BAC AL844887 restored normal *her1* expression in *tor*^{b644} mutants (Figure 2.1A). BAC map position and sequence (CR848819, CR936374, AL844887, and BX649265) are available at http://zfin.org.

2.3.4 CRISPR/Cas9 mutagenesis

An optimal target site, 5'-GGGCACCCCTAAGGCTCCTG-3', in the 5' coding sequence of *pnrc2* was identified using the ZiFit Targeter software package[133,134]. *pnrc2*-targeting gRNA (5'- CAGGAGCCTTAGGGGTGCCC-3') and *Cas9* mRNA[135] were synthesized and co-injected into 1-cell stage embryos (135 ng and 200 ng, respectively) as described[136]. At 24 hpf, a subset of injected embryos were individually screened by high-resolution melting analysis (HRMA) to assess target site mutation efficiency in somatic cells. Remaining embryos were raised and crossed to AB wild-type adults; F1 adults were screened for germline transmission of CRISPR-induced mutations using HRMA. HRMA revealed two unique *pnrc2* mutant alleles transmitted by an individual F0 founder at a transmission rate of ~13% (2 of 15 F1 individuals). We recovered one allele, *pnrc2*^{oz22}, and outcrossed *pnrc2*^{oz22} heterozygotes to the AB wild-type strain for two generations before intercrossing for phenotypic analyses.

2.3.5 DNA extraction and *pnrc2*^{oz22} genotyping strategy

Individual embryos and adult fin tissue were lysed in 50 ul 1X ThermoPol Buffer (NEB) at 95°C for 10 minutes, digested at 55°C for 1-4 hours using 25-50 ug Proteinase K (BP1700, ThermoFisher), followed by Proteinase K inactivation at 95°C for 10 minutes. 1 ul of DNA extract was used as template in a standard 25 ul reaction with Taq polymerase according to manufacturer's protocol (NEB). To molecularly identify *pnrc2*^{oz22} carriers after PCR amplification, samples were digested with 20 units NsiI-HF (NEB) to distinguish cleavable wild-type from un-

cleavable mutant amplicons. Reaction products were analyzed on a 2% agarose gel stained with Gel Red (Biotium).

2.3.6 Morpholino injection

The *pnrc2* splice-blocking morpholino (sbMO) sequence is: 5′-ACTGGATGTCACCctagcagaagaca-3′ (uppercase, sequence complementary to exon 3; lower case, sequence complementary to intron 2) (Gene Tools, LLC). The *upf1* sbMO, 5'-TTTTGGGAGTTTATACCTGGTTGTC-3', was published previously[137]. The *rbfox1l* sbMO, 5'-GCATTTGTTTTACCCCAAACATCTG-3', and *rbfox2* sbMO, 5'-TATAATGCTTTATATACCCCGAACA-3', was published previously[138,139]. Morpholinos were diluted to 0.1–2 ng/nl in 0.2M KCl and 0.1% phenol red and injected into the yolk of 1-cell stage embryos. *pnrc2* sbMO dose was optimized by determining the highest dose that gave reproducible and rescuable phenotypic defects with no toxicity. *upf1*, *rbfox1l*, and *rbfox2* sbMO doses were performed according to published methods using doses that gave reproducible phenotypic defects matching published results[137-139]. Embryos were incubated at 28.5°C until 6 hours post fertilization (hpf) and then transferred to 25°C thereafter, except for a subset of *rbfox1l/rbfox2* double-injected and uninjected control embryos that were incubated at 28.5°C until 24 hpf and subsequently scored for ability to move.

2.3.7 mRNA injection

Full-length *pnrc2* cDNA was amplified by RT-PCR and subcloned into expression vector pCS2+ [140,141] to generate plasmid *SP6-pnrc2-cDNA* (TLG109).

For rescue experiments, *pnrc2* mRNA was synthesized using the SP6 mMessage Machine Kit (Life Technologies), diluted in 0.2M KCl with 0.1% phenol red, and injected into 1-cell stage embryos (150–600 pg mRNA per embryo).

2.3.8 In situ hybridization

Whole mount in situ hybridization was performed as previously described[142,143] using DIG-labeled antisense probes. The full-length *pnrc2* cDNA was amplified by RT-PCR and subcloned into pBSKS+ (Stratagene), linearized with BamHI, and transcribed using T7 RNA polymerase to make DIG-labeled antisense *pnrc2* riboprobe (Roche Life Science). The same construct was linearized with XhoI and transcribed using T3 RNA polymerase to make DIG-labeled sense *pnrc2* riboprobe. Riboprobes for *her1, her7, dlc, dld*, and *Venus* were made as previously described[100,118]. In situ hybridization chain reaction (HCR-ISH) was performed using a combination of five anti-sense 50-nt probes spanning the *her1* transcript according to published procedures[144,145] and a zebrafish-specific protocol provided by Molecular Instruments. Probe targeting sequences (5' to 3') were:

1) GGGTTTTGAAGTCGCGAATCTAAAGTATTATCCAGAAGAAGCGTTCGCAG,

2) CGCCTTGATCTCTCGCAGTCGCGGTTTTAGTCCTAATATACTCAACAGCC,

3) GAGAATGGAGGAGAGCTGCTTGAAAAGCCTGGAGACGGCGGAGGAGAAAT,

4) TCACCTGAAGATGAGGTCCTGGGACGACCGGTAATGAAGTCGTTGAGAGA, and

5) TCGTCTCAGAGTCCGTGGTTGAGAGGATTGAACAGAGCCACTAAACCGCA.

2.3.9 RNA analysis

Whole embryos (n=20 per time point or condition) were solubilized in Trizol for RNA extraction (Life Technologies). 1 ug total RNA was purified and reverse transcribed into cDNA with random primers and Superscript III reverse transcriptase (RT) according to the manufacturer's instructions (Life Technologies). Expression analysis of *pnrc2* using primer pairs spanning constitutive exons 2 and 3 were used for RT-PCR-based detection of *pnrc2* transcript (Figure 2.4G, Figure 2.8K). Splicing of *pnrc2* using primer pairs spanning within and across each of three constitutive exons of the 3146 nt *pnrc2* mRNA were used for RT-PCR-based detection of spliced and unspliced *pnrc2* transcript (Figure 2.8K-L).

2.3.10 Plasmid construction and Transgenesis

The heat-shock reporter *hsp70l:Venus-her1* 3'UTR was assembled by PCR amplification and restriction digestion of the *hsp70l* promoter from Tol2kit construct #222 (entry plasmid *p5E-hsp70l)*[146], in parallel with restriction digestion of the *Venus-her1* 3'UTR sequence from the *her1:her1-Venus* plasmid[118], followed by ligation of both fragments into a modified version of pBSKS+ plasmid containing flanking I-SceI meganuclease recognition sites[147]. The *Venus-her1* 3'UTR fragment isolated from plasmid *her1:her1-Venus* contains the *Venus* coding sequence followed by 1.1 kb of *her1* 3' noncoding sequence that includes the annotated 724-nt *her1* 3'UTR and native *her1* pA signal sequence[118].

Constructs were sequence confirmed. Transgenic lines were generated as previously described using I-SceI-based transgenesis[147].

2.3.11 Stably transgenic heatshock assay

Adult fish carrying the stable *hsp70l:Venus-her1* 3'UTR transgene that transmits as a single Mendelian locus were crossed to AB wild-type fish and resulting progeny were either injected at the 1-cell stage with 6 ng splice-blocking *pnrc2* morpholino (sbMO) or were set aside as uninjected control siblings. Progeny were raised to mid-segmentation, heat-shocked at 37°C for 15 minutes, and fixed in 4% PFA at 0, 20, and 30 minutes post-heat-shock and processed for *Venus* in situ hybridization.

2.3.12 Immunohistochemistry

All embryos described below were immunostained following standard protocols using 4% PFA fixation, dehydration and rehydration in a methanol series, and incubation in blocking solution for 1 hour. Tg(*her1:her1-Venus*)^{bk15} embryos were immunostained in 2% BSA/2% goat serum/1% DMSO/0.1% Tween-20/PBS blocking solution with 1:1000 dilution chicken anti-GFP that recognizes Venus protein (A10262, Life Technologies), and 1:400 dilution goat anti-chicken Alexa-Fluor-488 (A11039, ThermoFisher). Mid-segmentation embryos from wild-type and *pnrc2*^{oz22} crosses were immunostained in 2% BSA/5% goat serum/0.1% Tween-20/PBS blocking solution with 1:200 dilution anti-zdc2 that recognizes DeltaC protein (ab73336, Abcam) according to previously published methods[32] or immunostained in 2% BSA/10% goat

serum/0.5% Triton X-100/PBS blocking solution with 1:100 anti-zdd2 that recognizes Dld protein according to previously published methods[148] (ab73331, Abcam), followed by 1:800 dilution goat anti-mouse Alexa-Fluor-488 (A11001, ThermoFisher). Nuclear counter-staining was performed by transferring and mounting dissected in situ-hybridized embryos from 80% glycerol into SlowFade Gold Antifade Mountant with DAPI (S36939, Thermo Fisher) and incubation at 4°C overnight prior to imaging.

2.3.13 Microscopy and Imaging

In situ hybridized embryos were mounted in Permount and imaged using an Axiocam HRc digital camera with AxioPlan2 microscope (Zeiss). Immunofluorescent embryos were dissected and flat mounted or whole mounted in 80% glycerol and imaged at 10x, 20x, and 60x magnification using MetaMorph software (Molecular Devices) on an Andor™ SpinningDisc Confocal Microscope (Oxford Instruments) with iXon Ultra EMCCD and Nikon Neo cameras; laser wavelength and intensity were set at 488 nm and 100% for Venus protein detection, 488 nm and 50% for Dlc protein detection, 488 nm and 100% for Dld protein detection, 561 nm and 30% for *her1* mRNA detection, 405 nm and 40% for DAPI detection, respectively, and bit depth at 16-bit. Maximum intensity projections using MetaMorph software are shown for Venus, Dlc, and Dld protein detection (Figure 2.7D-E, K-N). Single z-sections are shown for *her1* HCR-ISH and DAPI (Figure 2.7C-C', F-F'; Figure 2.13A-B'").

2.4 Results

2.4.1 *tortuga*^{b644} is a Chromosome 16 deficiency allele

The *tortuga*^{b644} allele is an ENU-induced deletion that leads to the post-transcriptional accumulation of segmentation clock transcripts[100]. Using genetic markers that distinguish wild-type AB and SJD mapping strains, we found that *b644* is a deficiency that maps to a 1.46 Mb region on Chromosome 16 spanning an interval of at least 20 known or predicted protein-coding RefSeq-annotated genes in genome assembly GRCz10/danRer10[149]. Haploid-based mapping revealed that the *tortuga* lesion lies 0.30 cM to the left and 0.37 cM to the right of the SSLP markers z13511 and z9511, respectively (Figure 2.1A). Using PCR-amplification of genomic regions (mostly in protein-coding genes) that lie between the two SSLP markers, we characterized the extent of the deletion in diploid embryos derived from heterozygous *b644* intercrosses by identifying genes that fail to amplify in *tortuga* homozygous mutant versus wild-type sibling embryos (Figure 2.1B). To better map deletion breakpoints, we analyzed presence or absence of amplicons near the presumptive ends of the *tortuga* deletion region of Chromosome 16. At the end near z13511, an intergenic region located ~124 kb upstream of *pou3f2b* failed to amplify, indicating the break lies in a ~206 kb interval between *mms22l* and the intergenic region (Figure 2.1B). Similar analysis at the other end indicates that the other breakpoint lies in the ~2.9 kb genomic interval between exon 1 and intron 3 of *snip1* (Figure 2.1B).

2.4.2 Injection of a BAC that includes *pnrc2* rescues the *her1* expression defect in *tortuga* mutants

To narrow the list of relevant candidate gene(s) in the *tortuga* deficiency, we injected four BACs spanning regions of the deletion interval between *pou3f2b* to *snip1* into zebrafish embryos at the 1-cell stage and assessed *her1* expression phenotype. Because *tortuga* mutants do not survive beyond larval stages, BACs were injected into embryos from a heterozygous intercross, from which ~25% are homozygous for the *tor* deletion. Injection of zebrafish BAC clone AL844887 spanning nine full-length open reading frames rescues the *her1* expression defect in *tor* mutants in a dose-dependent manner (Figure 2.1A, Figure 2.2A-D).

2.4.3 Loss of *pnrc2* is associated with accumulation of *her1* mRNA in *tortuga* mutants

To identify the gene or genes on BAC AL844887 that restore proper *her1* expression in *tortuga* mutants, we first analyzed candidate gene expression by RT-PCR before and during segmentation. Of nine candidates present on BAC AL844887, only seven are expressed at relevant time points (Figure 2.2E; data not shown for *me1*). Of these seven, only *pnrc2*, *rragca,* and to a lesser extent, *akirin1*, are detectably expressed from BAC AL844887 when injected into *tortuga*^{b644} mutants (Figure 2.2F). We injected antisense morpholinos (MOs) into 1-cell stage wild-type embryos to determine whether knockdown of any of the three candidates recapitulated the *tor*-like *her1* expression defect. Injection of translation-blocking MOs targeting *akirin1* and *rragca* does not cause overt

morphological or *her1* expression defects (Figure 2.2I-J), and injection of maximal non-toxic doses of *akirin1* or *rragca* mRNA into *tortuga* mutants does not rescue *her1* expression defects (data not shown). In contrast, injection of *pnrc2* splice-blocking MOs (sbMOs), that effectively disrupt proper *pnrc2* splicing (Figure 2.2K-L), disrupts *her1* expression just as in *tortuga*^{b644} mutants (Figure 2.1C-D). Injection of a second *pnrc2*-targeting translation-blocking MO gave the same phenotype (Figure 2.1H; see Methods). Importantly, co-injection of MO-resistant *pnrc2* mRNA with *pnrc2* sbMO restores normal *her1* expression (Figure 2.1C-E; Table 2.1).

2.4.4 Pnrc2 restores proper *her1* expression in *tortuga* mutants

To determine whether Pnrc2 can also restore normal *her1* expression in *tortuga* mutants, we injected *pnrc2* mRNA into embryos from a *tor*^{b644} heterozygote intercross. To discriminate “rescued” *tor* mutants and wild-type siblings among injected intercross progeny, we developed a visual assay to unambiguously identify fish homozygous for the *tor* deletion. The *pou3f1* gene lies within the *tortuga* deletion (Figure 2.1A) and thus is not expressed in *tor*^{b644} mutant embryos, whereas in wild-type siblings, *pou3f1* mRNA is expressed anteriorly in a pattern easily distinguished from that of *her1* mRNA expression. By co-hybridizing *pou3f1* and *her1* antisense probes, *tor*^{b644} mutants are readily identified and assessed for rescue of *her1* expression. Using this assay, we find that *pnrc2* mRNA-injected *tortuga* mutants exhibit wild-type *her1* expression

(Figure 2.3A-D'; Table 2.2), indicating that Pnrc2 can restore proper *her1* expression in *tor* mutants.

2.4.5 Targeted mutation of *pnrc2* recapitulates the cyclic transcript accumulation phenotype of *tor*^{b644} mutants

Because the *tor*^{b644} allele is a multi-gene deficiency, we used CRISPR/Cas9 mutagenesis[136,150,151] to generate a nonsense *pnrc2* allele. We isolated a 17 bp deletion allele, *pnrc2*^{oz22} that causes an early frame shift and likely results in a truncated Pnrc2 protein. Compared to wild-type Pnrc2 (148 amino acids), the predicted mutant protein determined from sequenced genomic DNA contains the N-terminal 35 amino acids followed by 11 aberrant residues (Figure 2.3E), terminating well before the two highly conserved SH3 and NR box regions (Figure 2.1F). To determine whether the *pnrc2*^{oz22} frame-shifting allele fails to complement the *tor*^{b644} deletion allele, we crossed *pnrc2*^{oz22} and *tor*^{b644} heterozygotes and found that all *pnrc2*^{oz22}/*tor*^{b644} trans-heterozygote progeny display the *tor*^{b644} *her1* expression defect (Figure 2.3F-G). As expected, homozygous *pnrc2*^{oz22} mutants phenocopy the *tor*^{b644} *her1* expression defect (Figure 2.3H-H'). Additionally, expression of segmentation clock-associated *her7*, *dlc*, and *dld* transcripts is also abnormal in *pnrc2*^{oz22} mutants (Figure 2.4) and in the cases of *her1* and *dlc*, arise due to post-transcriptional accumulation of mRNA (Figure 2.5), all consistent with previous observations in *tor*^{b644} mutants using intronic and exonic in situ probes that distinguish nascent from processed transcripts[100]. Unlike *tor*^{b644} mutants, *pnrc2*^{oz22} mutants and *pnrc2*^{oz22}/*tor*^{b644}

trans-heterozygotes do not have neural degeneration and somite shape defects, suggesting these *tor* mutant phenotypes are caused by loss of function of another gene or genes in the *tor* deletion interval. *pnrc2*$^{oz22/oz22}$ embryos appear morphologically normal and survive through 6 days post fertilization, but very few survive to adulthood (data not shown). Reduced survivorship of zebrafish *pnrc2*$^{oz22/oz22}$ mutants contrasts with Pnrc2-null mice that survive to adulthood and are indistinguishable from wild-type littermates up to 12 months of age[101].

2.4.6 *pnrc2* is broadly expressed during segmentation

To characterize embryonic *pnrc2* expression, we performed whole mount in situ hybridization and found that *pnrc2* is broadly expressed, with slight enrichment in somites and neural tissue during segmentation stages (Figure 2.6A-F). RT-PCR analysis of mRNA extracted from wild-type embryos confirms that *pnrc2* is expressed across similar stages examined by in situ (Figure 2.6G). Expression at the 8-cell stage (Figure 2.1A) and at the 1- and 2-cell stages (data not shown) suggests that *pnrc2* transcripts are maternally provided.

2.4.7 The *her1* 3'UTR confers instability to transcripts in a Pnrc2-dependent manner

In previous studies, heat-shock-induced reporter transcripts containing *her1* or *her7* coding and 3'UTR sequences decayed rapidly post-induction[32]. Because 3'UTR sequences can influence mRNA stability[52,123,126], we hypothesized that the *her1* 3'UTR alone might be sufficient to trigger Pnrc2-mediated decay. We therefore developed a stable transgenic heat-shock reporter

line to drive expression of a *Venus* transcript followed by the *her1* 3'UTR. We compared reporter expression after heat-shock of uninjected and *pnrc2* sbMO-injected *hsp70l:Venus-her1* 3'UTR transgenic siblings across multiple time points. Heat-shock-induced *Venus* transcripts are almost completely absent by 30 minutes post heat-shock (pHS) in the reporter line (Figure 2.7A-C). However, injection of *pnrc2* sbMO into *hsp70l:Venus-her1* 3'UTR embryos negates the destabilizing effect of the *her1* 3'UTR (Figure 2.7D-F; Table 2.3). These results support our hypothesis that Pnrc2-mediated decay of *her1* transcripts occurs through destabilizing features of the *her1* 3'UTR.

2.4.8 *her1* expression is unaffected in embryos lacking maternal and zygotic Dicer function

It is well established that microRNAs (miRNAs) play an essential role in post-transcriptional gene regulation in developing zebrafish embryos[96,152-156]. Using TargetScan Fish[157], we find that predicted miRNA target sites are present throughout the *her1* 3'UTR and other cyclic transcript 3'UTRs (data not shown). The 3'UTRs of *her1*, *her7*, *dlc*, and *dld* lack a common predicted target site, however some target sites are present in at least two of the four 3'UTRs analyzed. We therefore reasoned that miRNAs might influence the decay of *her1* and other transcripts. Using maternal-zygotic *dicer* (*MZdicer*) mutants that lack Dicer-dependent miRNA processing[153], we find that segmenting *MZdicer* mutants, despite having severe morphogenesis defects[153], have a normal striped

her1 expression pattern (n=11/11), demonstrating that proper *her1* expression is independent of Dicer-dependent miRNA function (Figure 2.7G-H).

2.4.9 Pnrc2 and Upf1 may genetically interact to promote *her1* transcript decay

Human PNRC2 binds directly to nonsense-mediated decay (NMD) factors, including UPF1, and these interactions are required for decay of reporter mRNA in cultured cells[103,105]. We therefore predicted that Pnrc2 and Upf1 might also interact to promote decay of non-aberrant, cyclic transcripts during segmentation. To determine whether Pnrc2 and Upf1 cooperatively regulate cyclic mRNA decay, we co-injected MOs targeting both transcripts and examined *her1* expression. As expected, injection of *pnrc2* sbMO at the optimal dose ("moderate", 6 ng) causes strong *her1* misexpression, but has no effect at a sub-optimal ("low") dose (2 ng) (Figure 2.8A-C). Strikingly, co-injection of a sub-optimal dose of *pnrc2* sbMO (2 ng) with a sub-optimal dose of *upf1* sbMO (0.25 ng) results in a *her1* expression defect markedly similar to that observed with optimal doses of *pnrc2* sbMO alone (6 ng) (Figure 2.8B-E, quantified in F). Interestingly, single *upf1* knockdown at published (0.65 ng) or higher doses (2 ng) does not alter *her1* mRNA expression, but does induce the expected published phenotypes including neural necrosis and abnormal segment formation (data not shown)[137,158]. As a control, we injected a sub-optimal dose of *pnrc2* sbMO (2 ng) with an unrelated MO, *rbfox1l* sbMO, at the published 6 ng dose[138,139], and observed that *her1* mRNA expression is normal (Figure 2.9),

suggesting that *her1* misexpression in embryos co-injected with sub-optimal dose *pnrc2* and *upf1* sbMOs is not due to non-specific MO effects. To confirm effective *rbfox1l* knockdown, we co-injected *rbfox1l* and *rbfox2* sbMOs (6 ng each) in parallel experiments because neither sbMO produces an overt morphological phenotype when injected alone. We observed the expected paralysis phenotype in all double-injected embryos (n=27/27 paralyzed embryos at 24 hpf)[138,139], confirming that we were using an effective *rbfoxl1* sbMO dose in our experiments (n=27/27 paralyzed embryos at 24 hpf). Taken together, these results reveal that depletion of Upf1 sensitizes embryos to partial loss of Pnrc2. Although depletion of Upf1 alone does not affect *her1* expression, it is possible that low levels of Upf1 protein persist in *upf1* morphants and may be sufficient for cyclic mRNA clearance in the presence of normal levels of Pnrc2.

2.4.10 Unlike mRNAs, cyclic proteins do not accumulate upon Pnrc2 depletion

Our data indicate that Pnrc2 triggers decay of reporter mRNAs and natural cyclic transcripts like *her1*. Previous work has shown that embryos injected with *her1* mRNA at the 1-cell stage have severe somite patterning and boundary defects, as well as decreased expression of Her1 transcriptional targets like *dlc* and *her7*[32,113]. The morphological phenotype of embryos constitutively overexpressing *her1* contrasts sharply with that of *pnrc2*^{oz22} mutant embryos, which have normal somite numbers and boundaries (Table 2.4 and data not shown) despite dramatic accumulation of endogenous *her1* and other cyclic

transcripts. We therefore hypothesized that accumulated *her1* transcripts in *pnrc2*^{oz22} mutants do not result in increased Her1 protein. Because a Her1 antibody is lacking, we tested this idea by depleting *pnrc2* function in a validated transgenic cyclic reporter line, *Tg(her1:her1-Venus)*^{bk15}, that infers *her1* transcript and Her1 protein dynamics via detection of *her1-Venus* reporter mRNA and protein[118,131]. As expected, *her1-Venus* transcripts are misexpressed in *pnrc2* morphants carrying the cyclic reporter transgene, mirroring what is observed for endogenous *her1* transcripts (Figure 2.10A-B). Her1-Venus reporter protein expression, however, is indistinguishable between uninjected and *pnrc2* sbMO-injected transgenic embryos (Figure 2.10D-E). Her1-Venus protein expression is similarly unaffected in transgenic reporter embryos injected with sub-optimal doses of *pnrc2* sbMO (2 ng) and *upf1* sbMO (0.25 ng) as well as transgenic reporter embryos co-injected with an optimal dose of *pnrc2* sbMO (6 ng) together with higher dose of *upf1* sbMO (2 ng) (Figure 2.11). Together, the observed misexpression of *her1-Venus* mRNA, but not Her1-Venus protein, is consistent with our hypothesis that *pnrc2* mutants segment normally because accumulated *her1* transcripts do not result in abnormal levels of Her1 protein.

Discordant transcript and protein expression in *pnrc2* mutants and morphants might be due to nuclear retention of accumulated mRNA, so we employed in situ hybridization chain reaction (HCR-ISH)[144,145] coupled with DAPI nuclear counter staining to assess sub-cellular localization of *her1* mRNA. As a control for probe set specificity, we first performed *her1* HCR-ISH on wild-type

and *Df(Chr05:her1,her7,ndrg3a)*^{b567} homozygote embryos that lack the linked *her1* and *her7* genes[33] and find that *b567* homozygotes lack detectable signal (Figure 2.12). We then performed HCR-ISH on both wild-type and *pnrc2* mutants and find substantial cytoplasmic localization of *her1* mRNA in both conditions, suggesting that accumulated transcripts in *pnrc2* mutants are not retained in the nucleus and are properly exported to the cytoplasm (Figure 2.10C-C', F-F'; Figure 2.13A-A", B-B"). Because relative intensity of *her1* HCR-ISH in *pnrc2* mutants to wild-type embryos is high, levels have been reduced in *pnrc2* mutant panels (Figure 2.10F-F'; Figure 2.13B-B"). Intensity maps of raw *her1* HCR-ISH signal reflect the extent of *her1* mRNA accumulation in *pnrc2*^{oz22} mutants (Figure 2.13A"', B"'). Overall, despite the increase in *her1* mRNA levels, accumulated transcripts in *pnrc2* mutants are exported from the nucleus, consistent with our hypothesis that Pnrc2 promotes decay of cyclic mRNA, a process that likely employs cytoplasmic decay machinery[122,126].

Having established that *her1-Venus* reporter mRNA, but not protein, is misexpressed in *pnrc2* morphants, we next asked whether discordant expression occurs for other cyclic transcripts and proteins. Siblings from a *pnrc2*^{oz22} heterozygote intercross were split and processed in parallel for mRNA and protein expression analysis. While *pnrc2*^{oz22} homozygous mutants were readily distinguished from unaffected siblings based on *dlc* and *dld* mRNA misexpression (Figure 2.10G-J), there were no discernible differences in Dlc and Dld protein expression among sibling embryos (Figure 2.10K-N). Overall, we

provide evidence that despite the accumulation of cyclic transcripts in *pnrc2*^{oz22} mutants, cyclic protein expression is unaffected, which may help explain the absence of obvious segmentation phenotypes.

2.5 Discussion

In this work, we present evidence that Pnrc2 promotes the decay of cyclic mRNAs and that the *her1* 3'UTR is sufficient to trigger Pnrc2-mediated decay. Our work builds upon previous studies of Pnrc2-regulated mRNA decay and reveals natural, developmentally-regulated transcripts that are targets of Pnrc2-mediated decay. Zebrafish Pnrc2 shares significant similarity with human PNRC2. Residues in human PNRC2 that are required for decay of reporter mRNA containing a premature termination codon (PTC) are conserved in zebrafish, and include K109 (K119 in zebrafish), W114 (W124 in zebrafish), and the C-terminal KTLLK nuclear receptor domain (NR box) (KSLLK in zebrafish) (Figure 2.1F)[103,105]. PNRC2 does not bind mRNA directly in human cultured cells, but instead functions via interactions with decay factors SMG6, DCP1A, UPF1, and STAU1 to regulate decay of PTC-containing reporter transcript[62,103,105,127-129]. Our work shows that in segmenting zebrafish embryos, *pnrc2* and *upf1* may also interact to promote decay of natural, developmentally-regulated transcripts. Future identification of factors that participate in the Pnrc2-mediated decay process will define this key aspect of oscillatory gene regulation and to what extent it employs existing, well-characterized RNA decay machinery.

Cyclic transcript accumulation is due to loss of Pnrc2 in *tortuga* and *pnrc2* mutants

Because the *tor*^{b644} allele is a multi-gene deficiency, we generated a nonsense *pnrc2* allele. As expected, *pnrc2*^{oz22} mutants show misexpression of cyclic transcripts including the cyclic transcripts *her1*, *her7*, and *dlc*, as well as *dld* (Figures 2.3 and 2.4), and in the cases of *her1* and *dlc*, accumulate post-transcriptionally (Figure 2.5), all consistent with previous observations in *tor*^{b644} mutants[100]. Because an early frame shift *pnrc2* mutation has the same impact on *her1* post-transcriptional regulation as complete deletion of the *pnrc*2 locus, it is unlikely that accumulation of *her1* transcripts is due to loss or mutation of miRNA- or lncRNA-encoding genes at or near the *pnrc2* locus, but is instead due to loss of Pnrc2 protein.

Pnrc2 translation may be developmentally regulated

pnrc2 transcripts are maternally provided and broadly expressed (Figure 2.6), however *pnrc2* may be subject to translational regulation. Using global ribosomal profiling experiments in developing zebrafish embryos, Giraldez and colleagues showed that the *pnrc2* transcript contains a conserved upstream open reading frame (uORF) that lies out of frame with the Pnrc2-coding ORF and is preferentially associated with translational machinery during early embryonic stages[159]. The presence of two ORFs, an uORF and the Pnrc2-coding ORF, suggests that Pnrc2 translation may be affected by translation at the uORF, as has been demonstrated in other organisms and contexts[160-166]. An uORF can

also act as an NMD-inducing feature[167,168], adding another layer of possible post-transcriptional regulation. It is also interesting that transcripts encoding several NMD factors, like UPF2 and SMG factors, themselves contain uORFs that confer post-transcriptional regulation via feedback control[169]. Future development of antibodies for detection of zebrafish Pnrc2 and other decay factors will help to advance our understanding of Pnrc2-mediated decay in a developmental context.

Expression patterns of cyclic proteins appear normal despite accumulated cyclic transcripts in *pnrc2*-deficient embryos

It is remarkable that the dramatic accumulation of Pnrc2-regulated cyclic transcripts like *her1* in *tor* and *pnrc2* mutant embryos does not confer phenotypes typically associated with excess Her1, like somite boundary defects and down-regulation of Her1 transcriptional targets including *dlc* and *her7*[32,113]. Similarly, accumulation of *dlc* transcripts in *tor* and *pnrc2* mutants does not confer somite boundary defects associated with excess Dlc protein[114]. We find that *pnrc2* mutants lack such phenotypes and hypothesize that this is due to normal cyclic protein expression despite mRNA accumulation. It remains unclear why accumulated *her1* transcripts in *prnc2* mutants fail to produce defects associated with excess Her1, particularly because previous *her1* overexpression experiments included the full-length *her1* 3'UTR[32,113] that we now show confers Pnrc2-dependent instability. Overall, because Her1-Venus reporter protein and endogenous Dlc and Dld proteins are expressed normally despite misexpression of mRNA in *pnrc2*-deficient embryos (Figure 2.10; Figure 2.11), we suggest that

Pnrc2-mediated mRNA decay acts in addition to a regulatory layer that controls oscillatory protein expression. Although the *her1* transcript does not contain obvious NMD-inducing features such as an uORF and accumulated *her1* transcripts in *pnrc2* mutants do not appear retained in nuclei (Figure 2.10F', Figure 2.13B''), there are other mechanisms that may function to repress or prevent translation[155,170-174]. Alternatively, normal cyclic protein expression in *pnrc2* mutants might occur because protein decay machinery compensates for increased cyclic expression. Treatment of cultured mouse cells with ubiquitin-proteasome inhibitors stabilizes Hes1 protein (closely related to zebrafish Her1)[43] and mathematical modeling predicts short half-lives for zebrafish Her1 and Her7 proteins[39]. More recently, it has been shown that translational fusion of Her1 to Venus reporter protein confers protein instability[118] and measurements of Her7 protein half-life reveal rapid turnover of Her7 protein within 3.5 minutes[41]. Future investigation into destabilizing features that trigger rapid protein decay might provide insight into the contribution of protein decay in maintaining oscillatory expression.

Potential cis-regulatory elements reside in the *her1* 3'UTR

Our data show that the *her1* 3'UTR is sufficient to trigger Pnrc2-dependent decay of reporter mRNA. It is well known that 3'UTR sequences can influence mRNA stability by length-dependent, sequence, and/or structural feature recognition[52,123,126]. We favor the latter two possibilities because the *her1* 3'UTR is of average length with respect to the post-gastrulation zebrafish

transcriptome[155,157,175], and analysis of the *her1* 3'UTR using the mfold Web Server [176] predicts a stable stem-loop structure (data not shown). Future biochemical methods of structure probing coupled with deletion reporter assays will help determine if mfold-predicted structures are functionally relevant.

mRNA decay pathways include AU-rich element (ARE)-mediated[177], Staufen1 (Stau1)-mediated[178], nonsense-mediated[126], and miRNA-mediated[96,152,154-156] decay. Normal *her1* expression in *MZdicer* mutants (Figure 2.7G-H) suggests that miRNA-mediated decay does not contribute to *her1* oscillatory expression despite the presence of numerous predicted miRNA 3'UTR sites (data not shown), although we have not ruled out the possibility that Dicer-independent miRNAs contribute to *her1* mRNA decay. Additional motif searches of the *her1* 3'UTR using AREsite2[179] yield four ARE core motif ATTTA sequences in addition to numerous other ARE-related motifs for *her1* and other cyclic 3'UTRs that might promote mRNA decay (data not shown). Experiments using deletion reporter assays are underway that will functionally test the role of these and other potential regulatory elements.

We favor nonsense mediated decay (NMD) and/or Stau1-mediated decay (SMD), both of which are Upf1-dependent, as the most likely pathway(s) utilized to clear natural cyclic transcripts during segmentation. Upf1 and Pnrc2 promote decay of cyclic transcripts during segmentation (Figure 2.8; Figure 2.11) and others have shown that human PNRC2 acts as a decay adapter that physically interacts with decay factors DCP1 and UPF1 and can promote decapping activity

of Dcp2 *in vitro*[62,103,105,127-130]. Transcripts annotated in zebrafish EST and GenBank databases (GRCv10) for *her1*, *dlc*, and *dld* lack canonical NMD-inducing features (retained introns, premature termination codons, upstream ORFs, or intron-containing 3'UTRs), although there exists an intron-retained *her7* isoform. Global analyses of UPF1-binding sites in murine embryonic stem cells (mESCs) uncovered a large class of UPF1-3'UTR-bound mRNAs that undergo repression by NMD despite lacking canonical NMD-inducing features, although cyclic transcripts were not among those analyzed[180]. Because *upf1* knockdown alone does not affect *her1* expression, but partial knockdown of *pnrc2* together with *upf1* leads to accumulated *her1* mRNA (Figure 2.8; Figure 2.11 and data not shown), it is unlikely that Upf1 is absolutely required for Pnrc2-mediated decay of cyclic transcripts (although maternally-provided *upf1* function may mask such a function). Instead, it may be that Pnrc2 promotes decay through a combination of Upf1-dependent and -independent mechanisms. Alternatively, low levels of Upf1 protein may be sufficient for Pnrc2-mediated cyclic mRNA decay. Substantial depletion of Upf1 protein is achieved with splice-blocking morpholinos, however, Upf1 is faintly detected by immunoblot[137] and this may be sufficient for cyclic mRNA clearance when Pnrc2 levels are normal. Future biochemical and genetic interaction studies with known factors of NMD and SMD will further enhance our understanding of mechanisms that drive rapid decay of cyclic transcripts during segmentation.

2.6 Figures

Figure 2.1. The *tortuga*^{b644} allele is a 1.46 Mb deficiency that includes the *pnrc2* gene.

Haploid-based mapping revealed that the *tortuga* lesion lies 0.30 cM to the left (4/1434 recombinants) and 0.37 cM to the right (4/1083 recombinants) of the SSLP markers z13511 and z9511, respectively (A). The extent of the deletion was refined by PCR-based screening of regions within and around the deletion interval from pooled genomic DNA samples of 10 wild-type (WT) and 10 *tortuga* mutant embryos (B); regions that fail to amplify in mutants are deleted in the *tor*^{b644} allele (A, B). Among BACs spanning the deletion interval, only BAC AL844887 restores *her1* expression when injected into tor mutants (A; Figure 2.2A-D). In wildtype embryos, *her1* is expressed in a striped pattern (n = 54/54) (C). In contrast, embryos injected with 6 ng of *pnrc2* splice-blocking morpholino (sbMO) have a *tortuga*-like *her1* expression defect (n=37/39) (D). When *pnrc2* mRNA is co-injected with 4 ng *pnrc2* sbMO, *her1* expression is partially restored in a dose-dependent manner (n = 3/19 WT *her1* expression, 150 pg *pnrc2* mRNA; n = 7/17 WT *her1* expression, 600 pg *pnrc2* mRNA) (E; Table 2.1). Alignment of vertebrate Pnrc2 amino acid sequences reveals a conserved 10 amino acid N-terminus (purple) and conserved C-terminal SRC-Homology 3 (SH3) (red) and Nuclear Receptor (NR box) domains (F). Clustal alignments were performed in consultation with published alignments for vertebrate Pnrc2[181]. (Data in Figure 2.1A-E were generated by Thomas L. Gallagher.)

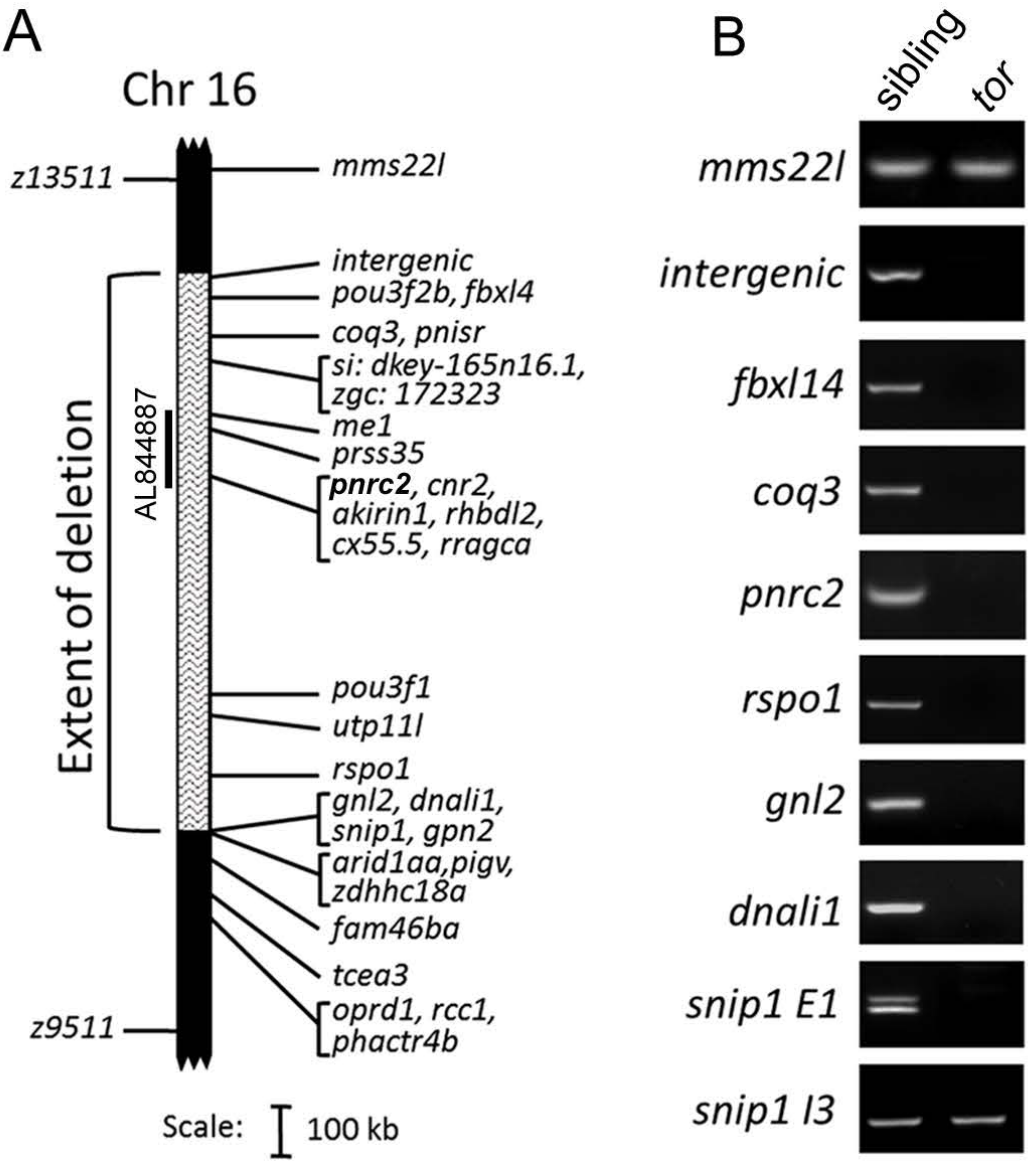

(Figure 2.1 continued on next page)

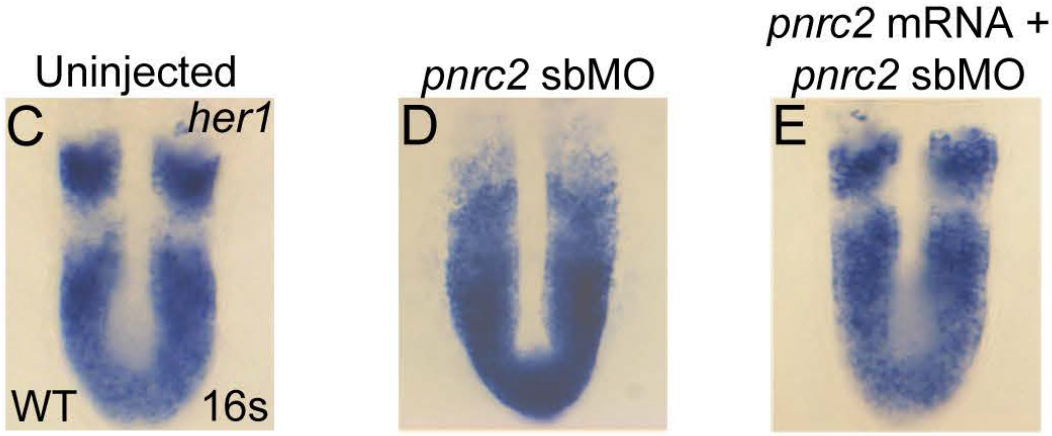

F

Pnrc2 proteins

```
zebrafish|  MGGGERYNIPDRPAPK--KSQPVSRGKQR-SRDQNG-VMHSAASGALGVPHHLRR
xenopus|    MGGGERFNIPGQHRNNLGK---QI-NRQK-LFDRNNQKM--------NTSH--TK
chicken|    MVGGERFNIPVPQSRNITKNHQQLKNRQKKNKDQNS-QM--------KKTY--MK
human|      MGGGERYNIPAPQSRNVSKNQQQL-NRQK-TKEQNS-QM--------KIVH--KK
cattle|     MGGGERYNIPAPQTRNVSKNQQQL-SRQK-TKDQNS-QM--------KIVH--KK
mouse|      MGGGERYNIPDPQSRNASKNQEQQ-NRQK-SKDQNSSQT--------KIAH--KK
rat|        MGGGERYNIPDPQSRNASKNQQQH-NRQK-TKDQNS-QM--------KIVH--KK


zebrafish|  GEKGTSYSWSPEARQAVSVDKKNGSVRFATPYDQNWESHL---NKLLSAQCGQNY
xenopus|    -DRGRGCGTS-LAWQAMQ----NGINNNAFSPNQNWSAGFPASKNLFTDEDNQNY
chicken|    KERGHGCNSLSGAWQAMQ---KAGKNNVHFPCNQNWSPNLSNRNLFFSPQTNQNY
human|      KERGHGYNSSAAAWQAMQ----NGGKNKNFPNNQSWNSSLSGPRLLFKSQANQNY
cattle|     KERGHTYNSSSAAWQAMQ----NGGKNKNFPNNQNWNSSLSSPTLLFKSQTNQNY
mouse|      KERGHGYNPAAAAWQAMQ----NGGKTKSLSNNSNWNAGLSSPSLLFKSQASQNY
rat|        KERGHGYNPS-----AVQ----NGGKTKSLSNNSNWNASLSSPSLLFKSQASQNY


zebrafish|  AGAKFSEPPSPSVLPKPPSHWVSLPMG-DHRELMTFQLKSLLKVQA  148 aa
xenopus|    AGAKFSEPPSPSVLPKPPSHWVLLSCSPAEKELMSFQLKTLLKVQA  135 aa
chicken|    AGAKFSEPPSPSVLPKPPSHWVPVSFKPSDKEIMTFQLKTLLKVQA  141 aa
human|      AGAKFSEPPSPSVLPKPPSHWVPVSFNPSDKEIMTFQLKTLLKVQV  139 aa
cattle|     AGAKFSEPPSPSVLPKPPSHWVPVSFNPSDKEIMTFQLKTLLKVQV  139 aa
mouse|      AGAKFSEPPSPSVLPKPPSHWVHVSLNPSDKETMTFQLKTLLKVQV  140 aa
rat|        AGAKFSEPPSPSVLPKPPSHWVHVSLNPSDKETMTFQLKTLLKVQV  134 aa
```

Figure 2.2. *pnrc2* is the best candidate within the tortuga interval for the gene regulating cyclic transcript decay.

Injection of 30 pg BAC AL844887 does not affect *her1* expression in wild-type sibling embryos (n=27/27) (A versus C), but does significantly reduce accumulation of *her1* transcripts in *tortuga*^{b644} mutants (n=10/10) (B versus D). BAC-injected *tor* mutants are indistinguishable from wild-type siblings and are identified by PCR-based genotyping of individual embryos after *her1* in situ hybridization (data not shown). (E) RT-PCR expression analysis of genes on BAC AL844887 reveals that seven are expressed during cleavage (C) and segmentation stages (S), with particularly robust detection of *pnrc2* and *akirin1*. In addition to RefSeq-annotated genes on BAC AL844887, *snap91* and *dopey1*, both of which lack RefSeq annotation, are detectably expressed during cleavage and segmentation stages (E). (F) RT-PCR expression analysis of genes on BAC AL844887 in *tortuga* mutants indicates that *pnrc2*, *rragca*, and to a lesser extent *akirin1* are expressed from injected BAC DNA. *dopey1, snap91*, *cnr2*, and *rhbdl2* are not expressed from the BAC (data not shown). (G-I) Injection of translation-blocking morpholinos (tbMOs) targeting *akirin1* and *rragca* into 1-cell stage wild-type embryos has no effect on the striped *her1* expression pattern observed in WT embryos (G vs I, J), but injection of a *pnrc2* tbMO has a dramatic effect (G vs H). A range of doses (1.5 ng-6 ng) was tested for each MO (n>50 per dose). (J) Schematic depicts primer and splice-blocking MO (sbMO) target location (*Figure 2.2 caption continued on page 52*)

(*Figure 2.2 caption continued from page 51)* on the *pnrc2* transcript. (K) RT-PCR splicing analysis was performed to detect both spliced and unspliced *pnrc2* transcript in uninjected wild-type and *pnrc2* morphant embryos (see Supplemental Methods). One primer combination was used to specifically amplify unspliced product (green and blue arrows in K) and exon-specific primers (orange and red arrows in K) were used to amplify both spliced and unspliced product for semi-quantitative splicing analysis[138]. Injection of *pnrc2* sbMO reduces normal *pnrc2* splicing by >70% knockdown in a dose-dependent manner (n=20 per dose) (L). Although intron retention alone does not disrupt *pnrc2* coding potential as this lies entirely in exon 3 (K), aberrant transcripts induced by *pnrc2* sbMO-injection coincide with elevated *her1* mRNA levels (Figure 2.1D) suggesting that *pnrc2* sbMOs are effective. Injection of either *pnrc2* splice-blocking (sbMO) or a *pnrc2* tbMO have similar, dose-dependent effects on *her1* expression when injected at doses ranging from 1.5-6 ng (n>50 per dose) (data not shown). All PCR products were sequenced. ORF=*pnrc2* open reading frame; KD=knockdown. (Data in Figure 2.2 were generated by Thomas L. Gallagher.)

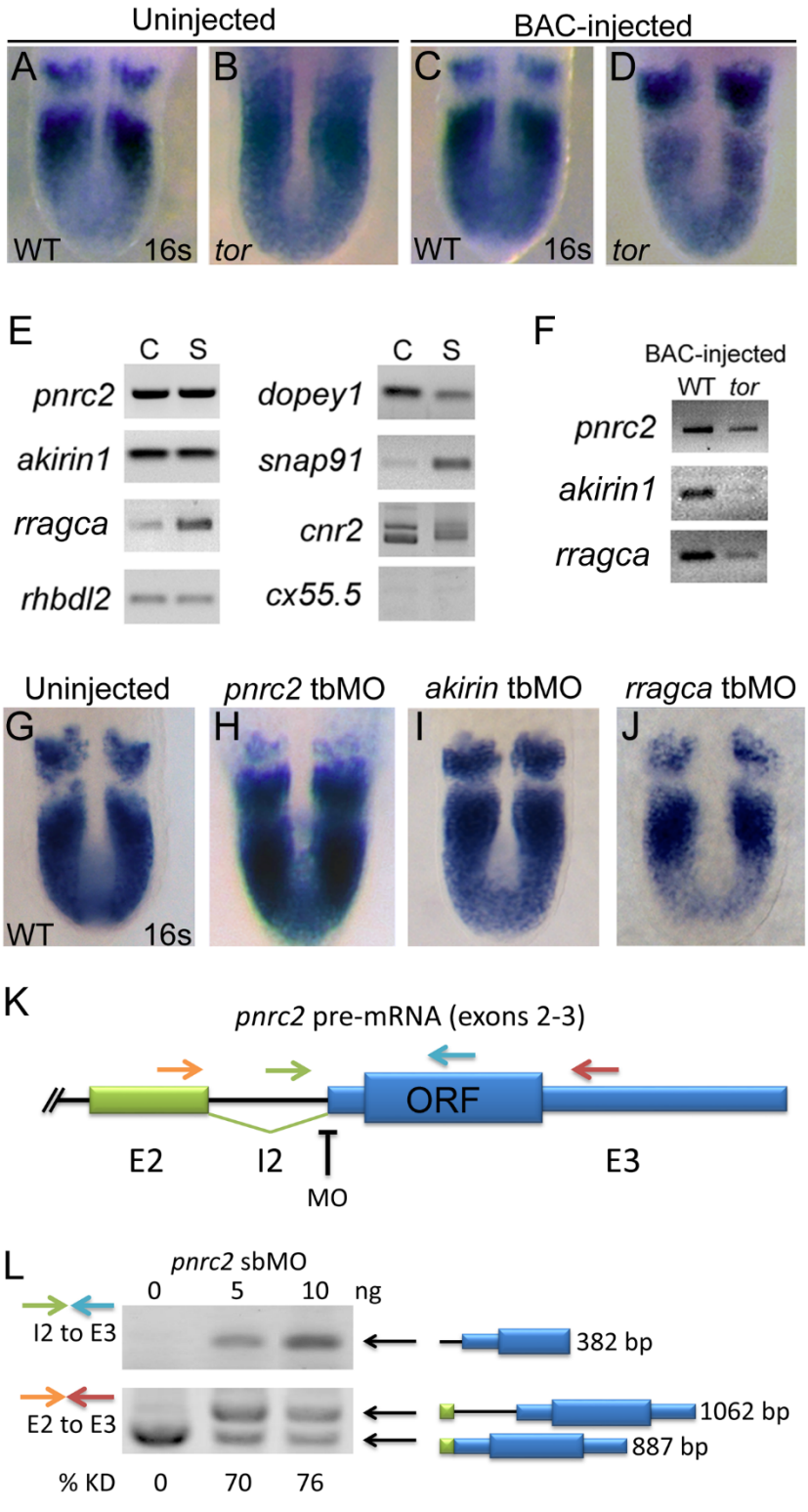
Uninjected
BAC-injected
A
WT
16s
B
tor
C
WT
16s
D
tor
E
C S
pnrc2
akirin1
rragca
rhbdl2
C S
dopey1
snap91
cnr2
cx55.5
F
BAC-injected
WT tor
pnrc2
akirin1
rragca
Uninjected
pnrc2 tbMO
akirin tbMO
rragca tbMO
G
WT
16s
H
I
J
K
pnrc2 pre-mRNA (exons 2-3)
ORF
E2
I2
MO
E3
L
pnrc2 sbMO
0 5 10 ng
I2 to E3
382 bp
E2 to E3
1062 bp
887 bp
% KD 0 70 76

Figure 2.3. *tor* mutant embryos are rescued by injection of *pnrc2* mRNA and phenocopied by frame-shifting mutation of the *pnrc2* locus.

Injection of 100 pg *pnrc2* mRNA has no effect in wild-type sibling embryos (n=15/15 non-mutant siblings) (A, A' vs B, B') but restores striped *her1* expression in *tor* mutant embryos (n=10/10 mutants) (C, C' vs D, D'; Table 2.2). In these experiments, rescued *tor*^{b644} mutant embryos were distinguished from wild-type siblings by lack of expression of *pou3f1*, a gene located in the *tor*^{b644} deficiency interval. Asterisks (*) mark the neural *pou3f1* expression domain. Arrows mark the *her1* expression domain (A-D), magnified in dorsal view to the right of each embryo (A'-D'). Using CRISPR-based mutagenesis, we induced a 17 bp deletion within the *pnrc2* coding sequence, creating an early frameshift allele, designated *pnrc2*^{oz22} (E). Predicted mutant protein sequence is based on sequenced genomic DNA (E). The *pnrc2*^{oz22} allele fails to complement the her1 accumulation phenotype of the *tor*^{b644} deletion allele (n = 4/15 embryos from a heterozygote intercross with *tor*-like *her1* accumulation) (F, G). Similar to *tor*^{b644} mutants, *pnrc2*^{oz22} mutant embryos lack a striped *her1* expression pattern (H, H'). (Data in Figure 2.3A-D' were generated by Thomas L. Gallagher.)

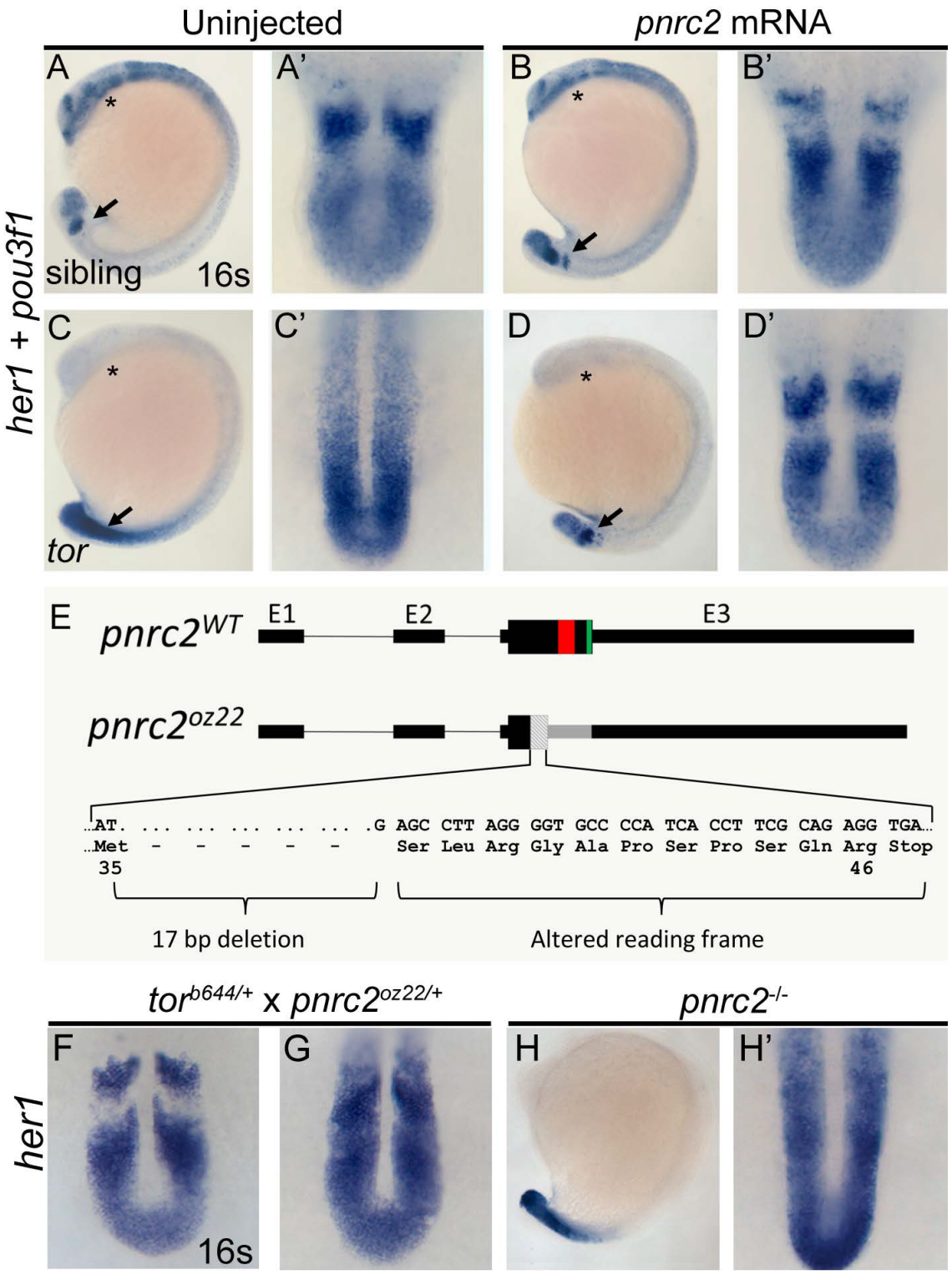
Uninjected
pnrc2 mRNA
her1 + pou3f1
A
A'
B
B'
sibling
16s
C
C'
D
D'
tor
E
pnrc2WT
E1
E2
E3
pnrc2oz22
…AT. ... ... .G AGC CTT AGG GGT GCC CCA TCA CCT TCG CAG AGG TGA…
…Met - - - - - Ser Leu Arg Gly Ala Pro Ser Pro Ser Gln Arg Stop
35
46
17 bp deletion
Altered reading frame
torb644/+ x pnrc2oz22/+
pnrc2-/-
her1
F
G
H
H'
16s

Figure 2.4. Segmentation clock transcripts accumulate in *pnrc2* mutant embryos.

Like *her1*, other segmentation clock genes, *dlc* (A, B), *dld* (C,D), and *her7* (E, F), are misexpressed in *pnrc2* mutant embryos, with expression detected throughout the presomitic mesoderm (PSM) in the expected one-quarter of embryos in a *pnrc2*^{oz22} intercross, n = 8/25 ($\mathbf{X}^2$ = 0.65, p = 0.4), 6/25 ($\mathbf{X}^2$ = 0.013, p = 0.9), and 8/25 ($\mathbf{X}^2$ = 0.65, p = 0.4), respectively (A-F).

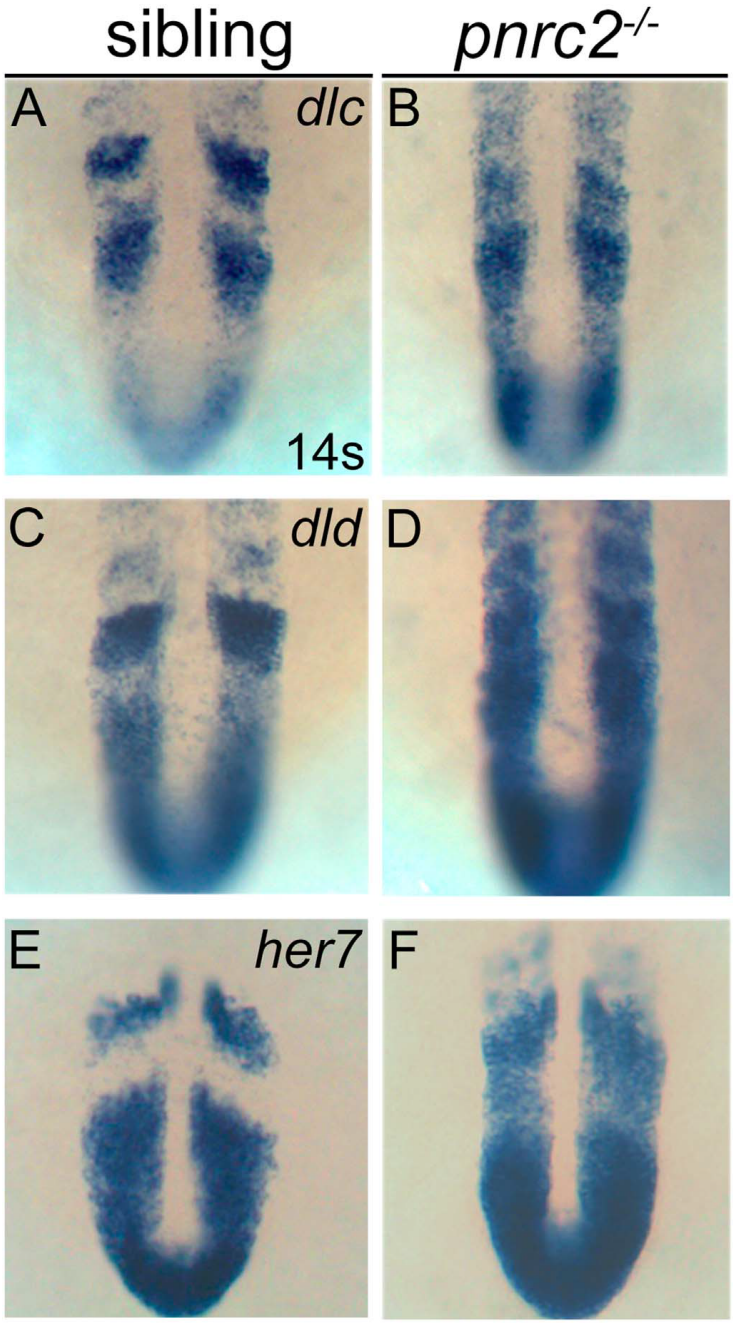
sibling
pnrc2-/-
A
dlc
14s
B
C
dld
D
E
her7
F

Figure 2.5. *her1* and *dlc* transcripts accumulate post-transcriptionally in *pnrc2*^{oz22} mutants.

Exonic in situ probes reveal that segmentation clock-associated *her1* and *dlc* transcripts are misexpressed in the expected one-quarter of embryos in a *pnrc2*^{oz22} intercross, n=13/57 (X^2=0.1, p=0.7) and n=8/30 (X^2=0.04, p=0.83), respectively (A, B and D, E). Intronic in situ probes, however, reveal no differences in expression among embryos from the same clutch, n=30/30 (X^2=10.0, p=0.0016) and n=45/45 (X^2=15.0, p=0.0001), respectively (C, F). These results are consistent with previous observations in *tor*^{b644} mutants using intronic and exonic in situ probes that distinguish nascent from processed transcripts[100]. (Data in Figure 2.5A-F were generated by Zachary T. Morrow.)

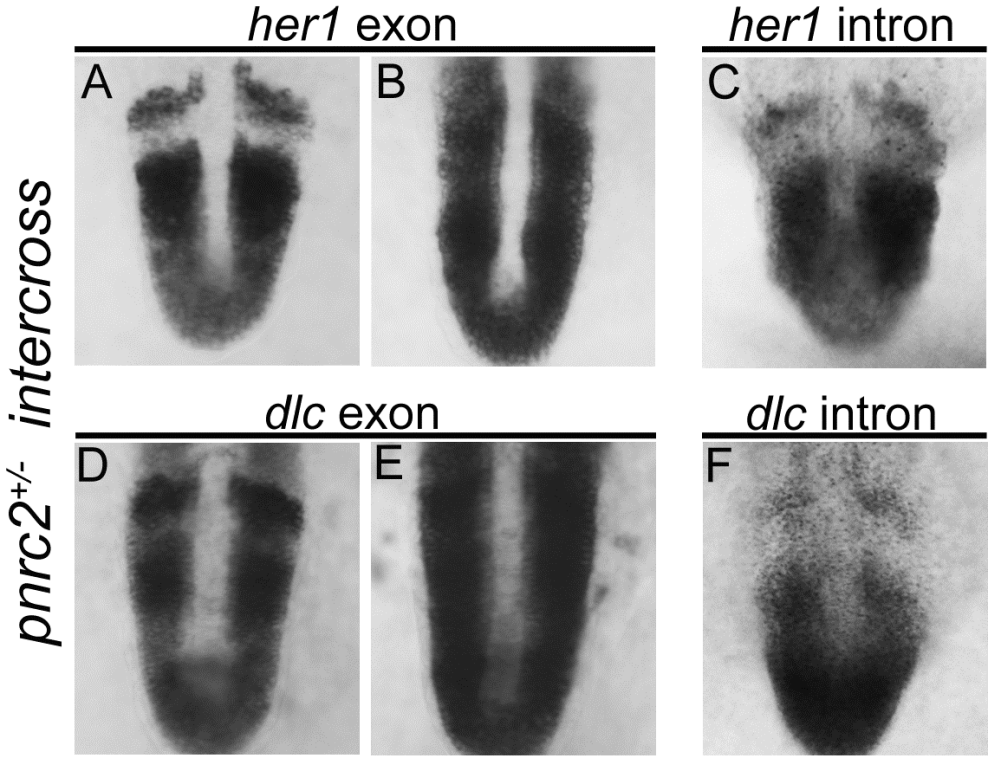
her1 exon
her1 intron
A
B
C
dlc exon
dlc intron
D
E
F
pnrc2$^{+/-}$ *intercross*

Figure 2.6. *pnrc2* is broadly expressed during segmentation stages. *pnrc2* transcripts are detected during early embryonic stages and throughout segmentation stages by in situ hybridization (n > 15 per time point) (A-F). As expected, there is no detectable staining with a *pnrc2* sense probe (n = 15/15) (data not shown). RT-PCR expression analysis for *pnrc2* at 2 hours post fertilization (2 h) through mid-segmentation (18 h) is consistent with in situ detection of *pnrc2* transcript (see Methods and Results) (G). (Data in Figure 2.6A-F were generated Thomas L. Gallagher.)

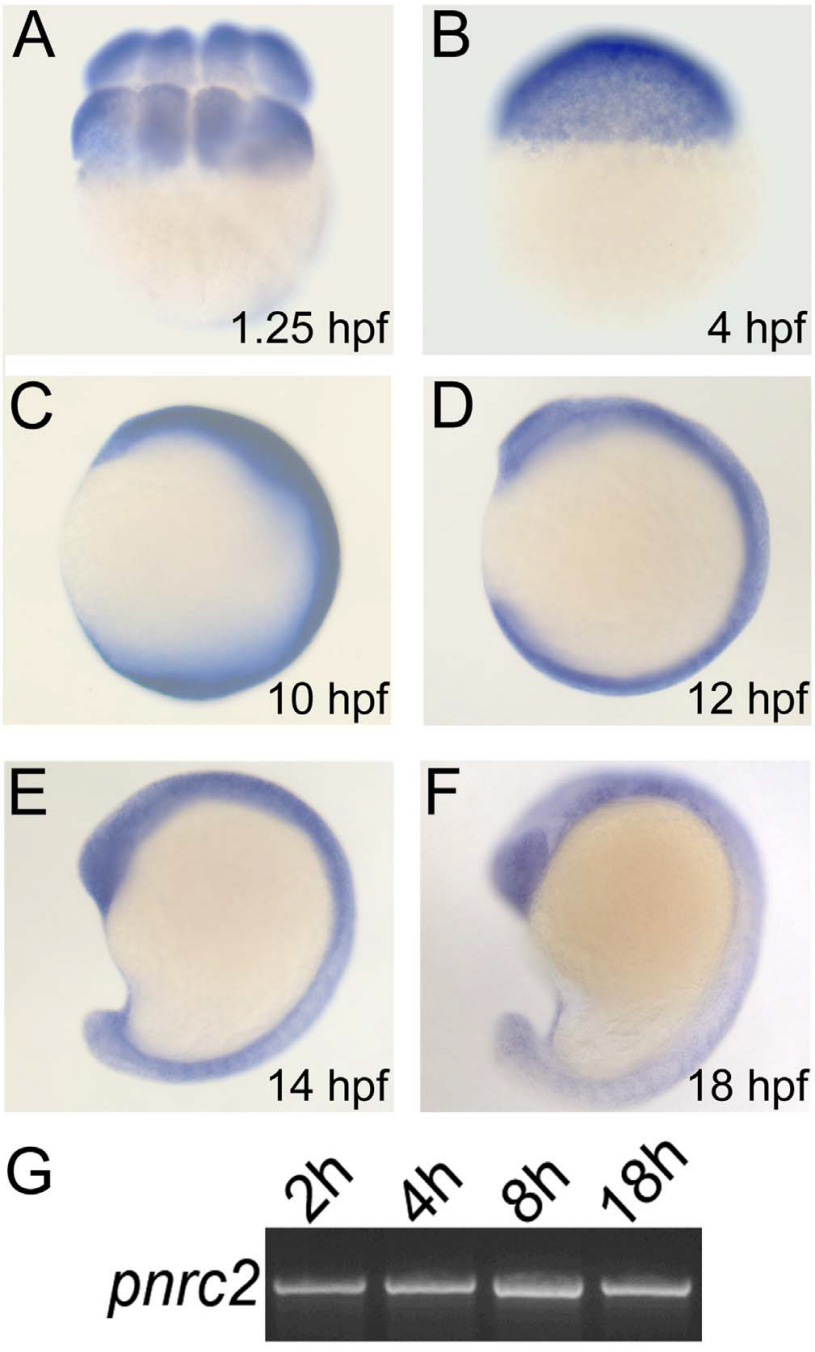
A
1.25 hpf
B
4 hpf
C
10 hpf
D
12 hpf
E
14 hpf
F
18 hpf
G
2h
4h
8h
18h
pnrc2

Figure 2.7. Pnrc2-mediated decay functions via 3'UTR recognition and does not require Dicer-dependent miRNAs.

Stably transgenic embryos carrying the *hsp70l:Venus her1 3'UTR* reporter were injected at the 1-cell stage with *pnrc2* sbMO or reserved as uninjected controls. Embryos were then raised to mid-segmentation stage, heat-shocked for 15 min, then collected at the indicated minutes post-heat-shock (pHS) and processed by *Venus* in situ hybridization (n=65, 6 ng *pnrc2* sbMO; n=55, uninjected controls) (A-F). Venus transcripts are not detected in the absence of heat-shock (n = 10) (not shown). To determine whether Dicer-generated miRNAs contribute to *her1* mRNA decay, *MZdicer* mutants (n = 11) and wild-type controls (n = 10) were raised to mid-segmentation stages (16–18 hpf) and processed by *her1* in situ hybridization (G, H). At this timepoint, *MZdicer* mutants are developmentally delayed relative to wild-type controls[153], and thus have a different overall shape. (Data in Figure 2.7A-F were generated by Thomas L. Gallagher and Nicolas L. Derr.)

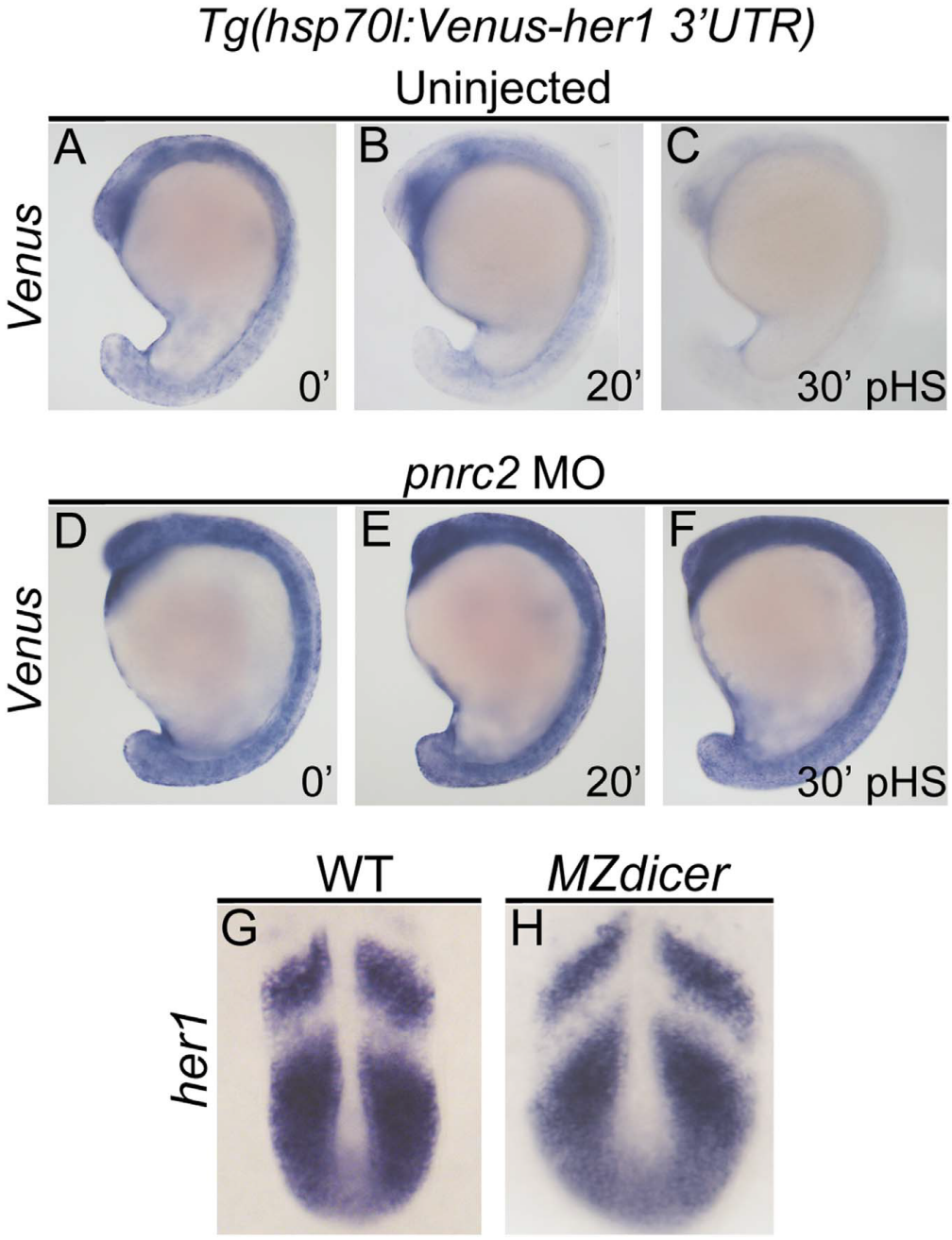
Tg(hsp70l:Venus-her1 3'UTR)
Uninjected
A
B
C
Venus
0'
20'
30' pHS
pnrc2 MO
D
E
F
Venus
0'
20'
30' pHS
WT
MZdicer
G
H
her1

Figure 2.8. *pnrc2* and the nonsense-mediated decay effector Upf1 promote decay of cyclic mRNA.

Injection of low dose pnrc2 sbMO (2 ng) has little to no effect on her1 expression (A, C), contrasting with the expected her1 misexpression observed after injection of moderate dose pnrc2 sbMO (6 ng) (B). Low dose injection of upf1 sbMO (0.25 ng) also has little effect on her1 expression (D), but when combined with a low dose of pnrc2 sbMO (2 ng), *her1* misexpression is observed in about 50% of injected embryos (E). The proportion affected in each condition is plotted on a bar graph that indicates significant differences between single morphants, double morphants, and controls (F). sbMO = splice-blocking MO; **** = $p < 0.0001$. (Data in Figure 2.8A-F were generated by Thomas L. Gallagher.)

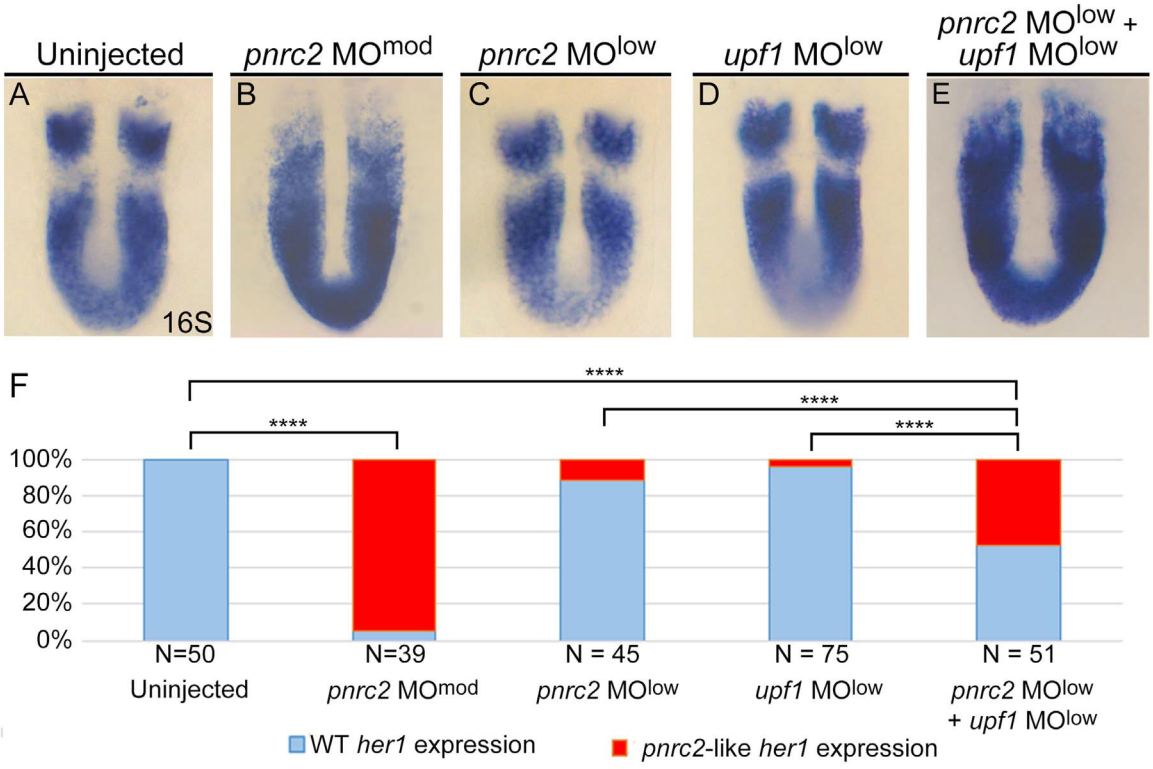
Uninjected
pnrc2 MOmod
pnrc2 MOlow
upf1 MOlow
pnrc2 MOlow + upf1 MOlow
A
B
C
D
E
16S
F
****
****
****
100%
80%
60%
40%
20%
0%
N=50
Uninjected
N=39
pnrc2 MOmod
N = 45
pnrc2 MOlow
N = 75
upf1 MOlow
N = 51
pnrc2 MOlow + upf1 MOlow
WT her1 expression
pnrc2-like her1 expression

Figure 2.9. *her1* expression is normal in embryos injected with a control MO, either alone or in combination with a sub-optimal dose of *pnrc2* sbMO. Injection of a sub-optimal dose of *pnrc2* sbMO (2 ng) has little to no effect on *her1* expression (A, C), contrasting with the expected *her1* misexpression observed after injection of a moderate dose of *pnrc2* sbMO (6 ng) (B). Injection of a moderate dose of an unrelated sbMO targeting *rbfox1l* (6 ng) either alone (D) or combined with a sub-optimal dose of *pnrc2* sbMO (2 ng) has no effect on *her1* expression (E). The proportion affected in each condition is plotted on a bar graph that indicates significant differences between single morphants, double morphants, and controls (F). To confirm effective *rbfox1l* knockdown, we co-injected *rbfox1l* and *rbfox2* sbMOs (6 ng each) in parallel experiments (neither sbMO produces an overt morphological phenotype when injected alone) and observed the expected paralysis phenotype in all double-injected embryos (n=27/27 paralyzed embryos at 24 hpf)[138,139], confirming that we were using an effective *rbfoxl1* sbMO dose in our experiments. sbMO = splice-blocking MO; **** = $p<0.0001$. (Data in Figure 2.9A-F were generated by Thomas L. Gallagher.)

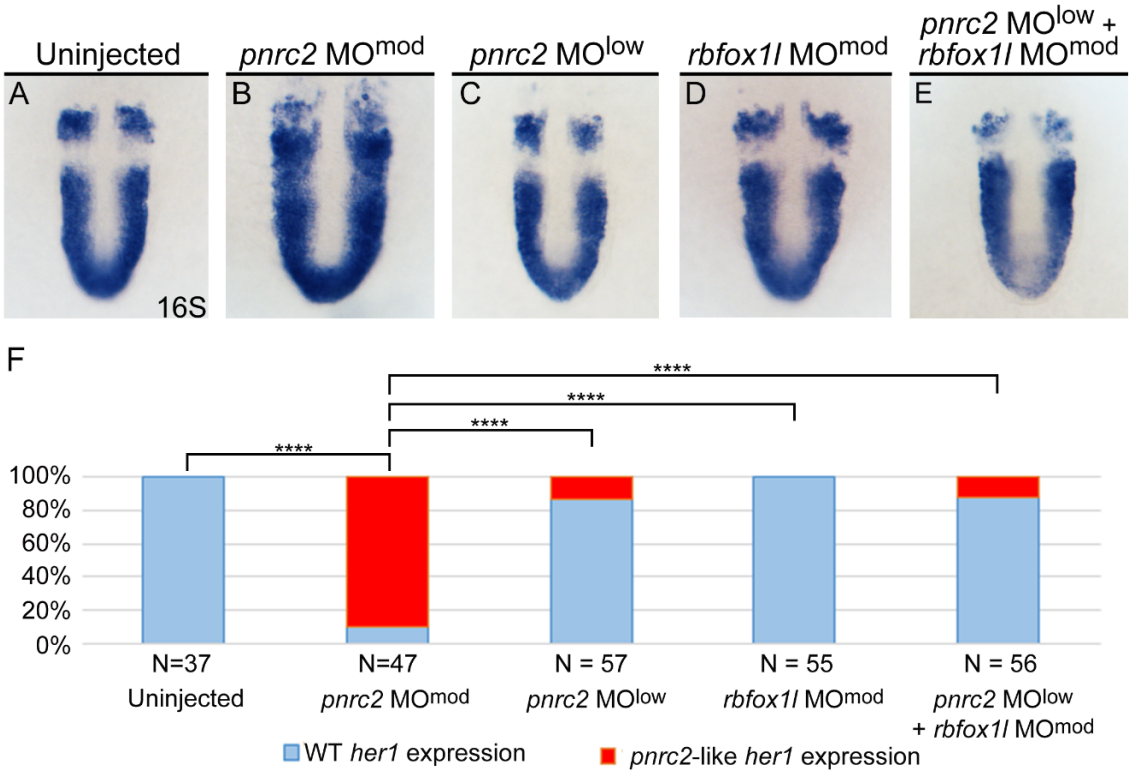
Uninjected
pnrc2 MOmod
pnrc2 MOlow
rbfox1l MOmod
pnrc2 MOlow + rbfox1l MOmod
A
B
C
D
E
16S
F
****
****
****
****
100%
80%
60%
40%
20%
0%
N=37
Uninjected
N=47
pnrc2 MOmod
N = 57
pnrc2 MOlow
N = 55
rbfox1l MOmod
N = 56
pnrc2 MOlow + rbfox1l MOmod
WT her1 expression
pnrc2-like her1 expression

Figure 2.10. Both reporter and endogenous cyclic transcripts accumulate in Pnrc2-depleted embryos, but protein expression appears normal.

Embryos carrying the *her1:her1-Venus*^{bk15} transgenic clock reporter were injected with *pnrc2* splice-blocking morpholino (sbMO) and processed to detect *Venus* transcripts (A, B) and Venus protein (D, E) at mid-segmentation stages. Representative embryos are shown in A (n=21/21); B (n=18/18), D (n=32/32), and E (n=29/29). Venus immunofluorescence panels (D, E) are at slightly higher magnification than *Venus* in situ panels (A, B). Detection of *her1* mRNA by in situ hybridization chain reaction (HCR-ISH) (C, F) is consistent with chromogenic NBT/BCIP-based in situ detection of endogenous *her1* transcript in wild-type and *pnrc2* mutant embryos (Fig. 2.3F, H'), with substantial cytoplasmic localization revealed by DAPI counter staining in 500X magnified view (C', F'). Because relative intensity of *her1* HCR-ISH in *pnrc2* mutants to wild-type embryos is high, levels have been reduced in *pnrc2* mutant panels (F-F'; see Figure 2.13A''', B'''). Misexpression of *dlc* and *dld* mRNA is detected throughout the presomitic mesoderm (PSM), formed somites and neurons in the expected one-quarter of embryos in a *pnrc2*^{oz22} intercross, n = 5/28 (X^2 = 0.76, p = 0.4) and n = 7/40 (X^2 = 1.2, p = 0.3), respectively (G-J). In contrast, *Dlc* and *Dld* protein expression is indistinguishable among siblings of the same *pnrc2*^{oz22} heterozygote intercross (K-N). Dlc and Dld immunolabeled embryos were genotyped prior to imaging and a subset of wild-type and mutant siblings were imaged by confocal microscopy with representative (*Figure 2.10 caption continued on page 69)*

(*Figure 2.10 caption continued from page 68)* embryos shown (K-N). Total genotyped individuals per representative panel: n = 5 (K), n = 6 (L), n=12 (M), n = 4 (N). Scale bars = 50 μm (D, F), 50 nm (F'), 100 μm (K). (Data in Figure 2.10A-F' were generated by Thomas L. Gallagher.)

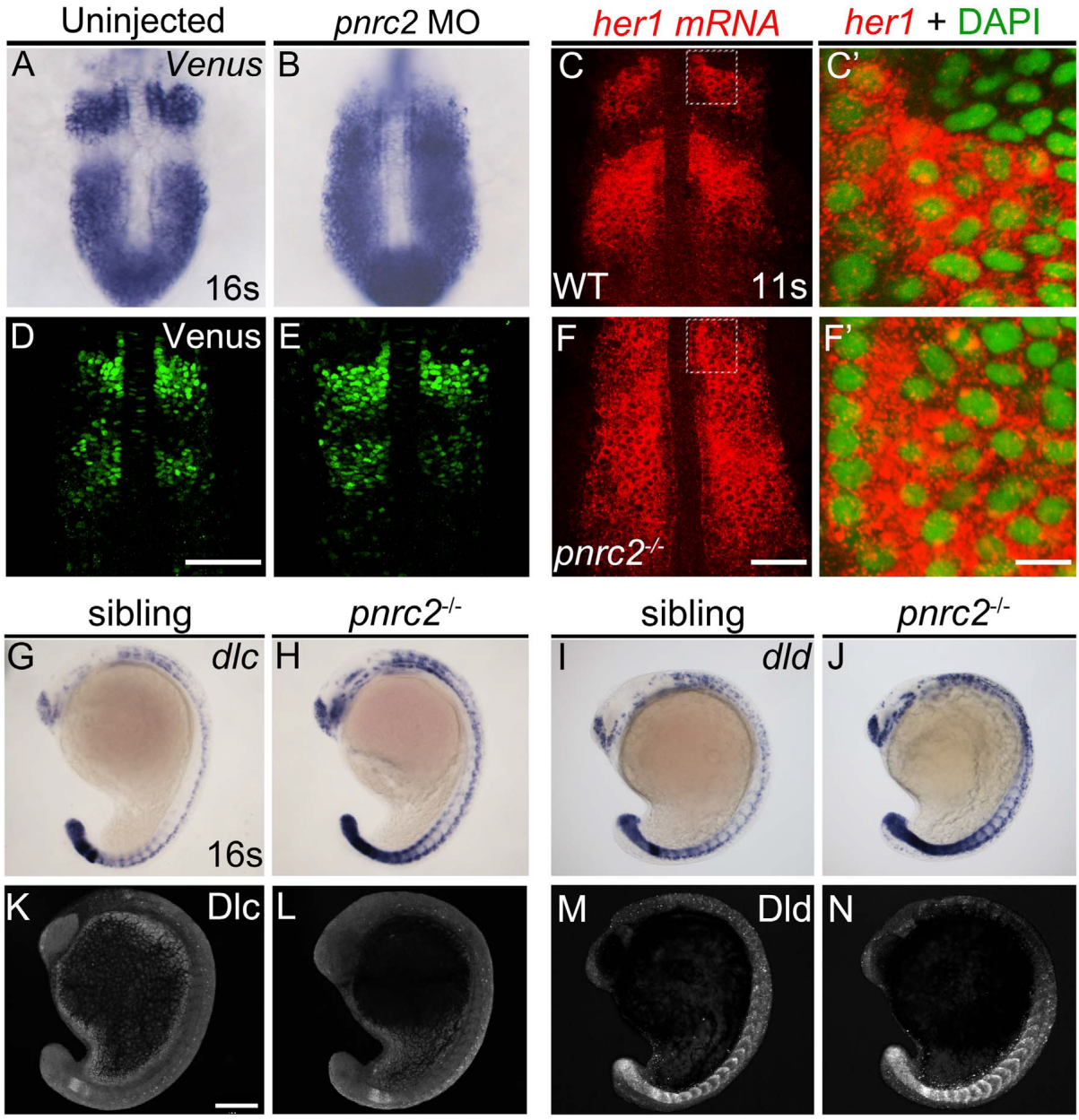
Uninjected
pnrc2 MO
her1 mRNA
her1 + DAPI
A
Venus
16s
B
C
WT
11s
C'
D
Venus
E
F
pnrc2-/-
F'
sibling
pnrc2-/-
sibling
pnrc2-/-
G
dlc
16s
H
I
dld
J
K
Dlc
L
M
Dld
N

Figure 2.11. *Venus* reporter transcripts accumulate in *pnrc2*- and *upf1*-deficient embryos, but Venus protein expression appears normal.

Embryos carrying the *her1:her1-Venus*^{bk15} transgenic clock reporter were injected with a moderate *pnrc2* sbMO dose (6 ng) or co-injected with low *pnrc2* and *upf1* sbMO doses (2 ng and 0.25 ng, respectively) to detect *Venus* transcripts (A-C) and Venus protein (D-F) at mid-segmentation stages. Representative embryos are shown in A (n=12), B (n=8), C (n=9), D (n=36), E (n=24), and F (n=27). Venus immunofluorescence panels (D-F) are at slightly higher magnification than *Venus* in situ panels (A-C). sbMO = splice-blocking MO; scale bar = 50 um (D-F). (Data in Figure 2.11A-F were generated by Thomas L. Gallagher.)

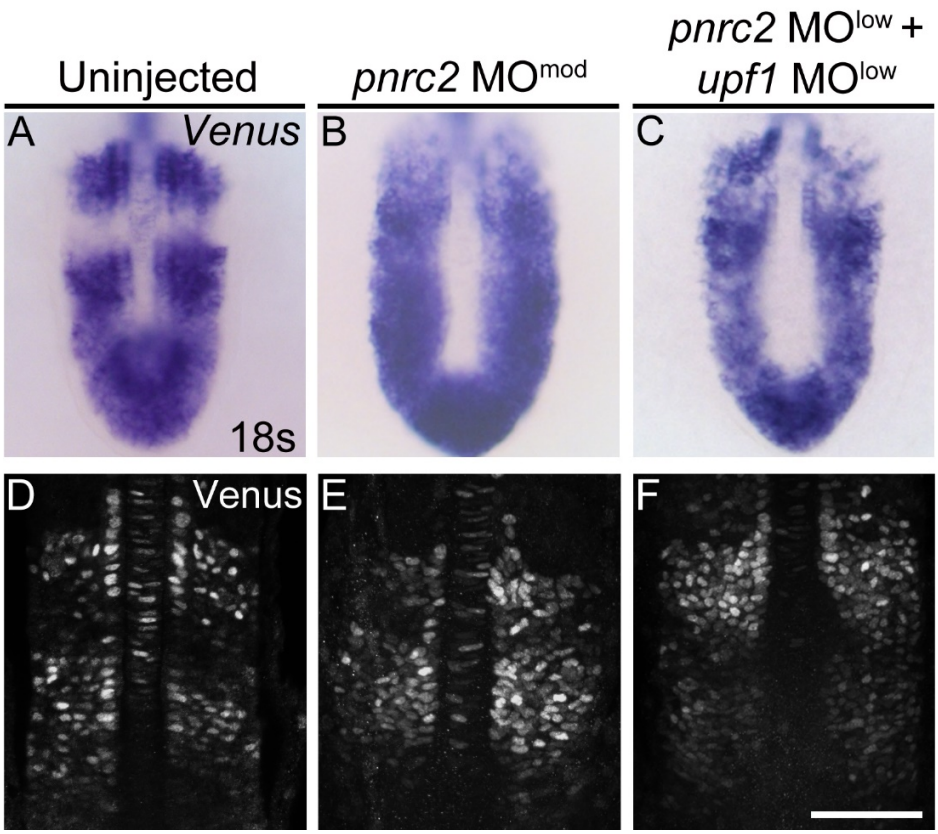
Uninjected
pnrc2 MOmod
pnrc2 MOlow +
upf1 MOlow
A
Venus
18s
B
C
D
Venus
E
F

Figure 2.12. *her1* transcripts are not detected in embryos homozygous for a *her1* deficiency.

Detection of *her1* mRNA by in situ hybridization chain reaction (HCR-ISH) by confocal microscopy reveals striped *her1* expression in the presomitic mesoderm (PSM) of wild-type embryos (A), mirroring what is observed by colorimetric in situ. As expected, *Df(Chr05:her1,her7,ndrg3a)*^{b567} homozygote embryos, imaged using the same laser intensity and exposure as wild-type embryos in A, lack detectable *her1* expression (B). Scale bar = 50 um. (Data in Figure 2.12A-B were generated by Thomas L. Gallagher.)

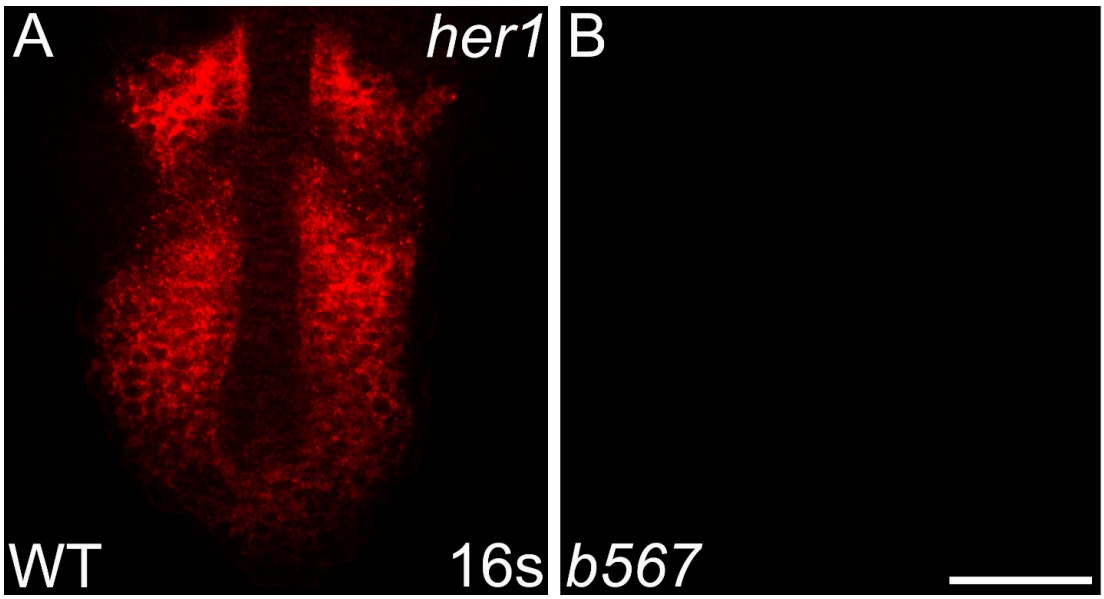
A
her1
WT
16s
B
b567

Figure 2.13. *her1* mRNA accumulates dramatically in *pnrc2*^{oz22} mutants. Detection of *her1* mRNA by in situ hybridization chain reaction (HCR-ISH) reveals *her1* misexpression throughout the presomitic mesoderm (PSM) of *pnrc2* mutants (A, B). Representative embryos are shown (n=5 in A, n=5 in B). Substantial cytoplasmic localization revealed with DAPI counter staining is apparent in both unaffected siblings and *pnrc*2 mutants (A', B', 470X magnified in A", B"). Because detection of *her1* mRNA in *pnrc2*^{oz22} mutants is very high relative to wild type, levels have been reduced in *pnrc2* mutant panels (B-B"). When wild-type and *pnrc2* mutants are imaged at the same laser level, raw intensity maps of *her1* HCR-ISH signal reveal the extent of *her1* mRNA accumulation in *pnrc2*^{oz22} mutants (A"', B"'). Scale bars = 50 um (B), 50 nm (B''). (Data in Figure 2.13A-B"' were generated by Thomas Gallagher.)

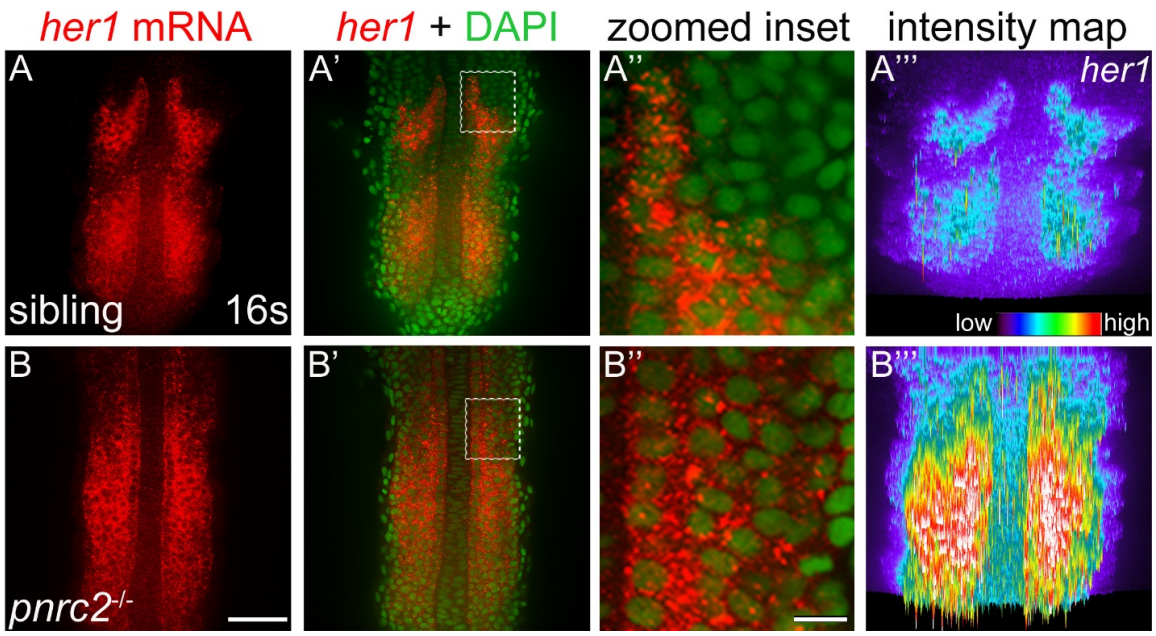
her1 mRNA
her1 + DAPI
zoomed inset
intensity map
A
A'
A''
A'''
her1
sibling
16s
low
high
B
B'
B''
B'''
pnrc2-/-

Table 2.1. Injection of pnrc2 mRNA partially restores normal *her1* expression in *pnrc2* morphants.

Condition	*her1* expression[a]		
	Normal	Partial *tor*-like	*tor*-like
Uninjected WT	54/54 (100%)	0/54 (0%)	0/54 (0%)
4 ng *pnrc2* sbMO	2/39 (5%)	28/39 (72%)	9/39 (23%)
4ng *pnrc2* sbMO + 150 pg *pnrc2* mRNA[b]	3/19 (16%)	12/19 (63%)	4/19 (21%)
4 ng *pnrc2* sbMO + 600 pg *pnrc2* mRNA[b]	7/17 (42%)	9/17 (53%)	1/17 (6%)

[a]Wild-type embryos were injected at the 1-cell stage with 4 ng *pnrc2* sbMO with and without increasing doses of MO-resistant *pnrc2* mRNA, raised to 16-18 hpf, and processed by *her1* in situ hybridization. Normal, *her1* is expressed in visible stripes separated by regions of low expression; Partial *tor*-like, *her1* stripes are distinguishable, but there is substantial *her1* detected between stripes; *to*r-like, *her1* expression is strong throughout the PSM with no obvious peaks or troughs.

[b]Chi-square analysis indicates a significant difference in *her1* expression between *pnrc2* morphants with and without co-injection of *pnrc2* mRNA. Co-injection of 150 pg and 600 pg of *pnrc2* mRNA significantly restores *her1* expression in morphants ($p<2.1 \times 10^{-3}$ and $p<8.8 \times 10^{-8}$, respectively). (Data in Table 2.1 were generated by Thomas L. Gallagher.)

Table 2.2. Injection of *pnrc2* mRNA restores normal *her1* expression in *tor*^{b644} mutants.

mRNA dose (pg)	Live Embryonic Phenotype		WT *her1* ISH/ WT genotype[b]	WT *her1* ISH/ *tor* genotype[b]	*tor her1* ISH/ *tor* genotype[b]
	WT[a]	neural degen[a]			
0	103	31	103/103	0/31	31/31
75	64	20	64/64	19/20[c]	1/20[d]
100	15	10	15/15	10/10[c]	0/10[d]

[a] At the 16-18 somite stage, *pnrc2* mRNA-injected embryos from a *tor*^{b644} heterozygote intercross were scored for neural degeneration, a non-somitic phenotype observed in *tor* mutants.

[b] After sorting by live phenotype, injected embryos were processed by *her1* in situ hybridization to assess phenotypic rescue and with *pou3f1* to identify individuals homozygous for the *tor* deletion. Representative embryos are shown in Figure 2.3.

[c] Both 75 and 100 pg doses correlate with restoration of normal *her1* expression. At the 100 pg dose, all *tor* mutants have a normal *her1* expression pattern.

[d] Chi-square analysis indicates a significant difference in *her1* expression among *pnrc2* mRNA-injected *tor* mutants compared to uninjected homozygous siblings ($p<4.7 \times 10^{-7}$ and $p<3.9 \times 10^{-3}$, for 75 pg and 100 pg doses, respectively). (Data in Table 2.2 were generated by Thomas L. Gallagher.)

Table 2.3. Pnrc2 is required for the transcript destabilizing effect of the *her1* 3'UTR.

***hsp70l:Venus-her1* 3'UTR Condition[a]**	**pHS recovery time[b]**	**Expression Level[c]**			**Number of embryos**	**Mean Expression**
		3	**2**	**1**		
Uninjected	0	20	0	4	24	2.7[d]
6 ng *pnrc2* MO	0	27	0	0	27	3.0[d]
Uninjected	20	0	0	6	6	1.0[d]
6 ng *pnrc2* MO	20	11	0	0	11	3.0[d]
Uninjected	30	0	8	17	25	1.3[d]
6 ng *pnrc2* MO	30	27	0	0	27	3.0[d]

[a]A stably transgenic male carrying a *hsp70l:Venus-her1* 3'UTR reporter was crossed to a wild-type female; half of the progeny were injected with *pnrc2* sbMO and the other half used as uninjected sibling controls.

[b]At 14-16 hpf, embryos were heat-shocked at 37°C for 15 minutes, followed by fixation at indicated post-heat shock (pHS) recovery times.

[c]Fixed embryos were processed and scored as described in Table 2.1. Embryos completely lacking *Venus* expression were not included because we could not discriminate the expected 50% of embryos that did not inherit the transgene from transgenic embryos lacking detectable *Venus* expression.

[d]Average expression levels reveal that *pnrc2* MO-injection into transgenic embryos dramatically stabilizes *Venus* transcript levels post heat-shock across the recovery time course of 30 minutes when compared to uninjected controls. (Data in Table 2.3 were generated by Thomas Gallagher.)

Table 2.4. *pnrc2* mutants segment normally.

Feature	**Genotype**		
	Wild type	***pnrc2*$^{+/-}$**	***pnrc2*$^{-/-}$**
Segment number	34.7 ± 0.7 (n = 14)	35.3 ± 0.3 (n = 14)	34.3 ± 0.4 (n = 14)

Sibling embryos from a *pnrc2*^{oz22} heterozygote intercross were raised to 36 hpf and processed by *cb1045* (*xirp2a*) in situ hybridization that reliably marks segment boundaries. PCR-based genotyping was performed for individuals after in situ hybridization and segment counts. No significant differences were observed between genotypes. Segment numbers are given as mean ± 95% confidence interval (Student's t test).

Chapter 3: Features of cyclic transcript 3'UTRs regulate Pnrc2-mediated decay during somitogenesis

This chapter is a manuscript in preparation for publication. The current reference for this publication is: Tietz, K. T., Gallagher, T. L., Mannings, M. C., Morrow, Z. T., Derr, N. L., & Amacher, S. L. (2019). Features of cyclic transcript 3'UTRs regulate Pnrc2-mediated decay during somitogenesis.
Contributions from authors other than myself will be denoted in the figure legends.

3.1 Abstract

Vertebrate segmentation is regulated by the segmentation clock, a biological oscillator that controls periodic formation of somites, or embryonic segments, which give rise to many mesodermal tissue types. This molecular oscillator generates cyclic gene expression with the same periodicity as somite formation in the presomitic mesoderm (PSM), an area of mesenchymal cells that give rise to mature somites. Molecular components of the clock include the *Hes/her* family of genes that encode transcriptional repressors, but additional genes cycle. Cyclic transcripts are cleared rapidly, and this depends upon the gene *pnrc2* (*proline-rich nuclear receptor co-activator 2*) that encodes an mRNA decay adaptor. Previously, we showed that the *her1* 3'UTR confers instability to otherwise stable transcripts in a Pnrc2-dependent manner, however, the

molecular mechanism(s) by which cyclic transcripts are cleared remained largely unknown. To identify features residing in the *her1* 3'UTR that are critical for Pnrc2-mediated decay, we developed an array of transgenic inducible reporter lines and find that the last 179 nucleotides (nts) of the *her1* 3'UTR is necessary and sufficient to confer rapid instability. Motif analysis reveals a Pumilio response element (PRE) and AU-rich element (ARE) within the last 179 nts of the *her1* 3'UTR, both of which are required for rapid turnover of reporter mRNA. Similar to the *her1* 3'UTR, the *dlc* 3'UTR also contains PRE and ARE motifs and confers instability to reporter mRNA. Taken together, we find that features including PREs and AREs residing within cyclic 3'UTRs promote instability. Our findings suggest that factors including Pumilio (Pum) and AU-rich binding proteins (ARE-BPs) may cooperate or act independently of Pnrc2 to promote the rapid turnover of clock-related transcripts during somitogenesis.

3.2 Introduction

Genetic oscillations underlie many cellular events and function in the regulation of critical developmental processes. A well-studied example of genetic oscillation is the segmentation clock, a rapid ultradian oscillator that generates periodic expression in developing embryos[3,22,111]. The segmentation clock controls vertebrate somitogenesis, the process by which the mesoderm is sequentially divided into segmental units called somites that later give rise to vertebrae and ribs, body musculature, and dermis. Molecular evidence for the segmentation clock was first observed in the *c-hairy* gene, a chick homolog of the

Drosophila pair rule gene *hairy*[21]. *c-hairy* encodes a member of the Hairy/Enhancer of split-related (Hes)/Hes-related (*her*) family of helix-loop-helix transcription factors that oscillate through a negative feedback loop in which the Hes/Her protein inhibits its own transcription[36,37,39,43]. Homologs of *hairy* have since been identified in vertebrate models such as mouse, fish, frog, and snake[23-26], and in each species, members of the *Hes/her* family undergo oscillatory expression in the presomitic mesoderm (PSM). Studies have shown mouse *hairy1* homolog *Hes7* and zebrafish *hairy1* homologs *her1* and *her7* are core segmentation genes that cycle in the PSM of each species with the same periodicity of segment formation[6,7,23,24,33-35,40]. Maintenance of oscillation periodicity requires many levels of regulation as a somite pair develops very rapidly in developing embryos (30 minutes in zebrafish, 90 minutes in mouse)[3,4]. Studies have explored transcriptional activation and the effect of negative feedback inhibition on oscillatory expression[32,36,39,42-44], and have emphasized the importance of post-transcriptional regulation in maintaining proper oscillatory periodicity[47,115-117]. Recent studies have demonstrated splicing[34,35] and mRNA export[45] are rate limited steps of oscillatory expression, and that cyclic transcript 3'UTRs can promote rapid decay of oscillating transcripts[32,48,116,118]. miRNAs have been shown to regulate decay of some cyclic transcripts[49,119-121], but specific mechanisms that govern cyclic transcript turnover are still not well-understood.

In a forward genetic screen, we discovered a zebrafish mutant, *tortuga* (*tor*), with disrupted cyclic expression[100]. Many genes are deleted in the *tor* deficiency allele, although loss of a single gene, *pnrc2*, is responsible for defects in cyclic expression[48]. Early studies showed Pnrc2 interacts with steroid hormone receptors in vitro and in yeast two-hybrid assays[55,102,104]. More recent studies described human PNRC2 as a decay adapter protein that interacts with decay factors such as UPF1, DCP1A, and STAU1, suggesting Pnrc2 functions in STAU1-mediated mRNA decay (SMD) and nonsense-mediated mRNA decay (NMD)[62,103,105,127-130]. Tethering of PNRC2 to reporter mRNAs confers instability[103,105,107], suggesting PNRC2 can recruit decay machinery when directly associated with transcripts. However, recent findings showed destabilization of NMD-inducing reporter transcripts is unaffected by *PNRC2* knockdown, suggesting PNRC2 is not necessary for NMD function[107]. This inconsistency in the field illustrates the need to better understand Pnrc2-mediated decay.

We previously showed *pnrc2* functions in clearance of cyclic transcripts such as *her1, her7,* and *deltaC (dlc)* during zebrafish segmentation[48]. Normally, clock-related transcript expression appears striped in the anterior PSM when observed at a single time point due to rapid oscillatory transcription followed by rapid mRNA decay; in *pnrc2*^{oz22} mutants, the accumulation of cyclic transcripts obscures the striped expression pattern even though cyclic transcription appears normal[48]. Our previous data provided evidence that *pnrc2* is maternally provided and zygotically expressed throughout somitogenesis[48]. We show here that

maternally provided *pnrc2* partially compensates for loss of zygotic *pnrc2* expression in the turnover of endogenous cyclic transcripts during somitogenesis. We show two cyclic transcripts 3'UTRs confer Pnrc2-mediated instability to reporter transcripts, suggesting a shared mechanism of 3'UTR regulation by Pnrc2 may function to destabilize cyclic transcripts. Through a series of inducible transgenic reporter lines containing various portions of the *her1* 3'UTR fused to reporter mRNA, we find the last 179 nucleotides (nts) of the 725 nt *her1* 3'UTR is necessary and sufficient to confer Pnrc2-dependent instability to reporter mRNA. We find the *dlc* 3'UTR confers Pnrc2-dependent instability as well, demonstrating 3'UTR-mediated instability elements function in both cyclic transcripts. Motif analysis comparing features of the last 179 nts of the *her1* 3'UTR to other cyclic transcript 3'UTRs, including the *dlc* 3'UTR, reveals two potential cis-regulatory motifs: a Pumilio response element (PRE) and an AU-rich element (ARE). We show precise disruption of the PRE or the ARE partially disrupts the destabilizing effect of the *her1* 3'UTR on reporter mRNA, suggesting both the ARE and PRE of the *her1* 3'UTR contribute to the rapid turnover of endogenous *her1* transcripts. This work suggests ARE-binding proteins (ARE-BPs) and Pumilio proteins may function with Pnrc2 in the 3'UTR-mediated turnover of cyclic transcripts during vertebrate segmentation.

3.3 Methods

3.3.1 Animal stocks and husbandry

Adult zebrafish strains (*Danio rerio*) were kept at 28.5°C on a 14 hour (h) light/10h dark cycle and obtained by natural spawning or *in vitro* fertilization, and were staged according to Kimmel et al (1995). The stable *hsp70l:Venus-her1 3'UTR-SV40*$^{oz44,\ oz45,\ oz46}$, *hsp70l:Venus-her1 3'UTR*Δ*1-362-SV40*$^{oz47,\ oz48,\ oz49,\ oz50}$, *hsp70l:Venus-her1 3'UTR*Δ*363-725-SV40*$^{oz51,\ oz52,\ oz53,\ oz54}$*, hsp70l:Venus-her1 3'UTR*Δ*1-546-SV40*$^{oz55,\ oz56,\ oz57,\ oz58,\ oz59}$, *hsp70l:Venus-her1 3'UTR*Δ*1-362;*Δ*547-725-SV40*$^{oz60,\ oz61}$*, hsp70l:Venus-her1 3'UTR*Δ*363-546-SV40*$^{oz62,\ oz63}$, *hsp70l:Venus-disrupted PRE her1 3'UTR-SV40*$^{oz69,\ oz70,\ oz71,\ oz72,\ oz73}$*, hsp70l:Venus-disrupted ARE her1 3'UTR-SV40*$^{oz74,\ oz75,\ oz76,\ oz77,\ oz78,\ oz79}$*, hsp70l:Venus-SV40*$^{oz64,\ oz65,\ oz66,\ oz67,\ oz68}$*, and hsp70l:Venus-dlc 3'UTR-SV40*$^{oz80,\ oz81,\ oz82,\ oz83}$ reporter lines, described below, were generated in this study and displayed in Table 3.1. Animal experiments were performed in accordance with institutional and national guidelines and regulations and were approved by the Ohio State University Animal Care and Use Committees.

3.3.2 DNA extraction and *pnrc2*^{oz22} and *Venus* genotyping strategy

Individual embryos and adult fin tissue were lysed in 50 ul 1X ThermoPol Buffer (NEB) at 95°C for 10 minutes, digested at 55°C for 1-4 hours using 25-50 ug Proteinase K (BP1700, ThermoFisher), followed by Proteinase K inactivation at 95°C for 10 minutes. 1 ul of DNA extract was used as template in a standard 25 ul reaction with Taq polymerase according to manufacturer's protocol (NEB).

To molecularly identify *pnrc2*^{oz22} carriers after PCR amplification, samples were digested with 20 units NsiI-HF (NEB) to distinguish cleavable wild-type (WT) from un-cleavable mutant amplicons. Reaction products were analyzed on a 2% agarose gel stained with Gel Red (Biotium). To identify carriers of the heat-shock inducible reporters, embryos were either screened post-heat shock (pHS) for Venus fluorescence or molecularly identified by PCR amplification of *Venus* coding sequence. Genotyping was performed with 1 ul of DNA extract as template in a standard 25 ul reaction with Taq polymerase according to manufacturer's protocol (NEB). Primers were designed to amplify presence of *Venus* coding sequence in the reporter lines and reaction products were analyzed on a 2% agarose gel stained with Gel Red (Biotium).

3.3.3 Plasmid construction and Transgenesis

The heat shock reporter construct *hsp70l:Venus-her1 3'UTR-SV40* was assembled using standard restriction digestion-based cloning and replacement of the 1.1 kilobase (kb) *her1* 3' noncoding sequence present in construct *hsp70l:Venus-her1 3'UTR* used in Gallagher et al (2017) with a synthetic 725 nt *her1 3'UTR* sequence directly fused to an *SV40* polyadenylation (polyA) sequence synthesized by GeneArt® Gene Synthesis (Invitrogen/Thermo Fisher Scientific). Truncation constructs of the *her1* 3'UTR, outlined in Figure 3.5, were generated by restriction digestion or PCR amplification of the *hsp70l:Venus-her1 3'UTR-SV40* plasmid, in parallel with removal of the full-length *her1* 3'UTR from the *hsp70l:Venus-her1 3'UTR-SV40* plasmid by restriction digestion, followed by

ligation of the truncated *her1 3'UTR* sequence into the digested *hsp70l:Venus-her1 3'UTR-SV40* plasmid. Modifications of the PRE and ARE sequences in the *her1* 3'UTR was performed by site-directed mutagenesis of the *hsp70l:Venus-her1 3'UTR-SV40* reporter using KOD polymerase (EMD Millipore) with mutagenic primers followed by DpnI digestion and transformation into *E. coli*. The full-length 1327 nt *dlc* 3'UTR was cloned by extracting total RNA from WT embyos at mid-segmentation with Trizol Reagent according to manufacturer procedures (Invitrogen/Thermo Fisher Scientific), followed by reverse-transcription with Superscript III (Invitrogen/Thermo Fisher Scientific) using a *dlc*-specific reverse primer followed by PCR amplification of the *dlc 3'UTR* using gene-specific primers containing restriction enzyme sites for cloning. In parallel, construct *hsp70l:Venus-her1 3'UTR-SV40* was digested to remove the *her1 3'UTR* followed by replacement with the *dlc* 3'UTR. Constructs were sequence confirmed. Transgenic lines were generated as previously described using I-SceI-based transgenesis[147], and at least two separate founder lines were analyzed for each transgene (Table 3.1) to minimize the impact of locus-specific insertional effects on transgene expression.

3.3.4 Heat shock assay

Adult fish carrying the stable reporter transgenes were crossed to AB WT fish. Resulting progeny were raised to mid-segmentation, heat shocked at 37°C for 15 minutes, and fixed in 4% PFA at defined intervals post-heat shock. Time points post-heat shock were determined through detection of Venus transcript by

in situ hybridization and qPCR analysis to best display turnover of the reporter. For transgenic lines illustrated in Figures 3.3 and 3.5, 0, 30, 60, and 90 minute time points post-heat shock were selected, for Figures 3.4 and 3.7, 30, 60, and 90 minute time points post-heat shock were selected, for Figure 3.6, 0, 30, and 60 minutes post-heat shock was selected. All transgenic lines were analyzed for *Venus* expression post-heat shock by colorimetric in situ hybridization or qPCR analysis in parallel (each method described below).

3.3.5 mRNA injection

Full-length *pnrc2* cDNA was generated as previously described[48] to create plasmid *SP6-pnrc2-cDNA* (pTLG109). For rescue experiments, WT and mutant *pnrc2* mRNAs were synthesized using the SP6 mMessage Machine Kit (Thermo Fisher), diluted in 0.2M KCl with 0.1% phenol red, and injected into 1-cell stage embryos (40 pg mRNA per embryo). All modifications of the *pnrc2* mRNA were performed by site-directed mutagenesis using KOD polymerase (EMD Millipore) with mutagenic primers followed by DpnI digestion and transformation into *E. coli*. All constructs were sequence verified.

3.3.6 In situ hybridization

Whole mount in situ hybridization was performed as previously described[142,143] using DIG-labeled antisense probes. Riboprobes for *her1, dlc*, and *Venus* were made as previously described[100,118].

3.3.7 RNA extraction

Whole embryos at mid-segmentation (n=10 per time point or condition) were solubilized in Trizol for RNA extraction and purified following standard procedures (Life Technologies). 0.5 -1 ug total RNA was purified and reverse transcribed using random primers or gene specific reverse primers and Superscript III reverse transcriptase (RT) according to the manufacturer's instructions (Life Technologies).

3.3.8 Quantitative PCR

Quantitative PCR was performed using PowerUp SYBR Green Master Mix (Thermo Fisher Scientific), following manufacture's procedures and 4.5 ul cDNA (diluted 1:50) in 10 ul reactions. Negative controls included no-template for each primer set. All reactions were subjected to thermal melting to confirm that each reaction gave single peaks. All reactions were carried out in at least technical duplicate for each of three biological replicates per heat shock line and transcript levels were normalized to *mobk13 (mob4)*[182]. Cycle thresholds (C_t) were determined using the Bio-Rad CFX manager software. Changes in mRNA expression were calculated by $\Delta\Delta C_t = \Delta C_{t\ target} - \Delta C_{t\ control}$. Relative changes in mRNA expression levels are represented graphically as fold changes, wherein relative mRNA fold change = $2^{-\Delta\Delta Ct}$. All data analysis was performed in GraphPad (Prism8).

3.3.9 Microscopy and Imaging

In situ hybridized embryos were mounted in Permount and imaged using an Axiocam HRc digital camera with AxioPlan2 microscope (Zeiss). Immunofluorescent embryos were whole mounted in 80% glycerol and imaged at 20x magnification using MetaMorph software (Molecular Devices) on an Andor™ SpinningDisc Confocal Microscope (Oxford Instruments) with iXon Ultra EMCCD and Nikon Neo cameras; laser wavelength and intensity were set 488 nm and 50% for Dlc protein detection, 488 nm and 100% for Dld protein detection, and bit depth at 16-bit. Maximum intensity projections using MetaMorph software are shown for Dlc, and Dld protein detection (Figure 3.2A-B, C-D).

3.3.10 Immunohistochemistry

All embryos described below were immunostained following standard protocols using 4% PFA fixation, dehydration and rehydration in a methanol series, and incubation in blocking solution for 1 hour. Mid-segmentation embryos from wild-type and *pnrc2*^{oz22} crosses were immunostained in 2% BSA/5% goat serum/0.1% Tween-20/PBS blocking solution with 1:200 dilution anti-zdc2 that recognizes Dlc protein (ab73336, Abcam) according to previously published methods[32] or immunostained in 2% BSA/10% goat serum/0.5% Triton X-100/PBS blocking solution with 1:100 anti-zdd2 that recognizes Dld protein according to previously published methods[148] (ab73331, Abcam), followed by 1:800 dilution goat anti-mouse Alexa-Fluor-488 (A11001, ThermoFisher).

3.4 Results

3.4.1 Zygotic and maternal *pnrc2* promotes cyclic transcript decay

We previously showed that zygotically expressed *pnrc2* promotes decay of cyclic transcripts, including *her1* and *dlc*, during somitogenesis[48]. Because *pnrc2* transcript is detected in wild-type (WT) embryos at early time points including the 8-cell stage[48], we hypothesized that *pnrc2* is maternally provided and may partially compensate for loss of zygotic *pnrc2* function during somitogenesis. To examine maternal *pnrc2* function, we generated maternal-zygotic *pnrc2*^{oz22} (*MZpnrc2*) mutant embryos and compared expression of cyclic transcripts to WT embryos, maternal *pnrc2*^{oz22} *(Mpnrc2)* embryos that possess zygotic *pnrc2* function, and zygotic *pnrc2*^{oz22} (*Zpnrc2*) mutant embryos that have maternal but lack zygotic *pnrc2* function. Consistent with previous results[48], both *her1* and *dlc* transcripts are misexpressed in *Zpnrc2* embryos (Figure 3.1A vs B, E vs F). Interestingly, *her1* and *dlc* expression appear normal in *Mpnrc2* embryos (Figure 3.1A vs C, E vs G), suggesting *pnrc2* zygotic function is sufficient to regulate turnover of cyclic transcripts during somitogenesis. Although zygotic *pnrc2* function is sufficient to promote *her1* and *dlc* transcript decay, *MZpnrc2* embryos lacking both maternal and zygotic *pnrc2* function show an enhanced misexpression phenotype compared to *Zpnrc2* embryos (Figure 3.1B vs D, F vs H). Because colorimetric in situ hybridization is qualitative, we quantified *her1* and *dlc* transcript levels by quantitative PCR (qPCR). To distinguish between transcriptional and post-transcriptional effects, primers that separately anneal to

spliced and unspliced transcript were employed. *MZpnrc2* mutant embryos exhibit ~4-fold accumulation of spliced *her1* and *dlc* transcripts whereas *Mpnrc2* sibling embryos exhibit WT levels of *her1* and *dlc* spliced transcripts (Figure 3.1I and K), indicating that *her1* and *dlc* transcripts accumulate post-transcriptionally in *MZpnrc2* mutants. These results are consistent with our previous work that showed *pnrc2* mutant embryos accumulate clock-associated transcripts due to a post-transcriptional defect[48,100]. Surprisingly, despite accumulation of clock-associated transcripts in *MZpnrc2* mutants and WT transcript levels in *Mpnrc2* mutants, qPCR analysis reveals a ~2-fold decrease of unspliced *her1* and *dlc* transcripts in both *MZpnrc2* and *Mpnrc2* mutants compared to WT embryos (Figure 3.1J and L). Together, these results suggest maternally-provided and zygotically-expressed *pnrc2* promotes the rapid turnover of *her1* and *dlc* transcripts during somitogenesis.

3.4.2 Unlike mRNAs, cyclic proteins do not accumulate in *MZpnrc2* mutants.

Our previous work showed that protein expression of cyclic transcripts such as *dlc* and the segmentation clock-associated transcript *deltaD* (*dld)* are unaffected in zygotic *pnrc2* mutants[48]. To determine if protein expression is also unaffected in *MZpnrc2* mutants, we examined endogenous Dlc and Dld protein expression in *MZpnrc2* mutant and WT embryos by immunofluorescence. Interestingly, while *MZpnrc2* mutant embryos display ~4 fold higher levels of *dlc* transcript than WT embryos (Figure 3.1K), there are no discernible differences in

Dlc protein expression among *MZpnrc2* and WT embryos (Figure 3.2A-B, magnified in A'-B'). Similarly, there are no discernible differences in Dld protein expression among *MZpnrc2* and WT embryos (Figure 3.2C vs D), despite a dramatic accumulation of *dld* transcript in *MZpnrc2* mutant embryos (data not shown). These data provide evidence that despite accumulation of clock-associated transcripts in *MZpnrc2* mutants, clock-associated protein expression is unaffected, which may explain the absence of a morphological segmentation phenotype.

3.4.3 Pnrc2 restores proper *her1* expression in *MZpnrc2* mutants and requires specific residues residing within conserved domains.

Zebrafish *pnrc2* encodes a 148 amino acid protein with highly conserved C-terminal SRC-Homology 3 (SH3) and Nuclear Receptor-box (NR-box) domains[48]. Human PNRC2 interacts with the mRNA decapping enzyme DCP1A through the SH3 domain and with the nonsense-mediated mRNA decay (NMD) effector UPF1 through the NR-box domain and SH3 domain[103,105,130,183,184]. Mutation of W114A in the SH3 domain and deletion of the NR-box abrogates binding to DCP1A and UPF1 and these interactions are required to elicit decay of reporter mRNA[105,107]. Because depletion of zebrafish Upf1 sensitizes embryos to partial loss of Pnrc2 and the SH3 and NR-box domains are 100% identical between human and fish[48], we hypothesized these domains might be essential for Pnrc2-mediated decay of cyclic transcripts. We injected WT and mutant forms of *pnrc2* mRNA into *MZpnrc2* mutants and assayed rescue (Table 3.2). *Cerulean*

coding sequence was translationally fused to WT and mutant forms of *pnrc2* mRNA to validate injected mRNA expression (data not shown). Whereas injection of WT *Cer-pnrc2* mRNA restores proper *her1* expression in *MZpnrc2* mutants, injection of *Cer-pnrc2* mRNA containing the W124A mutation (orthologous to human PNRC2 W114A) into *MZpnrc2* mutants did not restore proper *her1* expression (Table 3.2). Injection of *Cer-pnrc2* with NR-box deletion, however, restored *her1* expression in ~50% of *MZPnrc2* mutant embryos (Table 3.2). Overall, these results suggest that interaction of Pnrc2 with known decay machinery may be necessary for turnover of non-aberrant cyclic transcripts.

3.4.4 The *her1* 3'UTR confers instability to transcripts in a Pnrc2-dependent manner.

While aberrant mRNAs containing well-described features such as premature termination codons (PTCs) are targeted for decay, it remains unclear how non-aberrant cyclic mRNAs are targeted for decay. We set out to answer this question by performing cis-regulatory analysis through the use of inducible reporters. In previous studies, heat shock-induced reporter transcript containing the *her1* 3′UTR decayed rapidly post-induction[32,48] and this destabilizing effect requires Pnrc2 function[48]. To identify sequence elements within the *her1* 3'UTR that are required for Pnrc2-mediated decay, we modified our previously published transgenic heat shock reporter line[48] to drive expression of *Venus* transcript followed by various portions of the *her1* 3'UTR. Because a subset of reporter lines lack the endogenous *her1* polyadenylation (pA) signal, we included

an SV40 pA signal on all reporters, including the full length *her1* 3'UTR, so that all reporters utilize the same pA signal. Use of the SV40 pA was validated by 3' RACE in the last 179 nt *her* 3'UTR reporter used in Figure 3.4 that still maintains the endogenous pA signal (data not shown). As a control for baseline *Venus* stability, *Venus* transcript fused only to the SV40 pA signal (*Venus-SV40*) was developed and tested in parallel. Reporter mRNA containing the full-length *her1* 3'UTR (*Venus-her1 3'UTR-SV40*) is rapidly decayed between 30 to 90 minutes pHS when compared to reporter mRNA devoid of *her1* 3'UTR sequence (*Venus-SV40)* by in situ hybridization (Figure 3.3B-I), demonstrating that the full-length *her1* 3'UTR is sufficient to convey rapid instability. Quantification by qPCR analysis comparing fold-change of the *her1* 3'UTR containing reporter transcript from 30 minutes pHS to 60 and 90 minutes pHS reveals dramatic instability of the reporter by 90 minutes pHS (Figure 3.3J).To test Pnrc2 dependence for rapid reporter decay, *Mpnrc2* and the *MZpnrc2* mutant embryos were heat shocked and analyzed in parallel. *Mpnrc2* and WT embryos expressing *Venus-her1 3'UTR-SV40* reporter mRNA are indistinguishable across all pHS time points (Figure 3.3 F-M). In contrast, reporter mRNA in *MZpnrc2* mutant embryos is stabilized (Figure 3.3 N-Q), indicating that Pnrc2-mediated decay of *her1* transcript occurs through destabilizing features of the *her1* 3'UTR.

3.4.5 The last half of the *her1* 3'UTR promotes Pnrc2-mediated decay

To define regions of the *her1* 3'UTR that are necessary and sufficient for Pnrc2-dependent decay, we conducted truncation analysis of the *her1* 3'UTR.

Transgenic lines were generated with *hsp70l* promoter sequence driving expression of *Venus* coding sequence fused to either the first 362 nts or the last 363 nts of the *her1* 3'UTR followed by a SV40 pA. Induction of the reporter was performed as in Figure 3.3A, and time points of 30, 60, and 90 minutes pHS were examined because of lack of decay and/or continued induction from 0 to 30 minutes pHS (Figure 3.3 and data not shown). Reporter lines containing only the first 362 nts of the *her1* 3'UTR display minimal destabilization by 90 minutes pHS by in situ hybridization (Figure 3.4A-C). Reporter lines containing the last 363 nts of the *her1* 3'UTR display instability much like the *Venus-her1 3'UTR* reporter (Figure 3.4D-F). Consistent with in situ hybridization results, qPCR analysis comparing fold-change of the reporter fused to the last 363 nts of the *her1* 3'UTR displays dramatic instability by 90 minutes pHS (Figure 3.4G). qPCR analysis of the reporter carrying the first 362 nts of the *her1* 3'UTR displays minimal decay by 90 minutes pHS (Figure 3.4G). These data indicate the last 363 nts of the *her1* 3'UTR are necessary and sufficient to confer instability to reporter transcript.

3.4.6 The last 179 nucleotides of the *her1* 3'UTR are sufficient and necessary for Pnrc2-mediated decay of reporter transcripts

To identify specific features of the *her1* 3'UTR that confer destabilization, we conducted further truncation analysis on the last 363 nts of the *her1* 3'UTR. Heat-shock inducible transgenic lines were generated as previously described carrying only the last 179 nts of the *her1* 3'UTR. Reporters fused to the last 179 nts of the *her1* 3'UTR become destabilized from 30 to 90 minutes pHS by in situ

hybridization (Figure 3.4H-J). Destabilization of the reporter by the last 179 nts of the *her1* 3'UTR is similar to the destabilization observed by the full-length *her1* 3'UTR and the last 363 nts of the *her1* 3'UTR by in situ hybridization (Figure 3.3F-I and Figure 3.4D-F vs Figure 3.4H-J), suggesting instability elements of the *her1* 3'UTR were not lost in the truncation. Overall, the collection of various truncations of the *her1* 3'UTR, summarized in Figure 3.5, indicate that the last 179 nts are required for instability. To determine if destabilizing features within the last 179 nts of the *her1* 3'UTR are Pnrc2-dependent, we examined destabilization of the last 179 nt *her1* 3'UTR reporter in *Mpnrc2* and *MZpnrc2* mutant backgrounds. *MZpnrc2* mutants display persistence of the reporter at time points pHS not observed in WT embryos (Figure 3.4H-M). In *Mpnrc2* mutants, the reporter is destabilized similar to WT embryos (data not shown). These experiments reveal similar results compared to the full-length *her1* 3'UTR reporter (Figure 3.3F-Q), but persistence of the last 179 nt *her1* 3'UTR reporter does not appear as robust in *MZpnrc2* mutants as the full-length *her1* 3'UTR reporter, suggesting *her1* 3'UTR elements outside those in the last 179 nts may be important for recruitment of a Pnrc2-containing decay complex.

3.4.7 The *dlc* 3'UTR confers instability to reporter transcript in a Pnrc2-dependent manner.

Pnrc2 function is important for proper *her1* expression and also promotes proper *dlc* expression. To determine if the *dlc* 3'UTR contains features that promote Pnrc2-dependent decay, we modified our heat shock inducible system

to drive expression of *Venus* transcript followed by the full-length 1327 nt *dlc* 3'UTR that includes an SV40 pA (*Venus-dlc 3'UTR-SV40*) and compared reporter expression between WT, *Mpnrc2*, and *MZpnrc2* embryos. Time points of 0, 30, and 60 minutes pHS were chosen to best capture decay by in situ hybridization. We find that reporter expression is indistinguishable between WT and *Mpnrc2* mutant embryos across all time points observed (Figure 3.6A-C vs D-F). In contrast, reporter expression in *MZpnrc2* mutants is stabilized relative to WT and *Mpnrc2* mutant embryos at 30 and 60 minute time points (Figure 3.6A-F vs G-I). These data reveal that in addition to the *her1* 3'UTR, the *dlc* 3'UTR promotes Pnrc2-dependent transcript decay and suggests cyclic transcripts may contain a common Pnrc2-dependent decay feature(s) within their 3'UTRs.

3.4.8 Both *her1* and *dlc* 3'UTRs contain Pumilio response and AU-rich elements.

To determine if the *her1* and *dlc* 3'UTRs contain a common destabilizing feature, we searched for shared motifs using MEME analysis[185]. Because the last 179 nts of the *her1* 3'UTR is necessary and sufficient for Pnrc2-mediated decay, we compared this region with the *dlc* 3'UTR and identified two common motifs: a Pumilio response element (PRE) and an AU-rich element (ARE) (Figure 3.6J). The *her1* 3'UTR contains a single 5'UGUAHAUA PRE within the minimal destabilizing 179 nt region while the *dlc* 3'UTR contains three 5'UGUAHAUA PREs. The *her1* 3'UTR also contains a single 5'UAUUUAU ARE located near the PRE in the last 179 nts of the 3'UTR and the *dlc* 3'UTR contains three

5'UAUUUAU AREs. Because PREs and AREs are associated with mRNA instability[77,126], we focused on these motifs to determine their contribution to cyclic transcript turnover.

3.4.9 The *her1* PRE and ARE promote transcript decay.

To determine if the *her1* PRE and ARE promote decay of reporter transcript, we modified the *Venus-her1 3'UTR-SV40* reporter by mutation of the PRE or ARE and compared *Venus* expression in parallel with the unmodified *Venus-her1 3'UTR-SV40* reporter. The PRE in the *her1* 3'UTR was disrupted by replacement of PRE base positions 2 and 3 from GU to CC, a replacement that disrupts the ability of human PUMILIO to bind target mRNAs[186]. Reporter mRNA carrying the PRE mutation appears stabilized relative to unmodified *Venus-her1 3'UTR-SV40* reporter mRNA (Figure 3.7A-F). Consistent with in situ hybridization results, qPCR analysis reveals a stabilizing effect from PRE mutation, shifting the reporter half-life from 46.5 to 70.9 minutes when compared to the unmodified *Venus-her1 3'UTR-SV40* reporter (Figure 3.7G). To determine the contribution of the *her1* ARE, ARE positions 3-5 were changed from UUU to CCC, a replacement that disrupts ARE-binding protein association with target mRNAs[187]. Reporter mRNA carrying the ARE mutation also appears stabilized relative to unmodified *Venus-her1 3'UTR-SV40* reporter mRNA (Figure 3.7H), shifting reporter half-life from 46.5 to 57.0 minutes. Together, these results suggest that both the PRE and ARE in the *her1* 3'UTR promote transcript decay.

3.5 Discussion

In this work, we present evidence that Pnrc2 promotes 3'UTR-mediated mRNA decay of the cyclic genes *her1* and *dlc*. This work builds upon evidence that Pnrc2 promotes decay of non-aberrant transcripts[48,107], and identifies mRNA features that promote Pnrc2-mediated decay. Human PNRC2 is implicated in mRNA turnover through interactions with decay factors SMG6, DCP1A, UPF1, and STAU1, and studies have shown PNRC2 functions in decay of PTC-containing reporter transcripts[62,103,105,127-129]. However, a recent study found that levels of PTC-containing reporter transcripts were unaffected by PNRC2 knockdown[107]. These conflicting results suggest Pnrc2 function may be differentially required in different cell types, developmental stages, or environmental conditions, or may reflect partial redundancy of Pnrc2 with other decay factors and demonstrates a need to better understand Pnrc2-dependent decay in vivo. We show here the last 179 nts of the *her1* 3'UTR are necessary and sufficient for Pnrc2-dependent decay of non-PTC containing reporter mRNA. We show the full-length *dlc* 3'UTR also confers Pnrc2-mediated decay to reporter transcripts, demonstrating elements within cyclic transcript 3'UTRs are sufficient for triggering Pnrc2-dependent decay. Both the *her1* and *dlc* 3'UTRs contain at least one PRE and ARE, raising the possibility that Pnrc2 promotes decay via Pumilio and/or ARE-BPs. Future analysis examining interaction of Pum1, Pum2, and ARE-BPs with Pnrc2 will provide a better understanding of mechanisms by

which Pnrc2 regulates transcript stability and provide insight to pathways in which Pnrc2-mediated decay functions.

Maternal *pnrc2* also regulates cyclic transcript turnover

Zebrafish utilize a large contribution of maternally-provided mRNA and proteins due to external fertilization[188]. We show here maternal deposition of *pnrc2* partially compensates for loss of zygotic *pnrc2* during somitogenesis. Embryos without functional maternal and zygotic *pnrc2* display a stronger accumulation of *her1* and *dlc* transcripts compared to embryos without zygotic *pnrc2*, suggesting maternally provided *pnrc2* also mediates cyclic transcript stability (Figure 3.1). Interestingly, loss of functional maternal *pnrc2* has no consequence on *her1* and *dlc* transcript levels when *pnrc2* is still zygotically transcribed, suggesting zygotic *pnrc2* expression alone is sufficient to clear cyclic transcripts during somitogenesis. Because reporter expression in *Mpnrc2* mutant embryos is indistinguishable from reporter expression in wild-type embryos (Figure 3.3 and 3.6), it appears that zygotically-expressed *pnrc2* is sufficient to regulate cyclic transcript turnover. Incomplete compensation of *Zpnrc2* mutants by maternal *pnrc2* is likely the result of eventual depletion of maternal *pnrc2* during somitogenesis, but post-transcriptional processes such as splicing and/or translation may differ between zygotic *pnrc2* and maternal *pnrc2* and future studies should examine these processes in *Zpnrc2* and *Mpnrc2* mutants.

Other cyclic transcript 3'UTRs contain Pnrc2-dependent instability elements

Our previous work demonstrates the full-length *her1* 3'UTR is sufficient to confer Pnrc2-mediated decay[48], but it was unknown if other cyclic transcript 3'UTRs maintained this capacity. We show here the full-length *dlc* 3'UTR is also capable of destabilizing transcripts in a Pnrc2-dependent manner (Figure 3.6), suggesting a conserved mechanism of Pnrc2-dependent destabilization may regulate cyclic transcripts through 3'UTR interactions. The 1327 nt *dlc* 3'UTR is almost twice the length of the 725 nt *her1* 3'UTR, and more rapid destabilization of reporter constructs by the *dlc* 3'UTR may be attributed to decay factors such as UPF1 that display preference to longer 3'UTRs[189]. Identification of additional Pnrc2-regulated "destabilizing" 3'UTRs will provide a greater opportunity to identify and test conserved decay features of cyclic 3'UTRs and determine if 3'UTR length is a factor in Pnrc2-mediated decay. Future investigations should examine the 3'UTR of other endogenous Pnrc2-regulated transcripts such as *her7* and *dld* to determine if common conserved features regulate decay.

PRE and ARE motifs are found in multiple cyclic transcripts

Transcriptome-wide analyses show that the PRE is among the features most strongly correlated with mRNA instability[78-80], and a recent study found global enrichment of PREs and AREs in the 3'UTR of maternal transcripts rapidly degraded during zebrafish embryogenesis[81]. Our work provides evidence that disruption of the PRE and ARE in the *her1* 3'UTR affects destabilization of

reporter transcripts (Figure 3.7), suggesting these features may regulate instability of endogenous *her1* transcript. Cyclic transcripts such as *dlc* and *her7* and the clock-associated transcript *dld* also contain putative PRE and ARE motifs (Figure 3.6J and data not shown), suggesting PRE and ARE motifs may function in the regulation of multiple cyclic transcripts during somitogenesis. The *dlc* 3'UTR appears to confer more rapid destabilization of reporter transcripts than the *her1* 3'UTR, and this may be contributed to the presence of multiple PREs and AREs in the 3'UTR, allowing for recruitment of many decay factors. Because mutation of the PRE or ARE alone are not sufficient to fully stabilize reporter mRNA (Figure 3.7G-H), these motifs may function independently and future experiments should investigate the function of both the ARE and PRE sequences in the regulation of endogenous *her1*, *dlc*, *her7*, and *dld* expression through precise mutagenesis of both elements in the endogenous 3'UTR sequence.

We cannot rule out the possibility that decay features other than the PRE and ARE also function in the regulation cyclic transcripts. A canonical 5'UGCUGU Muscleblind-like 1 (MBNL1) binding motif is present in the last 179 nts of the *her1* 3'UTR and the *dlc* 3'UTR. MBNL1 regulates turnover of mRNA through 3'UTR interactions[190,191], and future studies should also examine function of the MBNL1 binding motif in cyclic transcript turnover. There is also potential for a secondary structure element that is sustained in the last 179 nts of the *her1* 3'UTR that recruits decay factors. Further mutagenesis experiments of the *her1*

3'UTR will help determine if features outside of the PRE and ARE also function to destabilize cyclic transcripts.

Pumilio proteins and ARE-BPs may regulate cyclic transcript expression during somitogenesis

PREs are well-studied binding sites for Pumilio proteins across a variety of species[74-76,192]. Studies have shown human PUM1 and PUM2 associate with overlapping sets of PRE-containing mRNAs[193-196], and both PUM1 and PUM2 must be simultaneously depleted to fully alleviate PRE-mediated repression[74,197], suggesting partial redundancy of PUM1 and PUM2 proteins. Pumilio proteins confer instability through recruitment of the major deadenylation machine, the Ccr4-Not complex (CNOT) to target mRNAs[74,82,83,198,199], but also repress protein levels through antagonism of poly(A)-binding protein (PABP)[74,198,200]. Repression by Pumilio proteins have been found to function in a range of biological processes including growth and development, gametogenesis, and neurogenesis[195,201-207], and dysfunction of Pumilio proteins have been linked to diseases such as neurodegeneration and cancer[201,206,208,209].

Zebrafish express both *pum1* and *pum2* transcript throughout somitogenesis[210], and our data suggests Pum1 and/or Pum2 may interact and regulate decay of *her1* and other cyclic genes. Normal cyclic protein levels in *MZpnrc2* mutants (Figure 3.2) may be explained by translational repression of accumulating cyclic transcripts by Pum1 and/or Pum2 and future genetic studies should examine cyclic transcript expression in *pum1* and *pum2* single mutants,

pum1; *pum2* double mutants, and *pum1*;*pum2*;*pnrc2* triple mutants. Because of the redundant function of human PUM1 and PUM2, we hypothesize *pum1*;*pum2* double mutants will impact cyclic transcript expression and anticipate both cyclic transcript and protein will accumulate in *pum1;pum2;pnrc2* triple mutants, leading to disrupted oscillatory expression and segmentation defects.

Interestingly, human *PNRC2* transcript and zebrafish *pnrc2* transcript both contain a PRE itself, and studies identifying direct interactions of human PUM1 and PUM2 identified *PNRC2* as a top target[192,193,196,211]. A recent study has also shown knockdown of PUM1 and PUM2 causes upregulation of *PNRC2* transcript[197], further supporting *PNRC2* expression itself is regulated by Pumilio proteins. These findings suggest Pumilio proteins may also indirectly regulate turnover of cyclic transcripts through regulation of Pnrc2 expression and future experiments should examine expression of *pnrc2* transcript and Pnrc2 protein in *pum1;pum2* mutants during somitogenesis.

Our data also show disruption of the ARE in the *her1* 3'UTR affects stability of reporter transcript (Figure 3.7H). Many factors recognize AREs and not only function to destabilize but also stabilize transcripts. Examples of well-studied destabilizing ARE-BPs are the ARE/poly(U)-binding/degradation factor 1 (AUF1), tristetrapolin (TTP), and KH-type splicing regulatory protein (KSRP)[66-68,72,210]. Other ARE-BPs such as TIA-1 and TIAR have been found to inhibit translation[212-214]. Similar to Pumilio-mediated repression, deadenylation is the first and rate-limiting step in degradation of many ARE-containing mRNAs[215-220].

Zebrafish orthologs of AUF1, KSRP, TTP, and TIA-1 are all expressed throughout somitogenesis[210], and future studies should investigate the role of ARE-BPs in the turnover of *her1* and *dlc* transcripts. Normal cyclic protein levels in *MZpnrc2* mutants (Figure 3.2) may also be explained by translational repression by ARE-BPs such as TIA-1 and future work should investigate the role of the ARE-BPs in the regulation of cyclic transcript and protein expression.

A recent study found inhibition of the CCR4-NOT deadenylation complex increases abundance of *her1* and *her7* transcripts in zebrafish and suggests features in the *her1* and *her7* 3'UTRs may recruit the CNOT deadenylase[221]. PRE and ARE motifs confer transcript instability through deadenylation, and our work and others raises the possibility that recruitment of the CNOT deadenylase to the *her1* 3'UTR may be through Pumilio proteins and/or ARE-BPs recognizing the PRE or ARE. Future biochemical and genetic approaches should examine interactions of the ARE and PRE motifs in cyclic transcripts to determine if Pum1, Pum2 and/or ARE-BPs directly bind and influence transcript stability.

Overall, we propose Pnrc2 regulates cyclic transcript expression through 3'UTR-mediated mRNA decay. Features in the last 179 nucleotides (nts) of the *her1* 3'UTR are necessary and sufficient to confer Pnrc2-mediated decay to reporter transcript and the *dlc* 3'UTR also confers Pnrc2-dependent decay to reporter transcript. We have identified a PRE and ARE motif in the last 179 nts of the *her1* 3'UTR and demonstrate that both motifs promote turnover of reporter transcripts. Future biochemical, molecular, and genetic studies of Pnrc2, Pum1,

Pum2, and ARE-BPs will provide a deeper understanding of regulators of the segmentation clock and post-transcriptional mechanisms that regulate oscillatory expression.

3.6 Figures

Figure 3.1. Maternal and zygotic *pnrc2* promotes proper *her1* and *dlc* expression.

Wild-type (WT), zygotic *pnrc2*^{oz22} (*Zpnrc2*), maternal *pnrc2*^{oz22} (*Mpnrc2*), and maternal-zygotic *pnrc2*^{oz22} (*MZpnrc2*) mutant embryos were raised to mid-segmentation stage (16-18 hpf) and probed for *her1* (A-D) and *dlc* expression (E-F) by in situ hybridization ($n \geq 10$ each). WT, *MZpnrc2*, and *Mpnrc2* mutant embryos (n = 10 each) were analyzed by qPCR using primers that span exon-exon boundaries to detect spliced *her1* (I) and *dlc* (K) transcripts or primers that span intron-exon boundaries to detect *her1* (J) and *dlc* (L) unspliced transcripts. *MZpnrc2* mutant embryos display ~4-fold higher levels of spliced *her1* and *dlc* mRNA by qPCR and *Mpnrc2* mutant embryos display similar levels of spliced *her1* and *dlc* mRNA compared to WT embryos by qPCR (I and K). Both *MZpnrc2* and *Mpnrc2* mutant embryos display a ~2-fold decrease in unspliced *her1* and *dlc* transcripts compared to WT embryos by qPCR (J and L). hpf = hours post-fertilization.

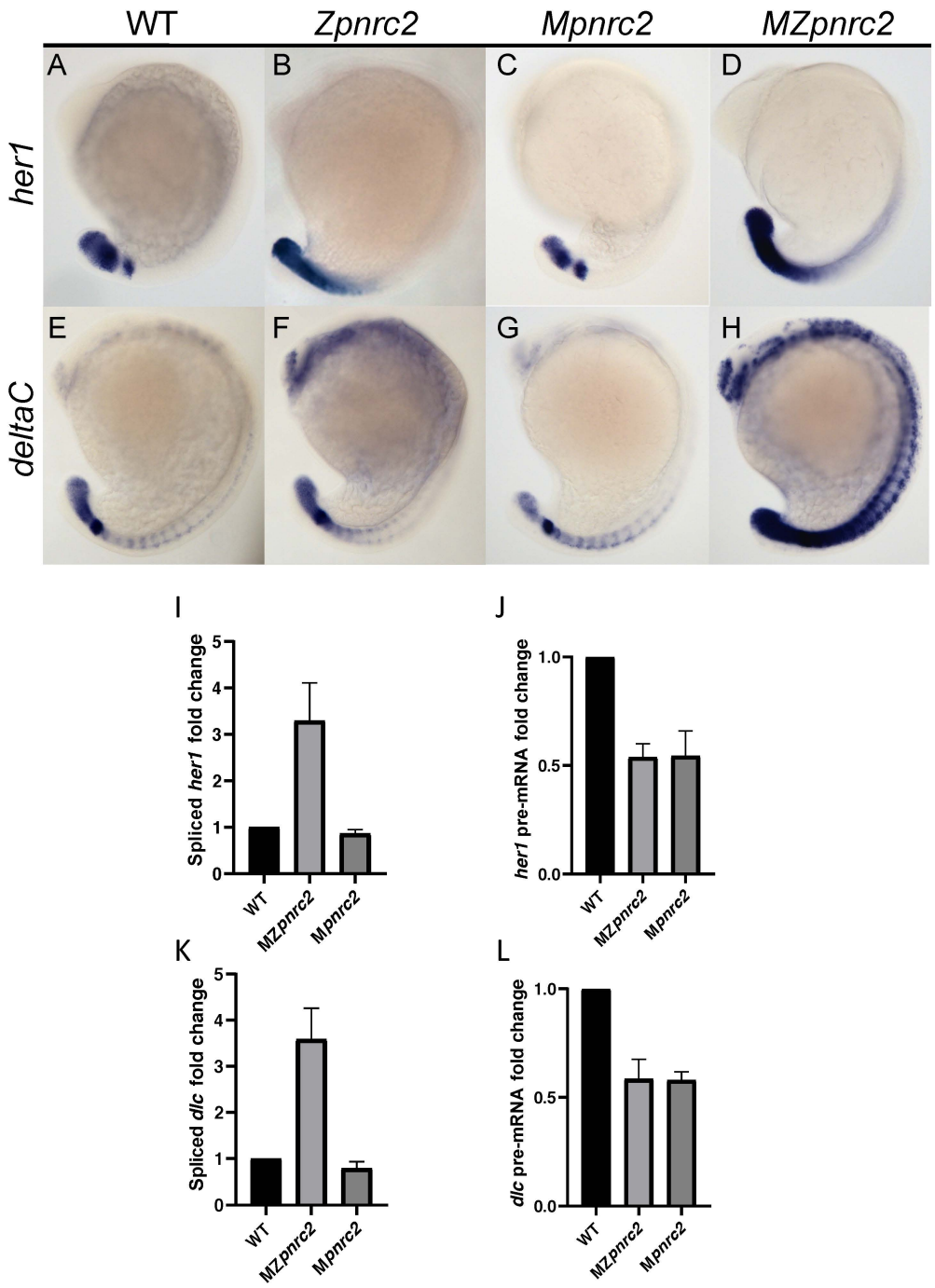
WT
Zpnrc2
Mpnrc2
MZpnrc2
A
B
C
D
her1
E
F
G
H
deltaC
I
Spliced her1 fold change
0
1
2
3
4
5
WT
MZpnrc2
Mpnrc2
J
her1 pre-mRNA fold change
0.0
0.5
1.0
WT
MZpnrc2
Mpnrc2
K
Spliced dlc fold change
0
1
2
3
4
5
WT
MZpnrc2
Mpnrc2
L
dlc pre-mRNA fold change
0.0
0.5
1.0
WT
MZpnrc2
Mpnrc2

Figure 3.2. Dlc and Dld protein levels are not elevated in maternal-zygotic *pnrc2*^{oz22} mutants during somitogenesis.

WT and *MZpnrc2* mutants were fixed during mid-segmentation and endogenous Dlc or Dld protein was detected by immunofluorescence (A-D) (n = 3 WT and n = 3 *MZpnrc2* mutants per antibody). (A') Magnified image of the PSM of the WT embryo probed for Dlc in A. (B') Magnified image of the PSM of the *MZpnrc2* mutant embryo probed for Dlc in B.

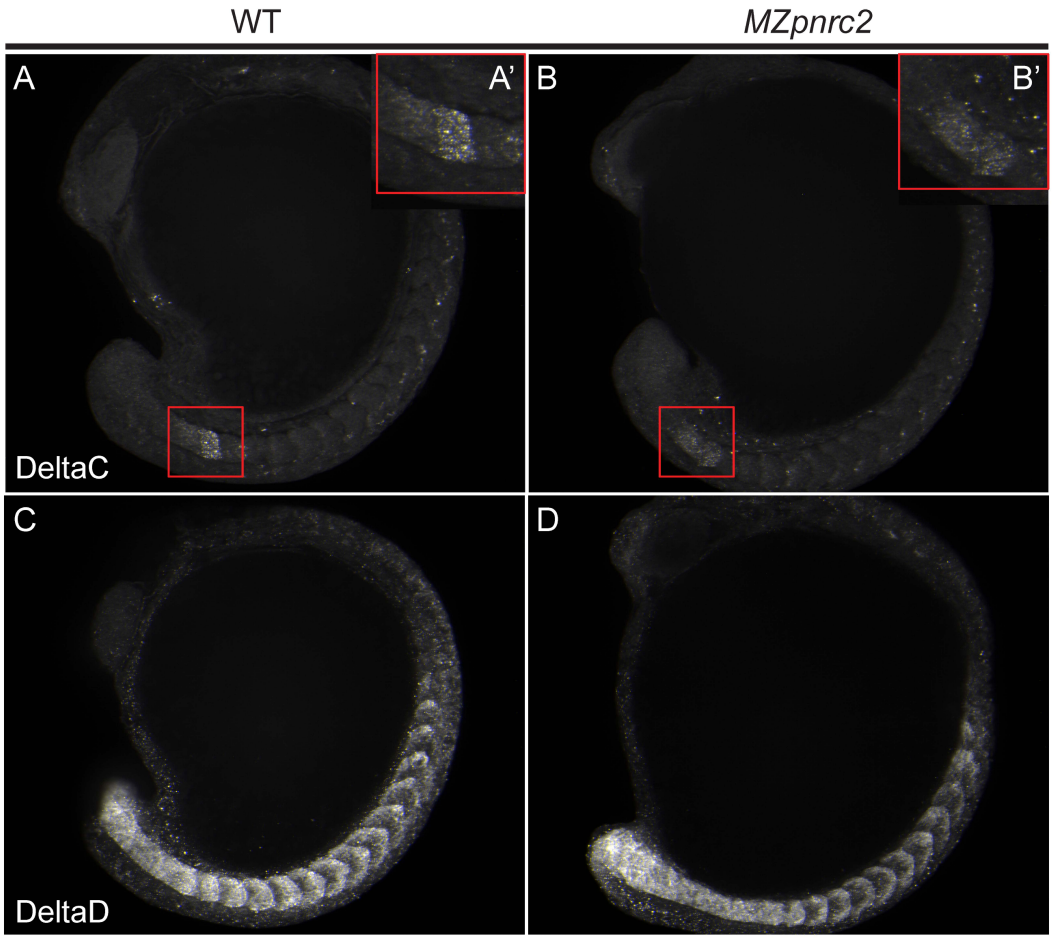
WT
MZpnrc2
A
A'
B
B'
DeltaC
C
D
DeltaD

Figure 3.3. The *her1* 3'UTR confers Pnrc2-dependent instability to reporter transcripts.

(A) Diagram illustrating the heat-shock protocol used for transgenic lines in this study. Transgenic embryos carrying the *hsp70l:Venus-her1 3'UTR-SV40* reporter or *hsp70l:Venus-SV40* reporter were raised to mid-segmentation stage, heat-shocked for 15 minutes, then collected at the indicated minutes pHS and processed by *Venus* in situ hybridization (B-I) ($n \geq 10$ embryos per time point). *Venus* transcript is not detected in the absence of heat-shock (n = 10) (not shown). (J) qPCR analysis comparing *Venus* transcript fold-change from 30 minutes pHS to 60 and 90 minutes pHS between the *hsp70l:Venus-her1 3'UTR-SV40* and *hsp70l:Venus-SV40* reporter lines (n = 10 per time point). (J-Q) Mid-segmentation stage *Mpnrc2* mutant embryos and *MZpnrc2* mutant embryos carrying the *hsp70l:Venus-her1 3'UTR-SV40* reporter were heat-shocked and processed by *Venus* in situ hybridization as previously stated ($n \geq 10$ embryos per time point). Representative embryos were genotyped post-imaging to confirm genotype. pHS = post heat-shock. (The *hsp70l:Venus-her1 3'UTR-SV40* and *hsp70l:Venus-SV40* reporters were constructed by Nicolas L. Derr.)

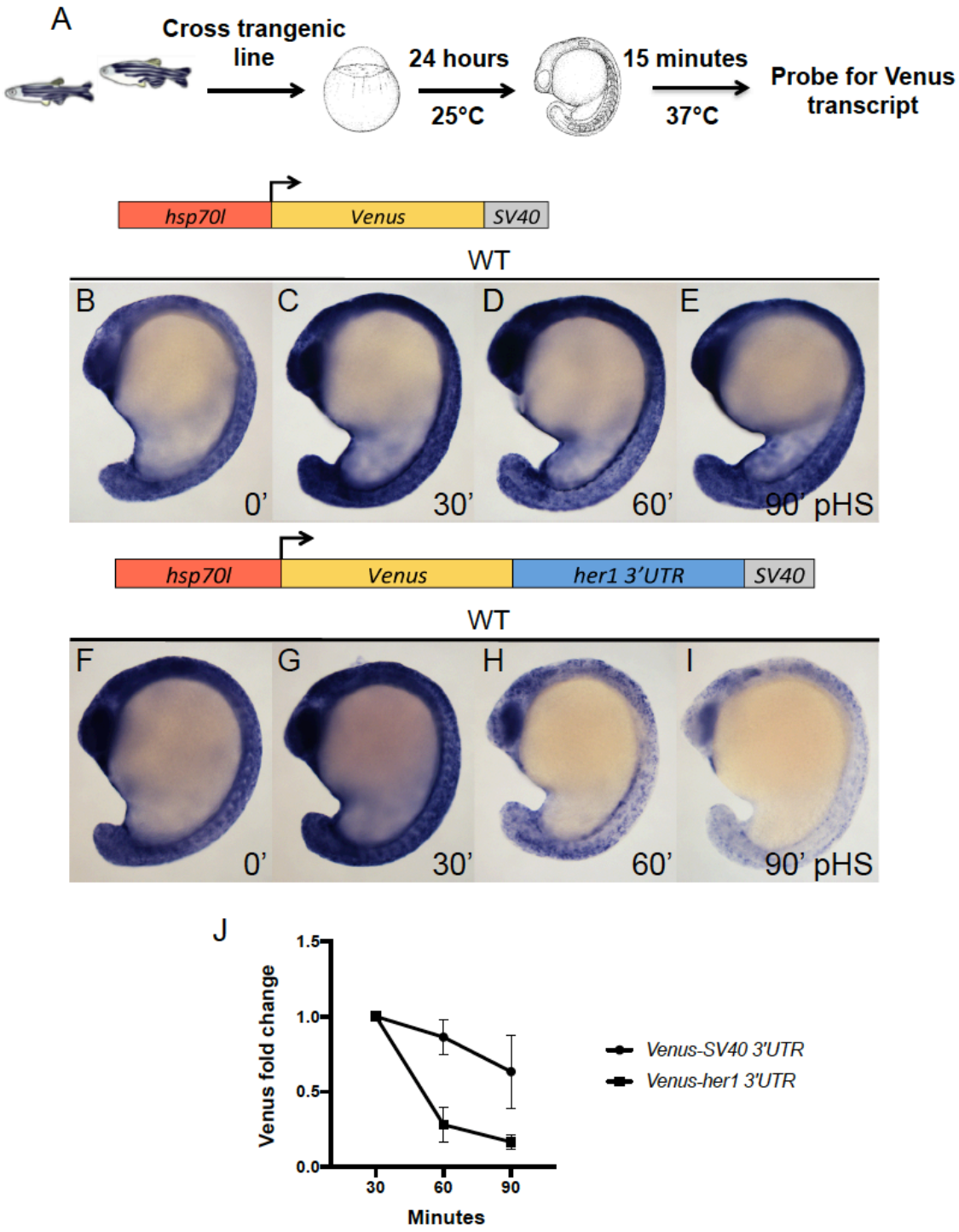

(*Figure 3.3 continued on next page*)

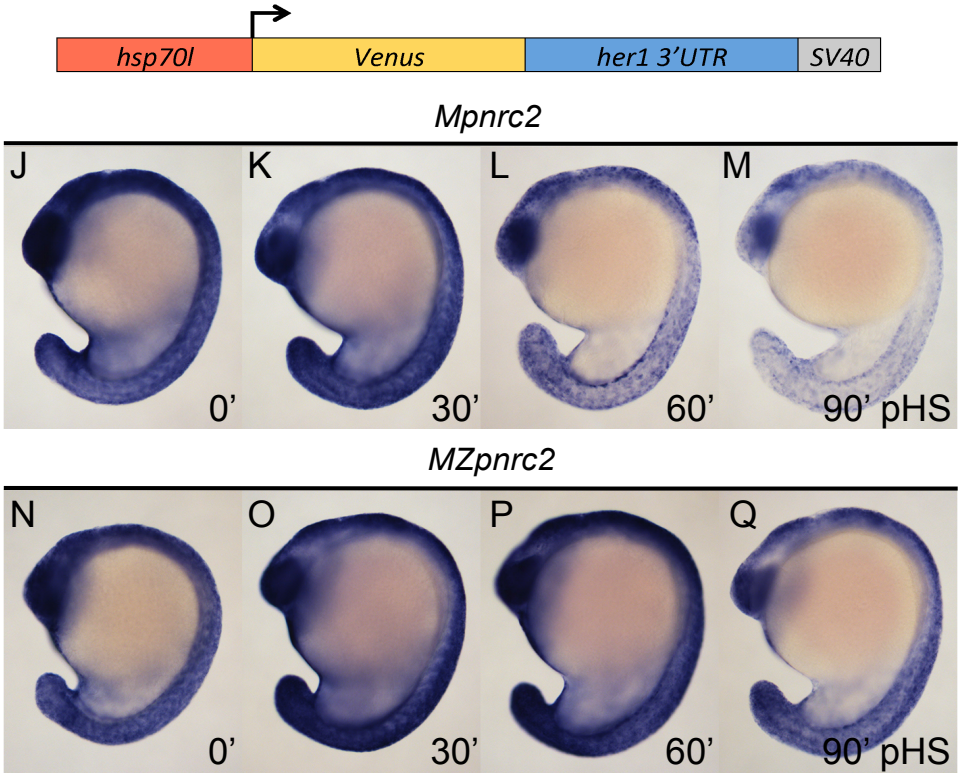
hsp70l
Venus
her1 3'UTR
SV40
Mpnrc2
J
K
L
M
0'
30'
60'
90' pHS
MZpnrc2
N
O
P
Q
0'
30'
60'
90' pHS

Figure 3.4. The last 179 nucleotides of the *her1* 3'UTR is sufficient for Pnrc2-mediated decay of reporter transcripts.

Transgenic embryos carrying the *hsp70l:Venus-her1 3'UTR∆363-725-SV40* reporter or *hsp70l:Venus-her1 3'UTR∆1-362-SV40* reporter were raised to mid-segmentation stage and heat-shocked for 15 minutes, then collected at the indicated minutes pHS and processed by *Venus* in situ hybridization (A-F) ($n \geq 6$ per time point). (G) qPCR analysis comparing *Venus* transcript fold-change from 30 minutes pHS to 60 and 90 minutes pHS between the *hsp70l:Venus-her1 3'UTR∆363-725-SV40* or *hsp70l:Venus-her1 3'UTR∆1-362-SV40* reporter lines (n = 10 per time point). Mid-segmentation stage WT and *MZpnrc2* mutant embryos carrying the *hsp70l:Venus-her1 3'UTR∆1-546-SV40* reporter construct were heat-shocked and processed by *Venus* in situ hybridization as previously stated (H-M) ($n \geq 10$ embryos per time point). Representative embryos were genotyped post-imaging to confirm genotype. pHS = post heat-shock; nts = nucleotides. (The *hsp70l:Venus-her1 3'UTR∆363-725-SV40* and *hsp70l:Venus-her1 3'UTR∆1-362-SV40* reporters were constructed by Nicolas L. Derr.)

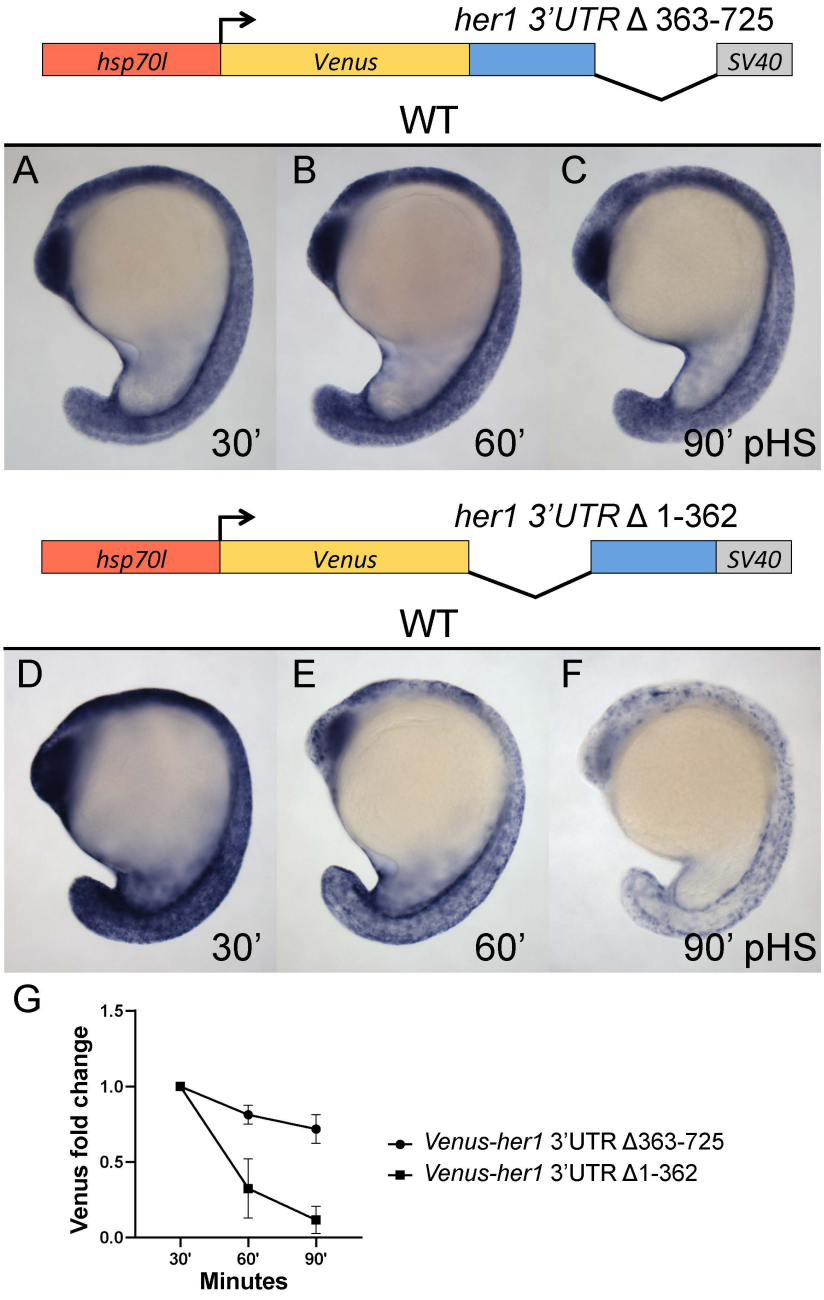

(*Figure 3.4 continued on next page*)

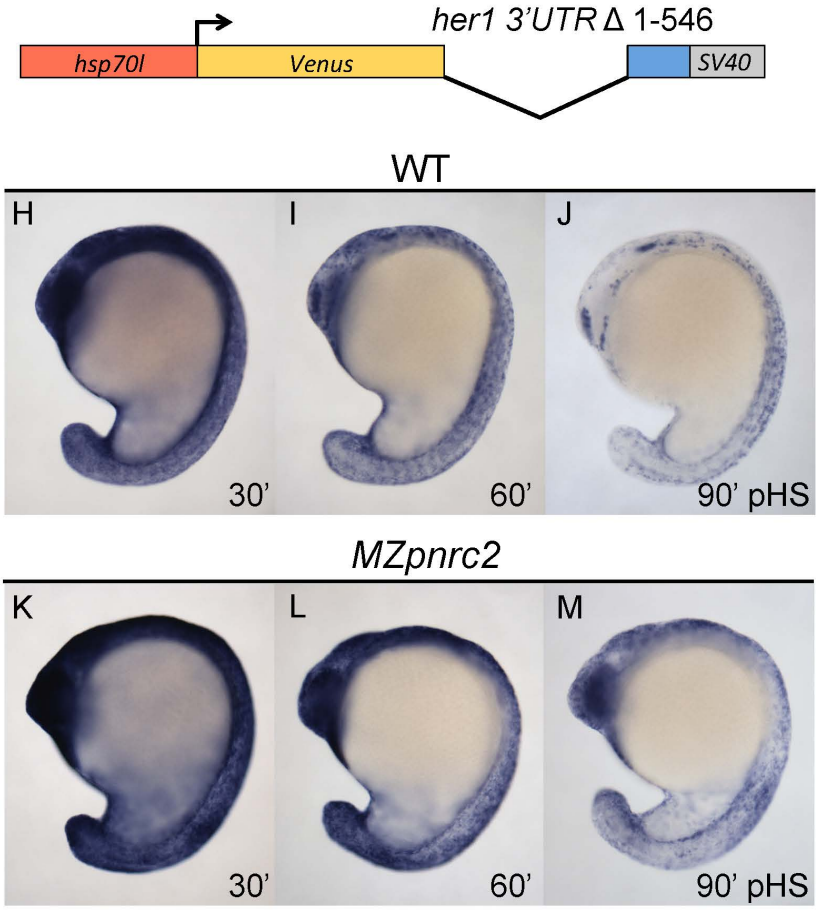
her1 3'UTR Δ 1-546
hsp70l
Venus
SV40
WT
H
I
J
30'
60'
90' pHS
MZpnrc2
K
L
M
30'
60'
90' pHS

Figure 3.5. Reporter constructs that contain the last 179 nucleotides of the *her1* 3'UTR become rapidly destabilized.

Summary of reporter destabilization in transgenic embryos carrying various truncations of the *her1* 3'UTR (A-F). All lines were raised to mid-segmentation stage and heat-shocked for 15 minutes, then collected and processed by *Venus* in situ hybridization at 0, 30, 60, and 90 minutes pHS. (A) *hsp70l:Venus-her1 3'UTR-SV40* reporter. (B) *hsp70l:Venus-her1 3'UTR∆1-362-SV40* reporter line. (C) *hsp70l:Venus-her1 3'UTR∆363-725-SV40* reporter. (D) *hsp70l:Venus-her1 3'UTR∆1-546-SV40* reporter. (E) *hsp70l:Venus-her1 3'UTR∆1-362;∆547-725-SV40* reporter. (F) *hsp70l:Venus-her1 3'UTR∆363-546-SV40* reporter. At least 2 separate stable lines were established and analyzed for each reporter construct (Table 3.1). pHS = post heat-shock. (The *hsp70l:Venus-her1 3'UTR-SV40, hsp70l:Venus-her1 3'UTR∆363-725-SV40,* and *hsp70l:Venus-her1 3'UTR∆1-362-SV40* reporters were constructed by Nicolas L. Derr.)

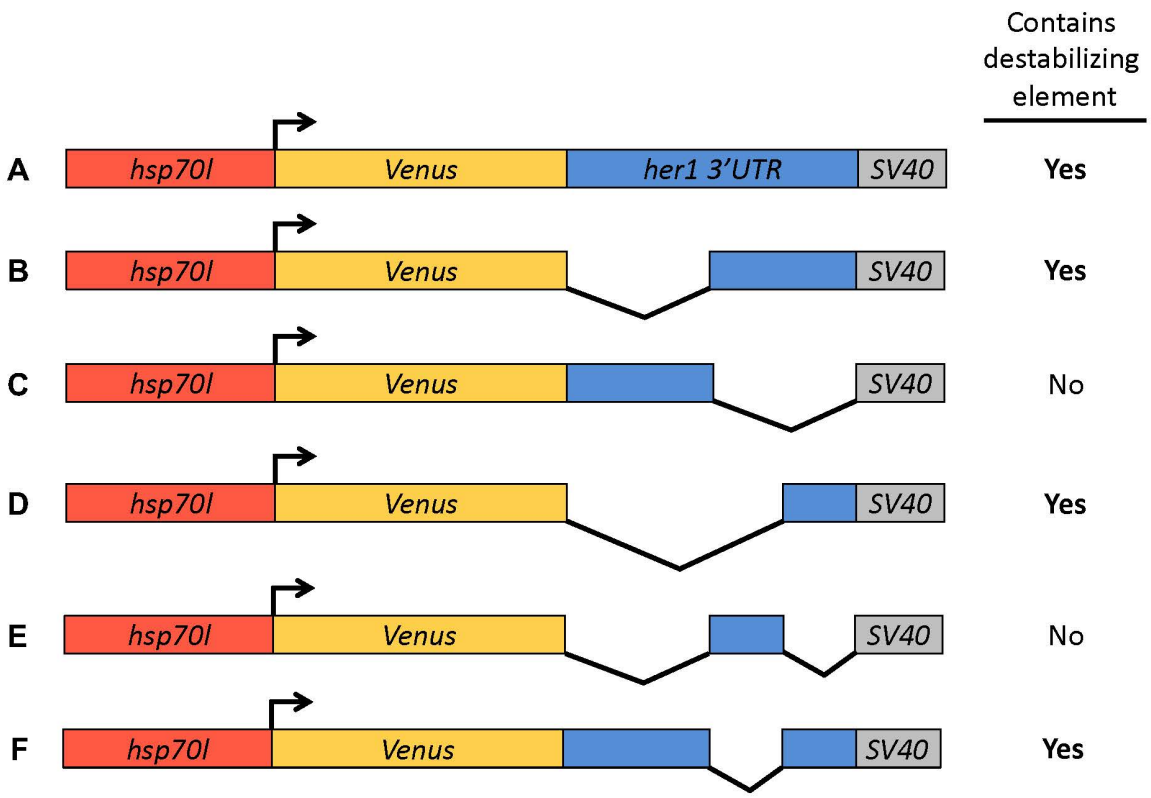
Contains destabilizing element
A
hsp70l
Venus
her1 3'UTR
SV40
Yes
B
hsp70l
Venus
SV40
Yes
C
hsp70l
Venus
SV40
No
D
hsp70l
Venus
SV40
Yes
E
hsp70l
Venus
SV40
No
F
hsp70l
Venus
SV40
Yes

Figure 3.6. The *dlc* 3'UTR confers Pnrc2-mediated decay to reporter transcripts.

Transgenic embryos carrying the *hsp70l:Venus-dlc 3'UTR-SV40* reporter were raised to mid-segmentation stage and heat-shocked for 15 minutes, then collected at the indicated minutes pHS and processed by *Venus* in situ hybridization (A-C) ($n \geq 10$ embryos per time point). *Mpnrc2* (D-F) and *MZpnrc2* mutant embryos (G-I) carrying the *hsp70l:Venus-dlc 3'UTR-SV40* reporter were heat-shocked and processed for *Venus* transcript as previously stated ($n \geq 10$ embryos per time point). Representative embryos were genotyped post-imaging to confirm genotype. (J) MEME analysis[185] identifies a PRE (yellow), and ARE (white) in the last 179 nts of the *her1* 3'UTR and in the full-length *dlc* 3'UTR. The *her1* 3'UTR contains a single 5' UGUAAAUA PRE, and the *dlc* 3'UTR contains three 5' UGUAHAUA PREs. The *her1* 3'UTR contains a single 5' UAUUUAU ARE and the *dlc* 3'UTR contains three 5' UAUUUAU AREs. pHS = post heat-shock; PRE = Pumilio response element; ARE = AU-rich element. (The *hsp70l:Venus-dlc 3'UTR-SV40* reporter was constructed by Zachary T. Morrow.)

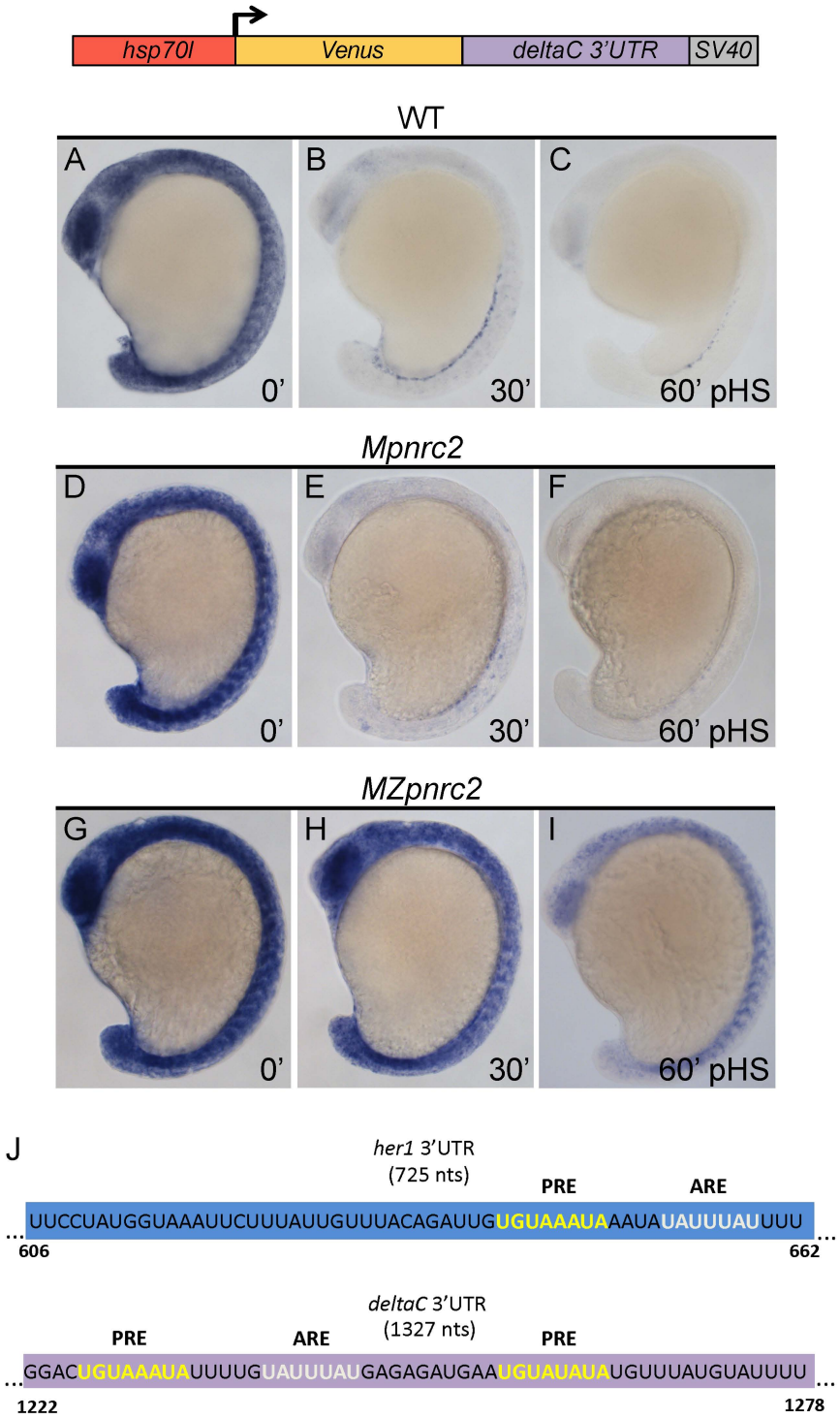
hsp70l
Venus
deltaC 3'UTR
SV40
WT
A
B
C
0'
30'
60' pHS
Mpnrc2
D
E
F
0'
30'
60' pHS
MZpnrc2
G
H
I
0'
30'
60' pHS
J
her1 3'UTR
(725 nts)
PRE
ARE
UUCCUAUGGUAAAUUCUUUAUUGUUUACAGAUUGUGUAAAUAAAUAUAUUUAUUUU
606
662
deltaC 3'UTR
(1327 nts)
PRE
ARE
PRE
GGACUGUAAAUAUUUUGUAUUUAUGAGAGAUGAAUGUAUAUAUGUUUAUGUAUUUU
1222
1278

Figure 3.7. The Pumilio response element and AU-rich element in the *her1* 3'UTR are necessary for normal turnover of reporter transcript.

Transgenic embryos carrying the *hsp70l:Venus-her1 3'UTR-SV40* reporter (A-C) or the embryos carrying the *hsp70l:Venus-her1 3'UTR-SV40* reporter with a 2 nt mutation in the PRE sequence (D-F) were raised to mid-segmentation stage and heat-shocked for 15 minutes, then collected at the indicated minutes pHS and processed by *Venus* in situ hybridization ($n \geq 10$ embryos per time point). (G) qPCR analysis comparing *Venus* transcript fold change from 30-minutes pHS to 60 and 90 minutes pHS between the *hsp70l:Venus-her1 3'UTR-SV40* reporter and the *hsp70l:Venus-her1 3'UTR-SV40* reporter with PRE mutation (n = 10 embryos per time point). Half-life calculation of the reporters display a 24.4-minute stabilization when the PRE is disrupted. (H) qPCR analysis comparing *Venus* transcript fold change from 30-minutes pHS to 60 and 90 minutes pHS between the *hsp70l:Venus-her1 3'UTR-SV40* reporter and the *hsp70l:Venus-her1 3'UTR-SV40* reporter with a 3 nt mutation in the ARE sequence (n = 10 per time point). The ARE in the *her1* 3'UTR is mutated from 5'UAUUUAU to 5'UACCCAU. Half-life calculation of the reporters display a 10.5-minute stabilization upon ARE disruption. pHS = post heat-shock; PRE = Pumilio response element; ARE = AU-rich element; nt = nucleotides.

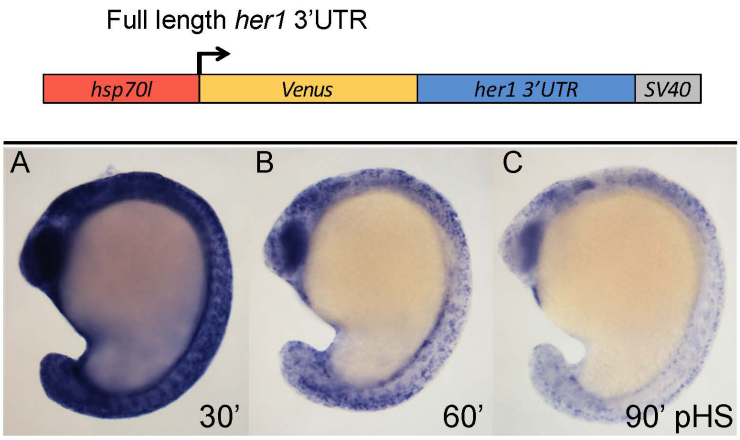
Full length her1 3'UTR
hsp70l
Venus
her1 3'UTR
SV40
A
B
C
30'
60'
90' pHS

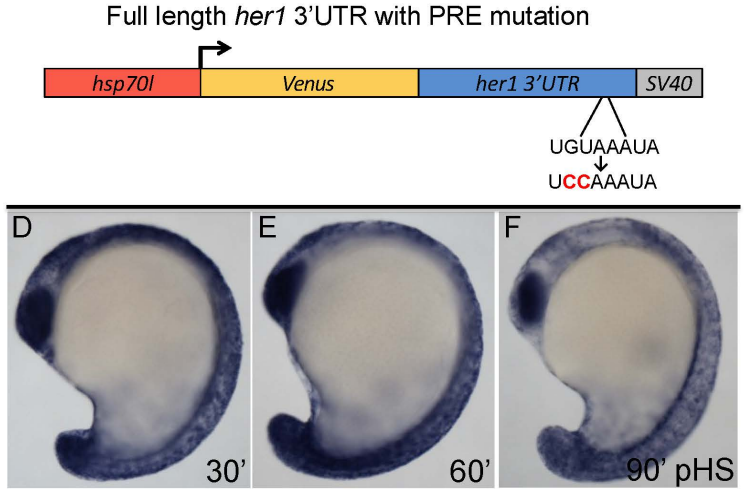
Full length her1 3'UTR with PRE mutation
hsp70l
Venus
her1 3'UTR
SV40
UGUAAAUA
UCCAAAUA
D
E
F
30'
60'
90' pHS

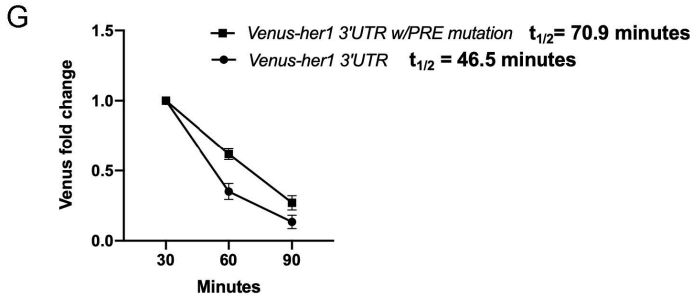
G
Venus-her1 3'UTR w/PRE mutation t1/2= 70.9 minutes
Venus-her1 3'UTR t1/2 = 46.5 minutes
Venus fold change
1.5
1.0
0.5
0.0
30
60
90
Minutes

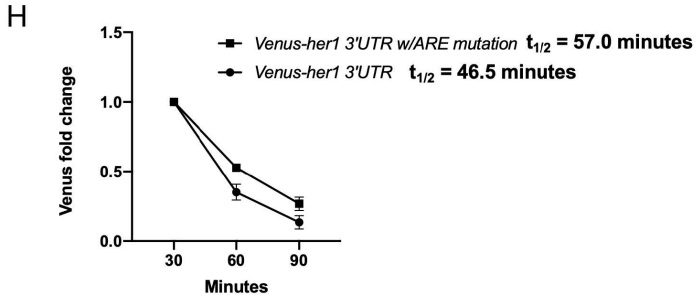
H
Venus-her1 3'UTR w/ARE mutation t1/2 = 57.0 minutes
Venus-her1 3'UTR t1/2 = 46.5 minutes
Venus fold change
1.5
1.0
0.5
0.0
30
60
90
Minutes

Table 3.1 List of transgenic lines generated in this study.

Allele	Transgene
oz44	*hsp70l:Venus-her1 3'UTR-SV40*
oz45	*hsp70l:Venus-her1 3'UTR-SV40*
oz46	*hsp70l:Venus-her1 3'UTR-SV40*
oz47	*hsp70l:Venus-her1 3'UTRΔ1-362-SV40*
oz48	*hsp70l:Venus-her1 3'UTRΔ1-362-SV40*
oz49	*hsp70l:Venus-her1 3'UTRΔ1-362-SV40*
oz50	*hsp70l:Venus-her1 3'UTRΔ1-362-SV40*
oz51	*hsp70l:Venus-her1 3'UTRΔ363-725-SV40*
oz52	*hsp70l:Venus-her1 3'UTRΔ363-725-SV40*
oz53	*hsp70l:Venus-her1 3'UTRΔ363-725-SV40*
oz54	*hsp70l:Venus-her1 3'UTRΔ363-725-SV40*
oz55	*hsp70l:Venus-her1 3'UTRΔ1-546-SV40*
oz56	*hsp70l:Venus-her1 3'UTRΔ1-546-SV40*
oz57	*hsp70l:Venus-her1 3'UTRΔ1-546-SV40*
oz58	*hsp70l:Venus-her1 3'UTRΔ1-546-SV40*
oz59	*hsp70l:Venus-her1 3'UTRΔ1-546-SV40*
oz60	*hsp70l:Venus-her1 3'UTRΔ1-362; Δ547-725-SV40*

oz61	*hsp70l:Venus-her1 3'UTR∆1-362; ∆547-725-SV40*
oz62	*hsp70l:Venus-her1 3'UTR∆363-546-SV40*
oz63	*hsp70l:Venus-her1 3'UTR∆363-546-SV40*
oz64	*hsp70l:Venus-SV40*
oz65	*hsp70l:Venus-SV40*
oz66	*hsp70l:Venus-SV40*
oz67	*hsp70l:Venus-SV40*
oz68	*hsp70l:Venus-SV40*
oz69	*hsp70l:Venus-disrupted PRE her1 3'UTR-SV40*
oz70	*hsp70l:Venus-disrupted PRE her1 3'UTR-SV40*
oz71	*hsp70l:Venus-disrupted PRE her1 3'UTR-SV40*
oz72	*hsp70l:Venus-disrupted PRE her1 3'UTR-SV40*
oz73	*hsp70l:Venus-disrupted PRE her1 3'UTR-SV40*
oz74	*hsp70l:Venus-disrupted ARE her1 3'UTR-SV40*
oz75	*hsp70l:Venus-disrupted ARE her1 3'UTR-SV40*
oz76	*hsp70l:Venus-disrupted ARE her1 3'UTR-SV40*
oz77	*hsp70l:Venus-disrupted ARE her1 3'UTR-SV40*
oz78	*hsp70l:Venus-disrupted ARE her1 3'UTR-SV40*
oz79	*hsp70l:Venus-disrupted ARE her1 3'UTR-SV40*
oz80	*hsp70l:Venus-dlc 3'UTR-SV40*
oz81	*hsp70l:Venus-dlc 3'UTR-SV40*

oz82	*hsp70l:Venus-dlc 3'UTR-SV40*
oz83	*hsp70l:Venus-dlc 3'UTR-SV40*

*Each oz number represents a separate founder line generated with each transgene, which should represent an independent transgene insertion event.

Table 3.2. Specific residues in the SH3 domain of Pnrc2 are necessary for rescue of *her1* accumulation in *MZpnrc2* mutants.

Condition	*her1* expression[a]		
	Normal	Accumulated	Percent affected
Uninjected	14/29	15/29	51.7%
Cerulean-pnrc2	48/49	1/49	2.0%
Cerulean-pnrc2$^{\Delta NR}$	22/27	5/27	18.5%
Cerulean-pnrc2$^{W->A}$	26/50	24/50	52.0%

[a]At the 16-18hpf, *pnrc2* mRNA-injected embryos from a *pnrc2*^{oz22} homozygous female crossed to *pnrc2*^{oz22} heterozygous male were processed by *her1* in situ hybridization to assess phenotypic rescue. The cross generates 50% MZ*pnrc2*^{oz22} mutants and 50% M *pnrc2*^{oz22} mutants. Because M*pnrc2*^{oz22} mutants display no *her1* accumulation as shown in Figure 3.1, only half of the embryos are expected to display the *her1* accumulation phenotype.

[b]Chi-square analysis indicates a significant difference in *her1* expression among *Cerulean-pnrc2* mRNA-injected *MZpnrc2* mutants versus uninjected embryos and no significant difference among *pnrc2*$^{W->A}$ mRNA-injected *MZpnrc2* mutants compared to uninjected embryos, $p < 0.0001$ and $p = 0.7773$ respectively**.** W->A = W114A mutation; ΔNR = deletion of Nuclear Receptor domain; hpf = hours post-fertilization. (Data in Table 3.2 were generated by Monica M. Mannings)

Chapter 4: Concluding remarks and Future work

4.1 Summary of Findings and Significance

My work investigates cis elements and trans-acting factors critical for cyclic transcript decay, a recognized but largely unexplored component of the segmentation clock[25]. I have determined zygotically expressed and maternally provided *pnrc2* contributes to clearing spliced *her1*, *her7*, *dlc*, and *dld* transcripts during somitogenesis (Chapter 2 Figure 2.3 and Figure 2.4; Chapter 3 Figure 3.1; data not shown) and show the *her1* 3'UTR confers Pnrc2-dependent instability to reporter transcripts (Chapter 2 Figure 2.7; Chapter 3 Figure 3.3). Sub-optimal depletion of both Pnrc2 and Upf1 causes accumulation of *her1* transcripts (Chapter 2 Figure 2.8), and specific residues in the SH3 domain of Pnrc2 are necessary for rescue of *MZpnrc2* mutants (Chapter 3 Table 3.2). Although cyclic transcripts accumulate in *pnrc2*^{oz22} mutants, I show cyclic protein levels do not (Chapter 2 Figure 2.10; Chapter 3 Figure 3.2), suggesting another mechanism of regulation ensures proper protein levels of segmentation clock genes such as rapid protein turnover or translational repression. I have determined the last 179 nts of the *her1* 3'UTR is necessary and sufficient to confer Pnrc2-dependent decay (Chapter 3 Figure 3.4 and Figure 3.5) and have shown the *dlc* 3'UTR also confers Pnrc2-dependent decay (Chapter 3 Figure 3.6), suggesting cyclic transcripts may be regulated through a conserved 3'UTR-mediated decay mechanism. I show *her1* transcript turnover is independent of Dicer-generated

miRNAs (Chapter 2 Figure 2.7) and identified conserved PRE and ARE motifs in the *her1* and *dlc* 3'UTRs (Chapter 3 Figure 3.6). Mutation of the PRE and ARE in the *her1* 3'UTR disrupts ability of the 3'UTR to convey normal turnover to reporter transcripts (Chapter 3 Figure 3.7), suggesting Pumilio and/or an ARE-BPs function to regulate transcript turnover during somitogenesis.

The purpose of this work is to define pathways regulating the rapid clock

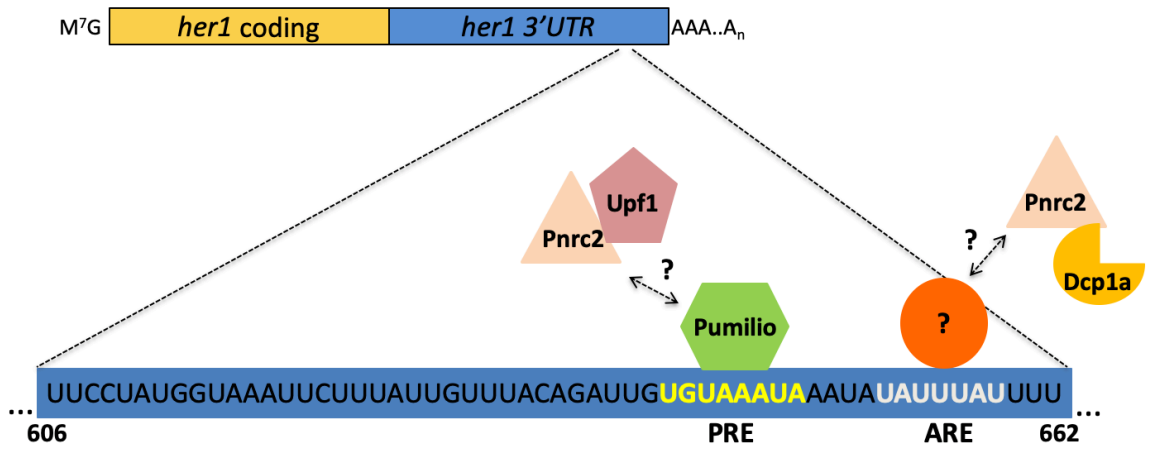

Figure 4.1. Potential decay factors involved in turnover of *her1* mRNA.

transcript turnover required to maintain Segmentation Clock function. Recent studies have determined that ultradian Hes oscillators are operating in other biological systems such as neural stem cells, embryonic stem cells and possibly even in cancer cells[222,223]. These oscillators regulate how cells respond to environmental signals and only by better understanding mechanisms of molecular oscillators will we learn to manipulate them in a developmental or cancerous context. I anticipate this work will be relevant to other oscillating systems and to other developmental processes where transcript clearance

facilitates developmental transitions and patterning. This work expands on our understanding of endogenous, non-aberrant targets of Pnrc2, and provides context to how Pnrc2 may regulate non-cyclic transcripts in other biological systems.

4.2 Future Directions

4.2.1 Identifying direct interactions of the *her1* and *dlc* 3'UTRs

There remain aspects of Pnrc2-mediated cyclic transcript turnover that are still not well-understood. A large question not yet addressed in these studies is the directness of Pnrc2-mediated decay. Does Pnrc2 directly bind to the *her1* and *dlc* 3'UTRs and drive instability or does Pnrc2 indirectly cause decay of these transcripts through regulation of another factor? To address this, future research should use biochemical assays using the *her1* and *dlc* 3'UTRs as bait to identify direct interactions. Because the *dlc* 3'UTR is 1327 nts long and non-specific interactions may create difficulties for pulldown experiments, I suggest first using the *her1* 3'UTR to detect interacting factors, then determine if relevant factors also interact with the *dlc* 3'UTR. The destabilizing last 179 nt "destabilizing" region of the *her1* 3'UTR should be used as bait for an RNA pulldown and the non-destabilizing upstream 184 nt "non-destabilizing" region of the *her1* 3'UTR should be used as a control. Lysates from mid-segmentation *MZpnrc2*^{oz22} mutants and wildtype embryos should be used to reveal relevant proteins that bind only when Pnrc2 is functional. Factors that bind only the destabilizing region of the *her1* 3'UTR should be the initial focus. Mutations of the

PRE and ARE in the *her1* 3'UTR that have been shown to affect destabilization of reporter transcripts should also be utilized in the pulldown to identify factors that uniquely bind when the PRE and/or ARE are intact. All pulldown experiments should be followed by western blot analysis for known decay factors and by mass spectrometry for unknown factors. Tethering of human PNRC2 to reporter transcripts has been shown to destabilize the reporter[103,107], suggesting direct interaction of PNRC2 to a target can affect stability. I hypothesize a Pnrc2-containing complex directly binds to specific decay elements in the *her1* and *dlc* 3'UTRs. I also hypothesize that Pumilio1 and/or Pumilio 2 interact with the PRE in the last 179 nts of the *her1* 3'UTR and Pumilio proteins will be detected using the destabilizing region of the *her1* 3'UTR. These experiments will provide support for direct or indirect regulation of cyclic transcripts by Pnrc2 and will also assist in identifying any ARE-BPs that interact with the destabilizing region of the *her1* 3'UTR.

4.2.2 Identifying direct interactions of Pnrc2

To complement the 3'UTR analysis, future research should also define interacting partners of Pnrc2 during somitogenesis. Decay factors that bind to the *her1* and *dlc* 3'UTRs should also be examined for direct interaction with Pnrc2. Commerically-available antibodies against Pnrc2 have been unsuccessful in zebrafish, but our lab has generated biochemically-tagged versions of Pnrc2 that do not interfere with cyclic transcript clearance as these modified versions of Pnrc2 are capable of rescuing *pnrc2*^{oz22} mutants (Chapter 3 Table 3.2). Using

these methods, future researchers should fuse either FLAG or GFP to Pnrc2 and conduct FLAG or GFP pulldowns using lysates from MZ*pnrc2*^{oz22} mutants to avoid binding competition from endogenous Pnrc2. Disruption of specific residues in Pnrc2 affects ability to rescue cyclic transcript turnover *pnrc2*^{oz22} mutants (Chapter 3 Table 3.2), and these non-functional versions of Pnrc2 could be used in the pulldown experiments as a controls to focus on factors that only recognize functional Pnrc2. It is important to note that critical decay factors may still bind to non-functional versions of Pnrc2 but become inactive because of the mutation. Because of this, researchers should initially examine the role of factors that bind only functional versions of Pnrc2 and later expand the search to all decay factors that recognize both functional and non-functional versions of Pnrc2. Human cell culture studies show PNRC2 interacts with UPF1 and DCP1A[103,107], and our own work supports a genetic interaction with Upf1 (Chapter 2 Figure 2.8). I hypothesize Upf1 and Dcp1a interact directly with Pnrc2 during somitogenesis and these factors function in 3'UTR-mediated decay of cyclic transcripts such as *her1* and *dlc*. These experiments will also provide evidence to whether Pumilio 1 and/or Pumilio 2 and a known ARE-BP directly interact with Pnrc2 during somitogenesis.

4.2.3 Determine if Pnrc2 and Pumilio proteins function in a common mRNA decay mechanism

Another important question remaining from this study is whether Pnrc2-mediated decay functions through the PRE and/or ARE in the *her1* 3'UTR, or if

there are alternative features in the last 179 nts of the *her1* 3'UTR that mediate Pnrc2-dependent instability (Figure 4.1). To address this, future work should utilize our heat-shock inducible reporter assay to examine reporter stability when fused to the *her1* 3'UTR with a disrupted PRE or ARE (Chapter 3, Figure 3.7) in the MZ*pnrc2*^{oz22} background. If Pnrc2 functions through the PRE or ARE, I hypothesize reporter stability will display no difference between MZ*pnrc2*^{oz22} mutants and WT embryos. If Pnrc2 functions through a separate feature in the last 179 nts of the *her1* 3'UTR, I hypothesize to see a cumulative effect on the reporter, leading to a more dramatic stabilization than observed with the PRE or ARE mutation alone (Chapter 3, Figure 3.7). If the data supports the latter hypothesis, then additional truncations or small internal deletions of the last 179 nts of the *her1* 3'UTR may identify additional Pnrc2-regulated destabilizing motifs. These experiments will help address if Pnrc2 functions through the PRE and ARE in the *her1* 3'UTR or if these motifs function separate from Pnrc2-mediated decay to mediate rapid turnover of cyclic genes.

4.2.4 Determine the post-transcriptional status of cyclic transcripts in *pnrc2*^{oz22} mutants

The post-transcriptional status of accumulated cyclic transcripts in *pnrc2*^{oz22} mutants is still unknown from this study. Removal of the poly(A) tail and the 5' cap is critical for efficient mRNA decay[224], and determining the status of both modifications on *her1* and *dlc* transcripts in *pnrc2*^{oz22} mutants will provide insight to what downstream process of mRNA decay Pnrc2 functions. Future

work could analyze the 5' cap status of *her1* and *dlc* transcripts by circularization RT-PCR (cRT-PCR)[225]. The 5' monophosphate of a decapped transcript can be ligated to its own 3' hydroxyl, causing circularization of the mRNA. Primers can be designed to only amplify products over the 5'- 3' junction, allowing the quantification of decapped *her1* and *dlc* transcripts compared to total RNA. This technique will be performed in RNA extractions from *MZpnrc2*^{oz22} mutant embryos and wildtype embryos. Human PNRC2 has been implicated in mRNA decapping by several reports[103,105,107,130], and I hypothesize that the ratio of decapped to capped *her1* and *dlc* transcripts will be decreased in *pnrc2*^{oz22} mutant embryos compared to WT embryos. Because inhibition of decapping can result in accumulation of deadenylated transcripts[226], I also expect that partially or completely deadenylated *her1* and *dlc* transcripts will be increased in *pnrc2*^{oz22} mutants. To examine the poly(A) tail status of *her1* and *dlc* transcripts in *MZpnrc2*^{oz22} mutants compared to wild-type embryos, a poly(A) tailing assay should be performed[224]. This method allows detection of mRNA products whose only difference in size will be the poly(A) tail length. I hypothesize that poly(A) tails on *her1* and *dlc* transcripts will be shortened in *pnrc2*^{oz22} mutants because of a decapping defect in the mutants. Shortening of the poly(A) tail affects translation rates and if the hypothesize is true, it may explain the lack of protein overexpression for Her1 and Dlc observed in *pnrc2*^{oz22} mutants (Chapter 2 Figure 2.10; Chapter 3 Figure 3.2). These experiments will help identify how Pnrc2

functions to regulate mRNA turnover during somitogenesis and may provide insight to how Pnrc2 regulates decay of other non-cyclic transcripts.

4.2.5 Identify mechanisms that regulate proper protein levels in *pnrc2*^{oz22} mutants

Another intriguing observation from this research is the near wild-type levels of cyclic proteins such as Her1 and Dlc in *pnrc2*^{oz22} mutants. Data reveals a ~4-fold increase of *her1* and *dlc* transcripts in MZ*pnrc2*^{oz22} mutants but protein levels appear unaffected (Chapter 2 Figure 2.10; Chapter 3 Figure 3.2). These results suggest that an additional regulatory mechanism is ensuring proper protein levels in *pnrc2*^{oz22} mutants to sustain oscillatory expression. I hypothesize a mechanism of translational repression or rapid protein turnover is maintaining proper cyclic protein levels in *pnrc2*^{oz22} mutants. To address if translation repression occurs in mutants, ribosomal profiling of *MZpnrc2*^{oz22} mutants and wild-type embryos could be performed to compare the association of ribosomes with *her1* and *dlc* transcripts. If translational repression is occurring, I hypothesize wild-type and *MZpnrc2*^{oz22} mutants will display similar levels of *her1* and *dlc* transcripts associated with active ribosomes. On the other hand, if accumulating transcripts are actively translated in *pnrc2*^{oz22} mutants, I hypothesize there will be a ~4-fold increase in *her1* and *dlc* transcripts associated with active ribosomes compared to wild-type embryos. If the data support the latter hypothesis, the protease inhibitor MG132[227-229] could be used to assay if rapid protein turnover is responsible for the maintenance of normal Her1 and Dlc

levels in *pnrc2*^{oz22} mutants. One could incubate *MZpnrc2*^{oz22} mutant embryos with MG132 during segmentation and observe spatial expression of endogenous Dlc by immunofluorescence (Chapter 2, Figure 2.10; Chapter 3, Figure 3.2) and quantify Dlc levels by western blot analysis. The *her1:her1-Venus*^{bk15} transgenic clock reporter (Chapter 2, Figure 2.10) could also be utilized to examine levels of Venus-Her1 protein in *MZpnrc2*^{oz22} mutants treated with the MG132 protease inhibitor. If rapid protein turnover is maintaining proper levels of Her1 and Dlc in *pnrc2*^{oz22} mutants, I hypothesize there will be a significant increase of Her1 and Dlc protein by immunofluorescence and western blot analysis in MG132-treated *pnrc2*^{oz22} mutant embryos compared to the untreated *pnrc2*^{oz22} mutant control. These experiments will be very informative to understanding mechanisms that function to ensure proper protein levels of cyclic genes during somitogenesis and will provide insight to why *pnrc2*^{oz22} mutants do not display a segmentation defect.

4.3 Conclusion

This work investigates the role and significance of RNA decay as a process of regulating sensitive genetic oscillations during development. Our current knowledge of the post-transcriptional regulation of cyclic transcripts is limited, and the studies detailed above and the proposed experiments will lead to a more complete understanding of the mechanisms controlling rapid decay of oscillating transcripts. Understanding regulatory features and factors that drive Pnrc2-mediated decay will also provide a better understanding of general

mechanisms regulating rapid transcript turnover in various cellular and developmental contexts.

References

1. Danks DM, Campbell PE, Jack I, Rogers J, Smith AL. Studies of the aetiology of neonatal hepatitis and biliary atresia. *Arch Dis Child*. 1977;52(5):360-367.

2. Gridley T. Notch signaling and inherited disease syndromes. *Hum Mol Genet*. 2003;12 Spec No 1:R9-13.

3. Oates AC, Morelli LG, Ares S. Patterning embryos with oscillations: structure, function and dynamics of the vertebrate segmentation clock. *Development*. 2012;139(4):625-639.

4. Kageyama R, Niwa Y, Isomura A, Gonzalez A, Harima Y. Oscillatory gene expression and somitogenesis. *Wiley Interdiscip Rev Dev Biol*. 2012;1(5):629-641.

5. Oates AC, Ho RK. Hairy/E(spl)-related (Her) genes are central components of the segmentation oscillator and display redundancy with the Delta/Notch signaling pathway in the formation of anterior segmental boundaries in the zebrafish. *Development*. 2002;129(12):2929-2946.

6. Holley SA, Julich D, Rauch GJ, Geisler R, Nusslein-Volhard C. her1 and the notch pathway function within the oscillator mechanism that regulates zebrafish somitogenesis. *Development*. 2002;129(5):1175-1183.

7. Gajewski M, Sieger D, Alt B, et al. Anterior and posterior waves of cyclic her1 gene expression are differentially regulated in the presomitic mesoderm of zebrafish. *Development*. 2003;130(18):4269-4278.

8. Li L, Krantz ID, Deng Y, et al. Alagille syndrome is caused by mutations in human Jagged1, which encodes a ligand for Notch1. *Nat Genet*. 1997;16(3):243-251.

9. Oda T, Elkahloun AG, Meltzer PS, Chandrasekharappa SC. Identification and cloning of the human homolog (JAG1) of the rat Jagged1 gene from the Alagille syndrome critical region at 20p12. *Genomics*. 1997;43(3):376-379.

10. Bulman MP, Kusumi K, Frayling TM, et al. Mutations in the human delta homologue, DLL3, cause axial skeletal defects in spondylocostal dysostosis. *Nat Genet*. 2000;24(4):438-441.

11. Whittock NV, Sparrow DB, Wouters MA, et al. Mutated MESP2 causes spondylocostal dysostosis in humans. *Am J Hum Genet*. 2004;74(6):1249-1254.

12. Sparrow DB, Chapman G, Wouters MA, et al. Mutation of the LUNATIC FRINGE gene in humans causes spondylocostal dysostosis with a severe vertebral phenotype. *Am J Hum Genet*. 2006;78(1):28-37.

13. Gekakis N, Staknis D, Nguyen HB, et al. Role of the CLOCK protein in the mammalian circadian mechanism. *Science*. 1998;280(5369):1564-1569.

14. Hogenesch JB, Gu YZ, Jain S, Bradfield CA. The basic-helix-loop-helix-PAS orphan MOP3 forms transcriptionally active complexes with circadian and hypoxia factors. *Proc Natl Acad Sci U S A*. 1998;95(10):5474-5479.

15. Akhtar RA, Reddy AB, Maywood ES, et al. Circadian cycling of the mouse liver transcriptome, as revealed by cDNA microarray, is driven by the suprachiasmatic nucleus. *Curr Biol*. 2002;12(7):540-550.

16. Panda S, Antoch MP, Miller BH, et al. Coordinated transcription of key pathways in the mouse by the circadian clock. *Cell*. 2002;109(3):307-320.

17. Storch KF, Lipan O, Leykin I, et al. Extensive and divergent circadian gene expression in liver and heart. *Nature*. 2002;417(6884):78-83.

18. Shimojo H, Ohtsuka T, Kageyama R. Oscillations in notch signaling regulate maintenance of neural progenitors. *Neuron*. 2008;58(1):52-64.

19. Cooke J. The problem of periodic patterns in embryos. *Philos Trans R Soc Lond B Biol Sci*. 1981;295(1078):509-524.

20. Cooke J, Zeeman EC. A clock and wavefront model for control of the number of repeated structures during animal morphogenesis. *J Theor Biol*. 1976;58(2):455-476.

21. Palmeirim I, Henrique D, Ish-Horowicz D, Pourquie O. Avian hairy gene expression identifies a molecular clock linked to vertebrate segmentation and somitogenesis. *Cell*. 1997;91(5):639-648.

22. Pourquie O. Vertebrate segmentation: from cyclic gene networks to scoliosis. *Cell*. 2011;145(5):650-663.

23. Bessho Y, Sakata R, Komatsu S, Shiota K, Yamada S, Kageyama R. Dynamic expression and essential functions of Hes7 in somite segmentation. *Genes Dev*. 2001;15(20):2642-2647.

24. Holley SA, Geisler R, Nusslein-Volhard C. Control of her1 expression during zebrafish somitogenesis by a delta-dependent oscillator and an independent wave-front activity. *Genes Dev*. 2000;14(13):1678-1690.

25. Li Y, Fenger U, Niehrs C, Pollet N. Cyclic expression of esr9 gene in Xenopus presomitic mesoderm. *Differentiation*. 2003;71(1):83-89.

26. Gomez C, Ozbudak EM, Wunderlich J, Baumann D, Lewis J, Pourquie O. Control of segment number in vertebrate embryos. *Nature*. 2008;454(7202):335-339.

27. Dubrulle J, McGrew MJ, Pourquie O. FGF signaling controls somite boundary position and regulates segmentation clock control of spatiotemporal Hox gene activation. *Cell*. 2001;106(2):219-232.

28. Aulehla A, Wehrle C, Brand-Saberi B, et al. Wnt3a plays a major role in the segmentation clock controlling somitogenesis. *Dev Cell*. 2003;4(3):395-406.

29. Sawada A, Shinya M, Jiang YJ, Kawakami A, Kuroiwa A, Takeda H. Fgf/MAPK signalling is a crucial positional cue in somite boundary formation. *Development*. 2001;128(23):4873-4880.

30. Naiche LA, Holder N, Lewandoski M. FGF4 and FGF8 comprise the wavefront activity that controls somitogenesis. *Proc Natl Acad Sci U S A*. 2011;108(10):4018-4023.

31. Vermot J, Gallego Llamas J, Fraulob V, Niederreither K, Chambon P, Dolle P. Retinoic acid controls the bilateral symmetry of somite formation in the mouse embryo. *Science*. 2005;308(5721):563-566.

32. Giudicelli F, Ozbudak EM, Wright GJ, Lewis J. Setting the tempo in development: an investigation of the zebrafish somite clock mechanism. *PLoS Biol*. 2007;5(6):e150.

33. Henry CA, Urban MK, Dill KK, et al. Two linked hairy/Enhancer of split-related zebrafish genes, her1 and her7, function together to refine alternating somite boundaries. *Development*. 2002;129(15):3693-3704.

34. Harima Y, Takashima Y, Ueda Y, Ohtsuka T, Kageyama R. Accelerating the tempo of the segmentation clock by reducing the number of introns in the Hes7 gene. *Cell Rep*. 2013;3(1):1-7.

35. Takashima Y, Ohtsuka T, Gonzalez A, Miyachi H, Kageyama R. Intronic delay is essential for oscillatory expression in the segmentation clock. *Proc Natl Acad Sci U S A*. 2011;108(8):3300-3305.

36. Bessho Y, Hirata H, Masamizu Y, Kageyama R. Periodic repression by the bHLH factor Hes7 is an essential mechanism for the somite segmentation clock. *Genes Dev*. 2003;17(12):1451-1456.

37. Chen J, Kang L, Zhang N. Negative feedback loop formed by Lunatic fringe and Hes7 controls their oscillatory expression during somitogenesis. *Genesis*. 2005;43(4):196-204.

38. Ay A, Holland J, Sperlea A, et al. Spatial gradients of protein-level time delays set the pace of the traveling segmentation clock waves. *Development*. 2014;141(21):4158-4167.

39. Lewis J. Autoinhibition with transcriptional delay: a simple mechanism for the zebrafish somitogenesis oscillator. *Curr Biol*. 2003;13(16):1398-1408.

40. Williams DR, Shifley ET, Braunreiter KM, Cole SE. Disruption of somitogenesis by a novel dominant allele of Lfng suggests important roles for protein processing and secretion. *Development*. 2016;143(5):822-830.

41. Ay A, Knierer S, Sperlea A, Holland J, Ozbudak EM. Short-lived Her proteins drive robust synchronized oscillations in the zebrafish segmentation clock. *Development*. 2013;140(15):3244-3253.

42. Gonzalez A, Manosalva I, Liu T, Kageyama R. Control of Hes7 expression by Tbx6, the Wnt pathway and the chemical Gsk3 inhibitor LiCl in the mouse segmentation clock. *PLoS One*. 2013;8(1):e53323.

43. Hirata H, Yoshiura S, Ohtsuka T, et al. Oscillatory expression of the bHLH factor Hes1 regulated by a negative feedback loop. *Science*. 2002;298(5594):840-843.

44. Schwendinger-Schreck J, Kang Y, Holley SA. Modeling the zebrafish segmentation clock's gene regulatory network constrained by expression data suggests evolutionary transitions between oscillating and nonoscillating transcription. *Genetics*. 2014;197(2):725-738.

45. Hoyle NP, Ish-Horowicz D. Transcript processing and export kinetics are rate-limiting steps in expressing vertebrate segmentation clock genes. *Proc Natl Acad Sci U S A*. 2013;110(46):E4316-4324.

46. Hilgers V, Pourquie O, Dubrulle J. In vivo analysis of mRNA stability using the Tet-Off system in the chicken embryo. *Dev Biol*. 2005;284(2):292-300.

47. Nitanda Y, Matsui T, Matta T, et al. 3'-UTR-dependent regulation of mRNA turnover is critical for differential distribution patterns of cyclic gene mRNAs. *Febs j*. 2014;281(1):146-156.

48. Gallagher TL, Tietz KT, Morrow ZT, et al. Pnrc2 regulates 3'UTR-mediated decay of segmentation clock-associated transcripts during zebrafish segmentation. *Dev Biol*. 2017;429(1):225-239.

49. Riley MF, Bochter MS, Wahi K, Nuovo GJ, Cole SE. Mir-125a-5p-mediated regulation of Lfng is essential for the avian segmentation clock. *Dev Cell*. 2013;24(5):554-561.

50. Muhlrad D, Decker CJ, Parker R. Deadenylation of the unstable mRNA encoded by the yeast MFA2 gene leads to decapping followed by 5'-->3' digestion of the transcript. *Genes Dev*. 1994;8(7):855-866.

51. Mangus DA, Evans MC, Jacobson A. Poly(A)-binding proteins: multifunctional scaffolds for the post-transcriptional control of gene expression. *Genome Biol*. 2003;4(7):223.

52. Chen CY, Shyu AB. Mechanisms of deadenylation-dependent decay. *Wiley Interdiscip Rev RNA*. 2011;2(2):167-183.

53. Li Y, Kiledjian M. Regulation of mRNA decapping. *Wiley Interdiscip Rev RNA*. 2010;1(2):253-265.

54. McGlincy NJ, Smith CW. Alternative splicing resulting in nonsense-mediated mRNA decay: what is the meaning of nonsense? *Trends Biochem Sci*. 2008;33(8):385-393.

55. Hentschke M, Borgmeyer U. Identification of PNRC2 and TLE1 as activation function-1 cofactors of the orphan nuclear receptor ERRgamma. *Biochem Biophys Res Commun*. 2003;312(4):975-982.

56. Le Hir H, Sauliere J, Wang Z. The exon junction complex as a node of post-transcriptional networks. *Nat Rev Mol Cell Biol*. 2016;17(1):41-54.

57. Kashima I, Yamashita A, Izumi N, et al. Binding of a novel SMG-1-Upf1-eRF1-eRF3 complex (SURF) to the exon junction complex triggers Upf1 phosphorylation and nonsense-mediated mRNA decay. *Genes Dev*. 2006;20(3):355-367.

58. Isken O, Kim YK, Hosoda N, Mayeur GL, Hershey JW, Maquat LE. Upf1 phosphorylation triggers translational repression during nonsense-mediated mRNA decay. *Cell*. 2008;133(2):314-327.

59. Mendell JT, Sharifi NA, Meyers JL, Martinez-Murillo F, Dietz HC. Nonsense surveillance regulates expression of diverse classes of mammalian transcripts and mutes genomic noise. *Nat Genet*. 2004;36(10):1073-1078.

60. Kim YK, Furic L, Desgroseillers L, Maquat LE. Mammalian Staufen1 recruits Upf1 to specific mRNA 3'UTRs so as to elicit mRNA decay. *Cell*. 2005;120(2):195-208.

61. Hosoda N, Kim YK, Lejeune F, Maquat LE. CBP80 promotes interaction of Upf1 with Upf2 during nonsense-mediated mRNA decay in mammalian cells. *Nat Struct Mol Biol*. 2005;12(10):893-901.

62. Cho H, Kim KM, Han S, et al. Staufen1-mediated mRNA decay functions in adipogenesis. *Mol Cell*. 2012;46(4):495-506.

63. Gong C, Kim YK, Woeller CF, Tang Y, Maquat LE. SMD and NMD are competitive pathways that contribute to myogenesis: effects on PAX3 and myogenin mRNAs. *Genes Dev*. 2009;23(1):54-66.

64. Bakheet T, Williams BR, Khabar KS. ARED 3.0: the large and diverse AU-rich transcriptome. *Nucleic Acids Res*. 2006;34(Database issue):D111-114.

65. Yamashita A, Chang TC, Yamashita Y, et al. Concerted action of poly(A) nucleases and decapping enzyme in mammalian mRNA turnover. *Nat Struct Mol Biol*. 2005;12(12):1054-1063.

66. Lykke-Andersen J, Wagner E. Recruitment and activation of mRNA decay enzymes by two ARE-mediated decay activation domains in the proteins TTP and BRF-1. *Genes Dev*. 2005;19(3):351-361.

67. Gratacos FM, Brewer G. The role of AUF1 in regulated mRNA decay. *Wiley Interdiscip Rev RNA*. 2010;1(3):457-473.

68. Briata P, Forcales SV, Ponassi M, et al. p38-dependent phosphorylation of the mRNA decay-promoting factor KSRP controls the stability of select myogenic transcripts. *Mol Cell*. 2005;20(6):891-903.

69. Hinman MN, Lou H. Diverse molecular functions of Hu proteins. *Cell Mol Life Sci*. 2008;65(20):3168-3181.

70. Abdelmohsen K, Gorospe M. Posttranscriptional regulation of cancer traits by HuR. *Wiley Interdiscip Rev RNA*. 2010;1(2):214-229.

71. von Roretz C, Di Marco S, Mazroui R, Gallouzi IE. Turnover of AU-rich-containing mRNAs during stress: a matter of survival. *Wiley Interdiscip Rev RNA*. 2011;2(3):336-347.

72. Sanduja S, Blanco FF, Dixon DA. The roles of TTP and BRF proteins in regulated mRNA decay. *Wiley Interdiscip Rev RNA*. 2011;2(1):42-57.

73. Schott J, Stoecklin G. Networks controlling mRNA decay in the immune system. *Wiley Interdiscip Rev RNA*. 2010;1(3):432-456.

74. Van Etten J, Schagat TL, Hrit J, et al. Human Pumilio proteins recruit multiple deadenylases to efficiently repress messenger RNAs. *J Biol Chem*. 2012;287(43):36370-36383.

75. Wang X, McLachlan J, Zamore PD, Hall TM. Modular recognition of RNA by a human pumilio-homology domain. *Cell*. 2002;110(4):501-512.

76. Filipovska A, Razif MF, Nygard KK, Rackham O. A universal code for RNA recognition by PUF proteins. *Nat Chem Biol*. 2011;7(7):425-427.

77. Goldstrohm AC, Hall TMT, McKenney KM. Post-transcriptional Regulatory Functions of Mammalian Pumilio Proteins. *Trends Genet*. 2018;34(12):972-990.

78. Schwanhausser B, Busse D, Li N, et al. Global quantification of mammalian gene expression control. *Nature*. 2011;473(7347):337-342.

79. Yang E, van Nimwegen E, Zavolan M, et al. Decay rates of human mRNAs: correlation with functional characteristics and sequence attributes. *Genome Res*. 2003;13(8):1863-1872.

80. Sharova LV, Sharov AA, Nedorezov T, Piao Y, Shaik N, Ko MS. Database for mRNA half-life of 19 977 genes obtained by DNA microarray analysis of pluripotent and differentiating mouse embryonic stem cells. *DNA Res*. 2009;16(1):45-58.

81. Rabani M, Pieper L, Chew GL, Schier AF. A Massively Parallel Reporter Assay of 3' UTR Sequences Identifies In Vivo Rules for mRNA Degradation. *Mol Cell*. 2017;68(6):1083-1094.e1085.

82. Lau NC, Kolkman A, van Schaik FM, et al. Human Ccr4-Not complexes contain variable deadenylase subunits. *Biochem J*. 2009;422(3):443-453.

83. Goldstrohm AC, Hook BA, Seay DJ, Wickens M. PUF proteins bind Pop2p to regulate messenger RNAs. *Nat Struct Mol Biol*. 2006;13(6):533-539.

84. Blewett NH, Goldstrohm AC. A eukaryotic translation initiation factor 4E-binding protein promotes mRNA decapping and is required for PUF repression. *Mol Cell Biol*. 2012;32(20):4181-4194.

85. Djuranovic S, Nahvi A, Green R. A parsimonious model for gene regulation by miRNAs. *Science*. 2011;331(6017):550-553.

86. Kozomara A, Griffiths-Jones S. miRBase: annotating high confidence microRNAs using deep sequencing data. *Nucleic Acids Res*. 2014;42(Database issue):D68-73.

87. Sunkar R, Li YF, Jagadeeswaran G. Functions of microRNAs in plant stress responses. *Trends Plant Sci*. 2012;17(4):196-203.

88. Shenoy A, Blelloch RH. Regulation of microRNA function in somatic stem cell proliferation and differentiation. *Nat Rev Mol Cell Biol*. 2014;15(9):565-576.

89. Chen X. Small RNAs and their roles in plant development. *Annu Rev Cell Dev Biol*. 2009;25:21-44.

90. Bushati N, Cohen SM. microRNA functions. *Annu Rev Cell Dev Biol*. 2007;23:175-205.

91. Ambros V. MicroRNAs and developmental timing. *Curr Opin Genet Dev*. 2011;21(4):511-517.

92. Wilson RC, Doudna JA. Molecular mechanisms of RNA interference. *Annu Rev Biophys*. 2013;42:217-239.

93. Rehwinkel J, Behm-Ansmant I, Gatfield D, Izaurralde E. A crucial role for GW182 and the DCP1:DCP2 decapping complex in miRNA-mediated gene silencing. *Rna*. 2005;11(11):1640-1647.

94. Behm-Ansmant I, Rehwinkel J, Doerks T, Stark A, Bork P, Izaurralde E. mRNA degradation by miRNAs and GW182 requires both CCR4:NOT deadenylase and DCP1:DCP2 decapping complexes. *Genes Dev*. 2006;20(14):1885-1898.

95. Nishihara T, Zekri L, Braun JE, Izaurralde E. miRISC recruits decapping factors to miRNA targets to enhance their degradation. *Nucleic Acids Res*. 2013;41(18):8692-8705.

96. Bazzini AA, Lee MT, Giraldez AJ. Ribosome profiling shows that miR-430 reduces translation before causing mRNA decay in zebrafish. *Science*. 2012;336(6078):233-237.

97. Chen CY, Shyu AB. AU-rich elements: characterization and importance in mRNA degradation. *Trends Biochem Sci*. 1995;20(11):465-470.

98. Bartel DP. MicroRNAs: target recognition and regulatory functions. *Cell*. 2009;136(2):215-233.

99. Mayr C, Bartel DP. Widespread shortening of 3'UTRs by alternative cleavage and polyadenylation activates oncogenes in cancer cells. *Cell*. 2009;138(4):673-684.

100. Dill KK, Amacher SL. tortuga refines Notch pathway gene expression in the zebrafish presomitic mesoderm at the post-transcriptional level. *Dev Biol*. 2005;287(2):225-236.

101. Zhou D, Shen R, Ye JJ, et al. Nuclear receptor coactivator PNRC2 regulates energy expenditure and adiposity. *J Biol Chem*. 2008;283(1):541-553.

102. Zhou D, Chen S. PNRC2 is a 16 kDa coactivator that interacts with nuclear receptors through an SH3-binding motif. *Nucleic Acids Res*. 2001;29(19):3939-3948.

103. Cho H, Kim KM, Kim YK. Human proline-rich nuclear receptor coregulatory protein 2 mediates an interaction between mRNA surveillance machinery and decapping complex. *Mol Cell*. 2009;33(1):75-86.

104. Zhou D, Ye JJ, Li Y, Lui K, Chen S. The molecular basis of the interaction between the proline-rich SH3-binding motif of PNRC and estrogen receptor alpha. *Nucleic Acids Res*. 2006;34(20):5974-5986.

105. Lai T, Cho H, Liu Z, et al. Structural basis of the PNRC2-mediated link between mrna surveillance and decapping. *Structure*. 2012;20(12):2025-2037.

106. Krol AJ, Roellig D, Dequeant ML, et al. Evolutionary plasticity of segmentation clock networks. *Development*. 2011;138(13):2783-2792.

107. Nicholson P, Gkratsou A, Josi C, Colombo M, Muhlemann O. Dissecting the functions of SMG5, SMG7, and PNRC2 in nonsense-mediated mRNA decay of human cells. *Rna*. 2018;24(4):557-573.

108. Levine JH, Lin Y, Elowitz MB. Functional roles of pulsing in genetic circuits. *Science*. 2013;342(6163):1193-1200.

109. Purvis JE, Lahav G. Encoding and decoding cellular information through signaling dynamics. *Cell*. 2013;152(5):945-956.

110. Sonnen KF, Aulehla A. Dynamic signal encoding--from cells to organisms. *Semin Cell Dev Biol*. 2014;34:91-98.

111. Hubaud A, Pourquie O. Signalling dynamics in vertebrate segmentation. *Nat Rev Mol Cell Biol*. 2014;15(11):709-721.

112. Harima Y, Imayoshi I, Shimojo H, Kobayashi T, Kageyama R. The roles and mechanism of ultradian oscillatory expression of the mouse Hes genes. *Semin Cell Dev Biol*. 2014;34:85-90.

113. Takke C, Campos-Ortega JA. her1, a zebrafish pair-rule like gene, acts downstream of notch signalling to control somite development. *Development*. 1999;126(13):3005-3014.

114. Soza-Ried C, Ozturk E, Ish-Horowicz D, Lewis J. Pulses of Notch activation synchronise oscillating somite cells and entrain the zebrafish segmentation clock. *Development*. 2014;141(8):1780-1788.

115. Cibois M, Gautier-Courteille C, Legagneux V, Paillard L. Post-transcriptional controls - adding a new layer of regulation to clock gene expression. *Trends Cell Biol*. 2010;20(9):533-541.

116. Fujimuro T, Matsui T, Nitanda Y, et al. Hes7 3'UTR is required for somite segmentation function. *Sci Rep*. 2014;4:6462.

117. Hanisch A, Holder MV, Choorapoikayil S, Gajewski M, Ozbudak EM, Lewis J. The elongation rate of RNA polymerase II in zebrafish and its significance in the somite segmentation clock. *Development*. 2013;140(2):444-453.

118. Delaune EA, Francois P, Shih NP, Amacher SL. Single-cell-resolution imaging of the impact of Notch signaling and mitosis on segmentation clock dynamics. *Dev Cell*. 2012;23(5):995-1005.

119. Bonev B, Stanley P, Papalopulu N. MicroRNA-9 Modulates Hes1 ultradian oscillations by forming a double-negative feedback loop. *Cell Rep*. 2012;2(1):10-18.

120. Tan SL, Ohtsuka T, Gonzalez A, Kageyama R. MicroRNA9 regulates neural stem cell differentiation by controlling Hes1 expression dynamics in the developing brain. *Genes Cells*. 2012;17(12):952-961.

121. Wong SF, Agarwal V, Mansfield JH, et al. Independent regulation of vertebral number and vertebral identity by microRNA-196 paralogs. *Proc Natl Acad Sci U S A*. 2015;112(35):E4884-4893.

122. Garneau NL, Wilusz J, Wilusz CJ. The highways and byways of mRNA decay. *Nat Rev Mol Cell Biol*. 2007;8(2):113-126.

123. Ghosh S, Jacobson A. RNA decay modulates gene expression and controls its fidelity. *Wiley Interdiscip Rev RNA*. 2010;1(3):351-361.

124. Houseley J, Tollervey D. The many pathways of RNA degradation. *Cell*. 2009;136(4):763-776.

125. Lykke-Andersen S, Jensen TH. Nonsense-mediated mRNA decay: an intricate machinery that shapes transcriptomes. *Nat Rev Mol Cell Biol*. 2015;16(11):665-677.

126. Schoenberg DR, Maquat LE. Regulation of cytoplasmic mRNA decay. *Nat Rev Genet*. 2012;13(4):246-259.

127. Cho H, Han S, Choe J, Park SG, Choi SS, Kim YK. SMG5-PNRC2 is functionally dominant compared with SMG5-SMG7 in mammalian nonsense-mediated mRNA decay. *Nucleic Acids Res*. 2013;41(2):1319-1328.

128. Cho H, Han S, Park OH, Kim YK. SMG1 regulates adipogenesis via targeting of staufen1-mediated mRNA decay. *Biochim Biophys Acta*. 2013;1829(12):1276-1287.

129. Cho H, Park OH, Park J, et al. Glucocorticoid receptor interacts with PNRC2 in a ligand-dependent manner to recruit UPF1 for rapid mRNA degradation. *Proc Natl Acad Sci U S A*. 2015;112(13):E1540-1549.

130. Mugridge JS, Ziemniak M, Jemielity J, Gross JD. Structural basis of mRNA-cap recognition by Dcp1-Dcp2. *Nat Struct Mol Biol*. 2016;23(11):987-994.

131. Shih NP, Francois P, Delaune EA, Amacher SL. Dynamics of the slowing segmentation clock reveal alternating two-segment periodicity. *Development*. 2015;142(10):1785-1793.

132. Postlethwait JH, Johnson SL, Midson CN, et al. A genetic linkage map for the zebrafish. *Science*. 1994;264(5159):699-703.

133. Sander JD, Maeder ML, Reyon D, Voytas DF, Joung JK, Dobbs D. ZiFiT (Zinc Finger Targeter): an updated zinc finger engineering tool. *Nucleic Acids Res*. 2010;38(Web Server issue):W462-468.

134. Sander JD, Zaback P, Joung JK, Voytas DF, Dobbs D. Zinc Finger Targeter (ZiFiT): an engineered zinc finger/target site design tool. *Nucleic Acids Res*. 2007;35(Web Server issue):W599-605.

135. Jao LE, Wente SR, Chen W. Efficient multiplex biallelic zebrafish genome editing using a CRISPR nuclease system. *Proc Natl Acad Sci U S A*. 2013;110(34):13904-13909.

136. Talbot JC, Amacher SL. A streamlined CRISPR pipeline to reliably generate zebrafish frameshifting alleles. *Zebrafish*. 2014;11(6):583-585.

137. Wittkopp N, Huntzinger E, Weiler C, et al. Nonsense-mediated mRNA decay effectors are essential for zebrafish embryonic development and survival. *Mol Cell Biol*. 2009;29(13):3517-3528.

138. Gallagher TL, Arribere JA, Geurts PA, et al. Rbfox-regulated alternative splicing is critical for zebrafish cardiac and skeletal muscle functions. *Dev Biol*. 2011;359(2):251-261.

139. Berberoglu MA, Gallagher TL, Morrow ZT, et al. Satellite-like cells contribute to pax7-dependent skeletal muscle repair in adult zebrafish. *Dev Biol*. 2017;424(2):162-180.

140. Rupp RA, Snider L, Weintraub H. Xenopus embryos regulate the nuclear localization of XMyoD. *Genes Dev*. 1994;8(11):1311-1323.

141. Turner DL, Weintraub H. Expression of achaete-scute homolog 3 in Xenopus embryos converts ectodermal cells to a neural fate. *Genes Dev*. 1994;8(12):1434-1447.

142. Broadbent J, Read EM. Wholemount in situ hybridization of Xenopus and zebrafish embryos. *Methods Mol Biol*. 1999;127:57-67.

143. Jowett T. Analysis of protein and gene expression. *Methods in Cell Biology*. 1998;59:63-85.

144. Choi HM, Beck VA, Pierce NA. Next-generation in situ hybridization chain reaction: higher gain, lower cost, greater durability. *ACS Nano*. 2014;8(5):4284-4294.

145. Choi HM, Chang JY, Trinh le A, Padilla JE, Fraser SE, Pierce NA. Programmable in situ amplification for multiplexed imaging of mRNA expression. *Nat Biotechnol*. 2010;28(11):1208-1212.

146. Kwan KM, Fujimoto E, Grabher C, et al. The Tol2kit: a multisite gateway-based construction kit for Tol2 transposon transgenesis constructs. *Dev Dyn*. 2007;236(11):3088-3099.

147. Thermes V, Grabher C, Ristoratore F, et al. I-SceI meganuclease mediates highly efficient transgenesis in fish. *Mech Dev*. 2002;118(1-2):91-98.

148. Wright GJ, Giudicelli F, Soza-Ried C, Hanisch A, Ariza-McNaughton L, Lewis J. DeltaC and DeltaD interact as Notch ligands in the zebrafish segmentation clock. *Development*. 2011;138(14):2947-2956.

149. Howe K, Clark MD, Torroja CF, et al. The zebrafish reference genome sequence and its relationship to the human genome. *Nature*. 2013;496(7446):498-503.

150. Hruscha A, Krawitz P, Rechenberg A, et al. Efficient CRISPR/Cas9 genome editing with low off-target effects in zebrafish. *Development*. 2013;140(24):4982-4987.

151. Hwang WY, Fu Y, Reyon D, et al. Efficient genome editing in zebrafish using a CRISPR-Cas system. *Nat Biotechnol*. 2013;31(3):227-229.

152. Giraldez AJ. microRNAs, the cell's Nepenthe: clearing the past during the maternal-to-zygotic transition and cellular reprogramming. *Curr Opin Genet Dev*. 2010;20(4):369-375.

153. Giraldez AJ, Cinalli RM, Glasner ME, et al. MicroRNAs regulate brain morphogenesis in zebrafish. *Science*. 2005;308(5723):833-838.

154. Mishima Y, Giraldez AJ, Takeda Y, et al. Differential regulation of germline mRNAs in soma and germ cells by zebrafish miR-430. *Curr Biol*. 2006;16(21):2135-2142.

155. Mishima Y, Tomari Y. Codon Usage and 3' UTR Length Determine Maternal mRNA Stability in Zebrafish. *Mol Cell*. 2016;61(6):874-885.

156. Jonas S, Izaurralde E. Towards a molecular understanding of microRNA-mediated gene silencing. *Nat Rev Genet*. 2015;16(7):421-433.

157. Ulitsky I, Shkumatava A, Jan CH, et al. Extensive alternative polyadenylation during zebrafish development. *Genome Res*. 2012;22(10):2054-2066.

158. Anastasaki C, Longman D, Capper A, Patton EE, Caceres JF. Dhx34 and Nbas function in the NMD pathway and are required for embryonic development in zebrafish. *Nucleic Acids Res*. 2011;39(9):3686-3694.

159. Lee MT, Bonneau AR, Takacs CM, et al. Nanog, Pou5f1 and SoxB1 activate zygotic gene expression during the maternal-to-zygotic transition. *Nature*. 2013;503(7476):360-364.

160. Gebauer F, Hentze MW. Molecular mechanisms of translational control. *Nat Rev Mol Cell Biol*. 2004;5(10):827-835.

161. Hood HM, Neafsey DE, Galagan J, Sachs MS. Evolutionary roles of upstream open reading frames in mediating gene regulation in fungi. *Annu Rev Microbiol*. 2009;63:385-409.

162. Medenbach J, Seiler M, Hentze MW. Translational control via protein-regulated upstream open reading frames. *Cell*. 2011;145(6):902-913.

163. Morris DR, Geballe AP. Upstream open reading frames as regulators of mRNA translation. *Mol Cell Biol*. 2000;20(23):8635-8642.

164. Sachs MS, Geballe AP. Downstream control of upstream open reading frames. *Genes Dev*. 2006;20(8):915-921.

165. Somers J, Poyry T, Willis AE. A perspective on mammalian upstream open reading frame function. *Int J Biochem Cell Biol*. 2013;45(8):1690-1700.

166. Wethmar K. The regulatory potential of upstream open reading frames in eukaryotic gene expression. *Wiley Interdiscip Rev RNA*. 2014;5(6):765-778.

167. Barbosa C, Peixeiro I, Romao L. Gene expression regulation by upstream open reading frames and human disease. *PLoS Genet*. 2013;9(8):e1003529.

168. Peccarelli M, Kebaara BW. Regulation of natural mRNAs by the nonsense-mediated mRNA decay pathway. *Eukaryot Cell*. 2014;13(9):1126-1135.

169. Popp MW, Maquat LE. Organizing principles of mammalian nonsense-mediated mRNA decay. *Annu Rev Genet*. 2013;47:139-165.

170. Mishima Y, Fukao A, Kishimoto T, Sakamoto H, Fujiwara T, Inoue K. Translational inhibition by deadenylation-independent mechanisms is central to microRNA-mediated silencing in zebrafish. *Proc Natl Acad Sci U S A*. 2012;109(4):1104-1109.

171. Takeda Y, Mishima Y, Fujiwara T, Sakamoto H, Inoue K. DAZL relieves miRNA-mediated repression of germline mRNAs by controlling poly(A) tail length in zebrafish. *PLoS One*. 2009;4(10):e7513.

172. Yasuda K, Kotani T, Ota R, Yamashita M. Transgenic zebrafish reveals novel mechanisms of translational control of cyclin B1 mRNA in oocytes. *Dev Biol*. 2010;348(1):76-86.

173. Takahashi K, Kotani T, Katsu Y, Yamashita M. Possible involvement of insulin-like growth factor 2 mRNA-binding protein 3 in zebrafish oocyte maturation as a novel cyclin B1 mRNA-binding protein that represses the translation in immature oocytes. *Biochem Biophys Res Commun*. 2014;448(1):22-27.

174. Subtelny AO, Eichhorn SW, Chen GR, Sive H, Bartel DP. Poly(A)-tail profiling reveals an embryonic switch in translational control. *Nature*. 2014;508(7494):66-71.

175. Li Y, Sun Y, Fu Y, et al. Dynamic landscape of tandem 3' UTRs during zebrafish development. *Genome Res*. 2012;22(10):1899-1906.

176. Zuker M. Mfold web server for nucleic acid folding and hybridization prediction. *Nucleic Acids Res*. 2003;31(13):3406-3415.

177. von Roretz C, Gallouzi IE. Decoding ARE-mediated decay: is microRNA part of the equation? *J Cell Biol*. 2008;181(2):189-194.

178. Park E, Maquat LE. Staufen-mediated mRNA decay. *Wiley Interdiscip Rev RNA*. 2013;4(4):423-435.

179. Fallmann J, Sedlyarov V, Tanzer A, Kovarik P, Hofacker IL. AREsite2: an enhanced database for the comprehensive investigation of AU/GU/U-rich elements. *Nucleic Acids Res*. 2016;44(D1):D90-95.

180. Hurt JA, Robertson AD, Burge CB. Global analyses of UPF1 binding and function reveal expanded scope of nonsense-mediated mRNA decay. *Genome Res*. 2013;23(10):1636-1650.

181. Valkov E, Muthukumar S, Chang CT, Jonas S, Weichenrieder O, Izaurralde E. Structure of the Dcp2-Dcp1 mRNA-decapping complex in the activated conformation. *Nat Struct Mol Biol*. 2016;23(6):574-579.

182. Hu Y, Xie S, Yao J. Identification of Novel Reference Genes Suitable for qRT-PCR Normalization with Respect to the Zebrafish Developmental Stage. *PLoS One*. 2016;11(2):e0149277.

183. Albers M, Kranz H, Kober I, et al. Automated yeast two-hybrid screening for nuclear receptor-interacting proteins. *Mol Cell Proteomics*. 2005;4(2):205-213.

184. Loh B, Jonas S, Izaurralde E. The SMG5-SMG7 heterodimer directly recruits the CCR4-NOT deadenylase complex to mRNAs containing nonsense codons via interaction with POP2. *Genes Dev*. 2013;27(19):2125-2138.

185. Bailey TL, Boden M, Buske FA, et al. MEME SUITE: tools for motif discovery and searching. *Nucleic Acids Res*. 2009;37(Web Server issue):W202-208.

186. Miles WO, Lepesant JM, Bourdeaux J, et al. The LSD1 Family of Histone Demethylases and the Pumilio Posttranscriptional Repressor Function in a Complex Regulatory Feedback Loop. *Mol Cell Biol*. 2015;35(24):4199-4211.

187. Lai WS, Carrick DM, Blackshear PJ. Influence of nonameric AU-rich tristetraprolin-binding sites on mRNA deadenylation and turnover. *J Biol Chem*. 2005;280(40):34365-34377.

188. Tadros W, Lipshitz HD. The maternal-to-zygotic transition: a play in two acts. *Development*. 2009;136(18):3033-3042.

189. Hogg JR, Goff SP. Upf1 senses 3'UTR length to potentiate mRNA decay. *Cell*. 2010;143(3):379-389.

190. Masuda A, Andersen HS, Doktor TK, et al. CUGBP1 and MBNL1 preferentially bind to 3' UTRs and facilitate mRNA decay. *Sci Rep*. 2012;2:209.

191. Wang ET, Ward AJ, Cherone JM, et al. Antagonistic regulation of mRNA expression and splicing by CELF and MBNL proteins. *Genome Res*. 2015;25(6):858-871.

192. Morris AR, Mukherjee N, Keene JD. Ribonomic analysis of human Pum1 reveals cis-trans conservation across species despite evolution of diverse mRNA target sets. *Mol Cell Biol*. 2008;28(12):4093-4103.

193. Galgano A, Forrer M, Jaskiewicz L, Kanitz A, Zavolan M, Gerber AP. Comparative analysis of mRNA targets for human PUF-family proteins suggests extensive interaction with the miRNA regulatory system. *PLoS One*. 2008;3(9):e3164.

194. Lu G, Hall TM. Alternate modes of cognate RNA recognition by human PUMILIO proteins. *Structure*. 2011;19(3):361-367.

195. Zhang M, Chen D, Xia J, et al. Post-transcriptional regulation of mouse neurogenesis by Pumilio proteins. *Genes Dev*. 2017;31(13):1354-1369.

196. Hafner M, Landthaler M, Burger L, et al. Transcriptome-wide identification of RNA-binding protein and microRNA target sites by PAR-CLIP. *Cell*. 2010;141(1):129-141.

197. Bohn JA, Van Etten JL, Schagat TL, et al. Identification of diverse target RNAs that are functionally regulated by human Pumilio proteins. *Nucleic Acids Res*. 2018;46(1):362-386.

198. Weidmann CA, Raynard NA, Blewett NH, Van Etten J, Goldstrohm AC. The RNA binding domain of Pumilio antagonizes poly-adenosine binding protein and accelerates deadenylation. *Rna*. 2014;20(8):1298-1319.

199. Joly W, Chartier A, Rojas-Rios P, Busseau I, Simonelig M. The CCR4 deadenylase acts with Nanos and Pumilio in the fine-tuning of Mei-P26 expression to promote germline stem cell self-renewal. *Stem Cell Reports*. 2013;1(5):411-424.

200. Chritton JJ, Wickens M. A role for the poly(A)-binding protein Pab1p in PUF protein-mediated repression. *J Biol Chem*. 2011;286(38):33268-33278.

201. Gennarino VA, Palmer EE, McDonell LM, et al. A Mild PUM1 Mutation Is Associated with Adult-Onset Ataxia, whereas Haploinsufficiency Causes Developmental Delay and Seizures. *Cell*. 2018;172(5):924-936.e911.

202. Siemen H, Colas D, Heller HC, Brustle O, Pera RA. Pumilio-2 function in the mouse nervous system. *PLoS One*. 2011;6(10):e25932.

203. Mak W, Fang C, Holden T, Dratver MB, Lin H. An Important Role of Pumilio 1 in Regulating the Development of the Mammalian Female Germline. *Biol Reprod*. 2016;94(6):134.

204. Xu EY, Chang R, Salmon NA, Reijo Pera RA. A gene trap mutation of a murine homolog of the Drosophila stem cell factor Pumilio results in smaller testes but does not affect litter size or fertility. *Mol Reprod Dev*. 2007;74(7):912-921.

205. Chen D, Zheng W, Lin A, Uyhazi K, Zhao H, Lin H. Pumilio 1 suppresses multiple activators of p53 to safeguard spermatogenesis. *Curr Biol*. 2012;22(5):420-425.

206. Gennarino VA, Singh RK, White JJ, et al. Pumilio1 haploinsufficiency leads to SCA1-like neurodegeneration by increasing wild-type Ataxin1 levels. *Cell*. 2015;160(6):1087-1098.

207. Zahr SK, Yang G, Kazan H, et al. A Translational Repression Complex in Developing Mammalian Neural Stem Cells that Regulates Neuronal Specification. *Neuron*. 2018;97(3):520-537.e526.

208. Naudin C, Hattabi A, Michelet F, et al. PUMILIO/FOXP1 signaling drives expansion of hematopoietic stem/progenitor and leukemia cells. *Blood*. 2017;129(18):2493-2506.

209. Kopp F, Elguindy MM, Yalvac ME, et al. PUMILIO hyperactivity drives premature aging of Norad-deficient mice. *Elife*. 2019;8.

210. Petryszak R, Keays M, Tang YA, et al. Expression Atlas update--an integrated database of gene and protein expression in humans, animals and plants. *Nucleic Acids Res*. 2016;44(D1):D746-752.

211. Van Nostrand EL, Pratt GA, Shishkin AA, et al. Robust transcriptome-wide discovery of RNA-binding protein binding sites with enhanced CLIP (eCLIP). *Nat Methods*. 2016;13(6):508-514.

212. Gueydan C, Droogmans L, Chalon P, Huez G, Caput D, Kruys V. Identification of TIAR as a protein binding to the translational regulatory AU-rich element of tumor necrosis factor alpha mRNA. *J Biol Chem*. 1999;274(4):2322-2326.

213. Piecyk M, Wax S, Beck AR, et al. TIA-1 is a translational silencer that selectively regulates the expression of TNF-alpha. *Embo j*. 2000;19(15):4154-4163.

214. Dixon DA, Balch GC, Kedersha N, et al. Regulation of cyclooxygenase-2 expression by the translational silencer TIA-1. *J Exp Med*. 2003;198(3):475-481.

215. Wilson T, Treisman R. Removal of poly(A) and consequent degradation of c-fos mRNA facilitated by 3' AU-rich sequences. *Nature*. 1988;336(6197):396-399.

216. Lieberman AP, Pitha PM, Shin ML. Poly(A) removal is the kinase-regulated step in tumor necrosis factor mRNA decay. *J Biol Chem*. 1992;267(4):2123-2126.

217. Peppel K, Baglioni C. Deadenylation and turnover of interferon-beta mRNA. *J Biol Chem*. 1991;266(11):6663-6666.

218. Laird-Offringa IA, de Wit CL, Elfferich P, van der Eb AJ. Poly(A) tail shortening is the translation-dependent step in c-myc mRNA degradation. *Mol Cell Biol*. 1990;10(12):6132-6140.

219. Shyu AB, Belasco JG, Greenberg ME. Two distinct destabilizing elements in the c-fos message trigger deadenylation as a first step in rapid mRNA decay. *Genes Dev*. 1991;5(2):221-231.

220. Brewer G, Ross J. Poly(A) shortening and degradation of the 3' A+U-rich sequences of human c-myc mRNA in a cell-free system. *Mol Cell Biol*. 1988;8(4):1697-1708.

221. Fujino Y, Yamada K, Sugaya C, et al. Deadenylation by the CCR4-NOT complex contributes to the turnover of hairy-related mRNAs in the zebrafish segmentation clock. *FEBS Lett*. 2018;592(20):3388-3398.

222. Kageyama R, Niwa Y, Shimojo H, Kobayashi T, Ohtsuka T. Ultradian oscillations in Notch signaling regulate dynamic biological events. *Curr Top Dev Biol*. 2010;92:311-331.

223. Sang L, Roberts JM, Coller HA. Hijacking HES1: how tumors co-opt the anti-differentiation strategies of quiescent cells. *Trends Mol Med*. 2010;16(1):17-26.

224. Hu W, Sweet TJ, Chamnongpol S, Baker KE, Coller J. Co-translational mRNA decay in Saccharomyces cerevisiae. *Nature*. 2009;461(7261):225-229.

225. Couttet P, Fromont-Racine M, Steel D, Pictet R, Grange T. Messenger RNA deadenylylation precedes decapping in mammalian cells. *Proc Natl Acad Sci U S A*. 1997;94(11):5628-5633.

226. Coller J, Parker R. Eukaryotic mRNA decapping. *Annu Rev Biochem*. 2004;73:861-890.

227. Daroczi B, Kari G, Ren Q, Dicker AP, Rodeck U. Nuclear factor kappaB inhibitors alleviate and the proteasome inhibitor PS-341 exacerbates radiation toxicity in zebrafish embryos. *Mol Cancer Ther*. 2009;8(9):2625-2634.

228. Winder SJ, Lipscomb L, Angela Parkin C, Juusola M. The proteasomal inhibitor MG132 prevents muscular dystrophy in zebrafish. *PLoS Curr*. 2011;3:Rrn1286.

229. Yogev O, Williams VC, Hinits Y, Hughes SM. eIF4EBP3L acts as a gatekeeper of TORC1 in activity-dependent muscle growth by specifically regulating Mef2ca translational initiation. *PLoS Biol*. 2013;11(10):e1001679.